Evolution of Seismic Response and Seismic Hazard at Goldex Mine's D1-Zone

by

Ray Stratton

A thesis submitted in partial fulfillment
of the requirements for the degree of
Master of Science (MASc) in Natural Resource Engineering

The Faculty of Graduate Studies
Laurentian University
Sudbury, Ontario, Canada

THESIS DEFENCE COMMITTEE/COMITÉ DE SOUTENANCE DE THÈSE
Laurentian Université/Université Laurentienne
Office of Graduate Studies/Bureau des études supérieures

Title of Thesis Titre de la thèse	Evolution of Seismic Response and Seismic Hazard at Goldex Mine's D1-Zone
Name of Candidate Nom du candidat	Stratton, Ray
Degree Diplôme	Master of Science
Department/Program Département/Programme	Natural Resources Engineering
Date of Defence Date de la soutenance	October 24, 2022

APPROVED/APPROUVÉ

Thesis Examiners/Examinateurs de thèse:

Dr. Marty Hudyma
(Supervisor/Directeur(trice) de thèse)

Dr. Philip Dirige
(Committee member/Membre du comité)

Dr. Marie-Helene Fillion
(Committee member/Membre du comité)

Dr. Mike Yao
(External Examiner/Examinateur externe)

Approved for the Office of Graduate Studies
Approuvé pour le Bureau des études supérieures
Tammy Eger, PhD
Vice-President Research (Office of Graduate Studies)
Vice-rectrice à la recherche (Bureau des études supérieures)
Laurentian University / Université Laurentienne

ACCESSIBILITY CLAUSE AND PERMISSION TO USE

ACCESSIBILITY CLAUSE AND PERMISSION TO USE

Abstract

This thesis observes both the evolution of the seismic response and associated seismic hazard at Goldex Mine's D1-zone over the time period including August 2018 until December 2020. A variety of evaluation methods have been used to discuss the changes in seismic response, the source mechanisms, and the associated hazards. Data visualization and analysis were performed using mXrap software (Australian Centre for Geomechanics).

Ultimately, the hazards of the change in seismic response are associated with significant or large seismic events occurring at times well outside of the normal blasting times. Understanding the role that both mining sequence and production constraints plays in the seismic response is key to understanding relative hazards. The change over time as the extraction ratio of the orebody increases is also considered.

Keywords

Seismicity, Mining, Seismic Hazard, Goldex Mine, Seismic Event Location, Seismic Event Time, Seismic Response to Mining.

Acknowledgments

I would like to take this opportunity to acknowledge and thank those who made this work possible.

I sincerely thank Chantale Doucet of Agnico Eagle Goldex Mine for her assistance throughout this work. I would also thank Goldex mine and Agnico Eagle for making available the rock mechanics data, seismic data and technical documents.

I would like to acknowledge the Australian Centre of Geomechanics for use and support of their mXrap software.

I thank Dr. Laura Brown for her tutelage in use of the mXrap software and her guidance in analysis.

Sincere thanks to my committee, including Dr. Philip Dirige, Dr. Marie-Hélène Fillion and Dr. Mike Yao for their constructive comments on my research and for their efforts in reviewing this thesis.

Thank you also to the wonderful staff at Laurentian University. This includes the assistance provided by Dr. Ramesh Subramanian in my various admissions endeavors and also Dr. Dean Millar, who was able to provide coaching while guiding my work at a point where otherwise it may have remained unfinished.

I cannot possibly thank my supervisor, Dr. Martin Hudyma, enough for all his efforts throughout this work. His unending patience for my many complications, as well as his guidance throughout the work, I will never forget. Dr. Hudyma is an invaluable asset to seismic research in any form, and I thank him for this opportunity to have learned from him.

I would like to express my sincerest appreciation to Austin Glover, a young man who has taught me so much about perseverance while solidifying my beliefs that learning is a lifelong endeavor.

Last but not least, I thank my partner throughout this time, Kim Ablitt. Without her assistance and support this work would never have been completed.

Table of Contents

List of Tables

List of Figures

Chapter 1

1 Introduction

As improvements in technology allow for mine expansion to deeper depths, so too must the evaluation of seismic hazard develop. This is an important step in understanding both the changes involved in deep mining and the hazards that workplace parties may be exposed to.

A significant source of hazards, as mining progresses deeper, is mining-induced seismicity. These hazards must be controlled during the extraction of rock underground, either for the purposes of access to the ore, or removal of the ore itself.

Seismic data was provided by the Agnico Eagle Goldex mine in Northern Quebec, Canada for the basis of this research. The focus of this thesis is the evolution of the seismic response, and associated hazards, during the initial development and subsequent extraction of the D1 ore zone, which spans approximately 800m-1250m below surface.

1.1 Underground Mine Seismicity

Both safety and productivity in underground mining can be impacted by seismic activity (Gibowicz and Kijko, 1994). As the depth of mining within a given mine deepens, associated stresses increase. This increase in stress will often either directly or indirectly result in more frequent seismic events, and may also generate larger events. These events can be expressed with either small amounts of energy over time, or violent failures of rock at the boundaries of an excavation referred to as a rockburst (Ortlepp, 1997).

1.2 Seismic Monitoring and Data Collection

An appropriately designed seismic system, maintained in good condition, can provide significant information about the seismic events taking place in the vicinity. Not only can the magnitudes and locations of events be determined, but significant additional information about the rock mass response can be obtained through various analysis and interpretation techniques. These analyses and interpretations will be explored in Sections 2.2 and 2.3.

1.3 Scope of Thesis

This thesis aims to evaluate the changes in seismic hazard from the time period prior to mining the D1 Zone at Goldex mine right up to intermediate/late-stage extraction of this same ore zone. This covers the time period starting August 2018 up to December 2020. This analysis focuses on the various events which occur in and around the excavations, and attempts to identify the general conditions which resulted in those events. The changes in general trends over time, and possible conditions that led to those circumstances are also evaluated.

There is some uncertainty about the pre-mining stress conditions and an appropriate constitutive relation for the geological units around the Goldex orebody. Consequently, stress conditions throughout the evaluation period, determined either through numerical modelling or *in situ* measurement techniques, is beyond the scope of this thesis.

1.4 Research Approach

This research is primarily an observational study using a natural experimentation approach. This is due to the Goldex Mine D1 Zone being a complex rock mass system, precluding a controlled experimental approach. The reason for this is that the rock mass itself contains significant variations in geology, structure, crystallization and other natural discontinuities which cannot be entirely determined. These uncertain conditions are compounded by the very nature of the mining exploration and development often resulting in incomplete information about the rock mass itself. Additionally, even within a given area, stress conditions can vary significantly in both direction and magnitude. Finally, the collection of seismic data during these unknowns cannot be replicated, it can only be gathered when the sum of these unknowns results in a seismic event, preventing statistical validation or analysis.

The aggregate of these conditions is an uncontrolled system for research purposes, requiring observational study. This research does so by observing the seismic data collected to either identify or infer patterns of the data, allowing for an extrapolation of that understanding into an evaluation of the changes in seismic hazard over time.

1.5 Outline of the Thesis

Chapter One introduces the thesis, stating the objectives and thesis scope.

Chapter Two discusses prior literature relevant to the thesis, including background information around core concepts discussed.

Chapter Three provides an introduction and general overview to the mine from which the data in this thesis was obtained.

Chapter Four presents the seismic response observed as a result of mining over the relevant timeframe.

Chapter Five discusses both the observations and the practical implications of the changes in seismic responses over time.

Chapter Six outlines the conclusions of this thesis while providing recommendations for future work.

Chapter 2

2 Literature Review

The sections in this chapter provide an overview of prior research necessary to understand the fundamental concepts presented in this thesis. This includes both investigation and insight into stress, structure, seismicity, seismic response, source mechanism, seismic source parameters and analysis techniques relevant to this thesis.

2.1 Terminology

The following terms are used in this thesis and are material to underground hard rock mining-induced seismicity research.

2.1.1 Stress and Strain

Stress is a term used to describe the internal forces in a body applied to the surfaces of that body (Brady and Brown, 2006). It is typically described as Pascals (N/m^2). In more general terms, stress is the load per unit area applied to a body.

Stresses can act both internally within a body on the surface or externally on that same surface. These external stresses are described as confining stresses.

With respect to mining, stress can be classified as either *in situ* (a combination result of tectonics, depth and make-up of overhead rock influence, and geological formation), or induced (a result of the excavation of openings as part of the mining process). *In situ* stresses are defined by principal stresses classified as major (σ_1), intermediate (σ_2) and minor (σ_3) (Brady and Brown, 2006).

The stress attributed to any local site within a mine (generally the area immediately surrounding an excavation) is the combination of both the *in situ* and mining-induced stresses (Gibowicz and Kijko, 1994). When this local stress exceeds the strength of the rock, the conditions for rockbursting can occur (Hoek and Brown, 1980).

Strain is the deformation of a rock mass under the applied stress. Strain can be broadly defined under three categories with respect to underground hard rock mining: elastic (it will recover to its previous state when the stress is removed), inelastic/plastic/brittle/ductile (it will not recover to its previous state when the stress is removed) and fracture/rupture.

In the context of an underground hard rock mine, the entire rock mass must be considered, which would include multiple rock types and also various discontinuities such as joints within the rock mass. Progression through the various portions of the stress-strain curve of a "moderately jointed hard rock mass" was described by Andrieux *et al*. (2008), resulting in Figure 1.

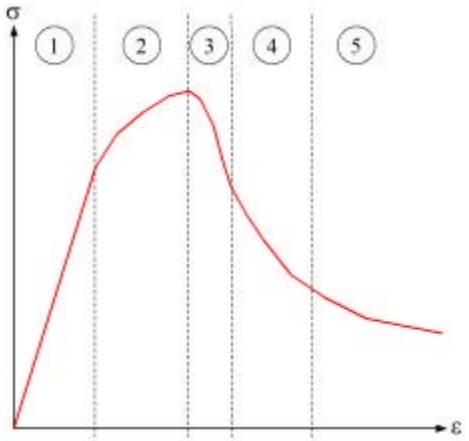

Figure 1 – Stress-strain curve of a typical moderately jointed hard rock under a given level of confinement (Andrieux *et al*., 2008)

Andrieux *et al*. (2008) continued to describe the five regions of the stress-strain curve as corresponding with the following response:

1. Elastic response, no permanent damage
2. Overall rock mass begins to experience damage, referred to as the “yielding phase”
3. Brittle response occurs post-peak strength has been reached, high amount of strain energy being released
4. Softening response, large volumes of rock are experiencing deformation with less energy per unit volume than in the brittle response
5. Residual phase, continued deformation as the rock mass sheds load. Despite failure, the rock mass continues to retain some load-bearing capacity

Since the density of discontinuities is a primary factor in being able to treat rock masses as uniform and isotropic (Hoek, 2006), with large enough rock masses, the scale is such that the density of those discontinuities is reduced to where their impact is minimal. Hoek had also observed that as intact rock specimen size increased, the strength of that rock decreased significantly, shown in Figure 2.

Rock mass properties

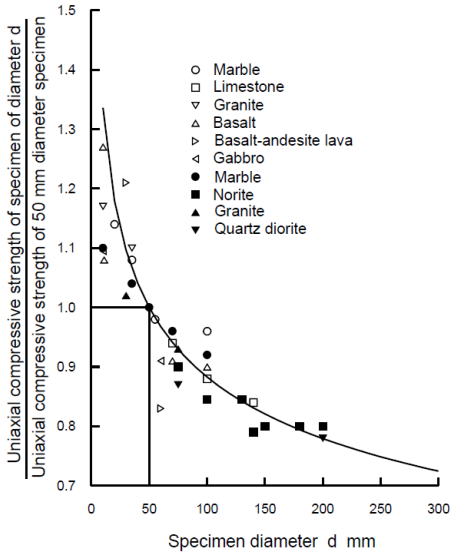

Figure 2 - Influence of specimen size on the strength of intact rock (Hoek, 2006)

Combining these observations, Hoek (2006) suggested that as the sample size increases, the strength of the rock mass will be a relatively constant value, compared to strength of smaller samples within the same rock mass, as illustrated in Figure 3.

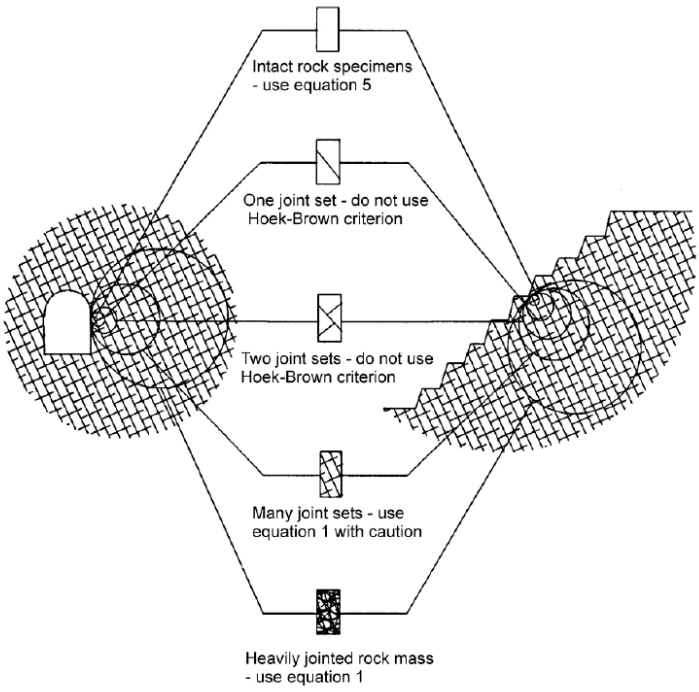

Figure 3 - Illustration showing sample size within a rock mass and the impact of discontinuities on strength of the sample (Hoek, 2006)

2.1.2 Structure

With respect to this thesis, structure refers to geological structures which exist as a result of the geological formation and tectonics. This may include geological/lithological units, bedding planes, veins, faults, joints, contacts between rock types, foliation within a rock type, and dykes. These structures often influence the location of seismic events, discussed further in Section 2.1.5.

2.1.3 Mining-Induced Seismicity

Seismicity is a vibration created due to inelastic deformation in a rock mass as a result of the loads applied to it. A seismic event is a stress driven dynamic wave generated by a sudden failure within the rock mass (Hedley, 1992). Mining-induced seismicity is a seismic event which has occurred as a result of stress changes due to the extraction of rock in a mining environment. These mining-induced seismic events can range in size, generally expressed in a logarithmic magnitude scale, from miniscule, posing very little hazard, to significant, potentially introducing substantial hazard.

As the elevation at which mining openings are being made deepens, the *in situ* stresses will increase. As more material is removed from any given mine, the mining-induced stresses will increase. This combination of factors can lead to the stresses and/or the strains exceeding the strength of some of the structures present, potentially resulting in mining-induced seismic events (Cook, 1976). The deeper the mine, the more extensive the mine, and the more complex the geology, will increase the likelihood of seismicity until at some point it becomes an inevitability in underground hard rock mines.

Modern seismic monitoring equipment can be used to pinpoint the location of where the rock is undergoing a seismic response. These seismic systems can also give information about the intensity of an event and considerable information about the nature of the rock mass failure that caused the seismic event.

2.1.4 Rock Mass Seismic Response to Mining

In hard rock mines, rock fails in a brittle manner at the pressures experienced in typical mining environments (Hoek and Brown, 1980). These failures and their associated seismic events can occur within very close proximity to underground openings, however it is possible that mining activities can generate failure and seismic events distant from mine excavations.

Proximity to openings means that the energy released is more likely to cause failure of the openings in some way, which can range from the engineered ground support entirely absorbing the energy; displacement and partial damage contained by engineered ground support; up to total failure of the opening and bursting/collapse. The greater the distance of the seismic event to the opening, the lower the hazard related to rock mass failure.

2.1.4.1 Rockbursts

When a seismic event causes violent and significant damage to a tunnel, or the excavation of a mine, it is referred to as a rockburst (Stacey and Ortlepp, 2001). Rockbursts are sudden, dynamic ejection of rock at a surface of an excavation. This occurs based on the strain at the excavation boundary, which is an extension of the stresses experienced by the rock mass.

The damage from the rockburst can be categorized as bulking, ejection or a rockfall induced by seismicity (Kaiser *et al*., 1996), as illustrated in Figure 4.

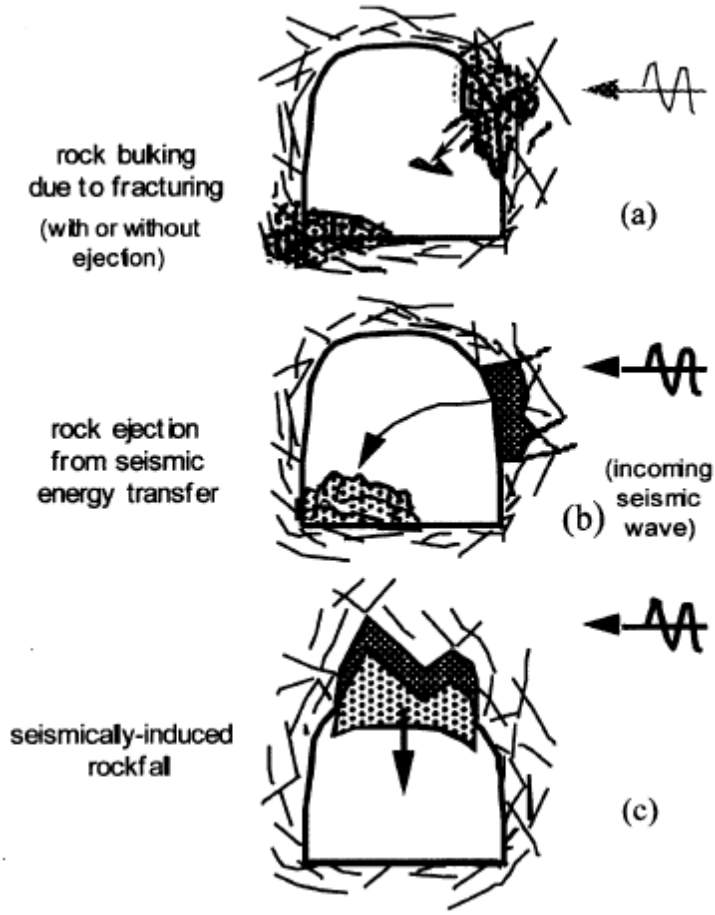

Figure 4 - Classifications of rockburst damage (Kaiser *et al.*, 1996)

There is an imperfect relation between event size and rockbursting. However, the larger the event, the greater the potential for damage.

2.1.4.2 Yielded Regions

The relation between stress and strain in hard rock is related to loading conditions. As confining pressures change, so does the stress-strain relation. An increase in confining pressure leads to more multi-axial loading conditions.

These changes in confining stress may lead to an increase in peak strength, noted by Wawersik and Fairhurst (1970), while also transitioning the rock mass from a brittle to more ductile

behaviour (Brady and Brown, 2006). Figure 5 shows the relation between the various confining pressures and the stress-strain response in a series of triaxial compression tests.

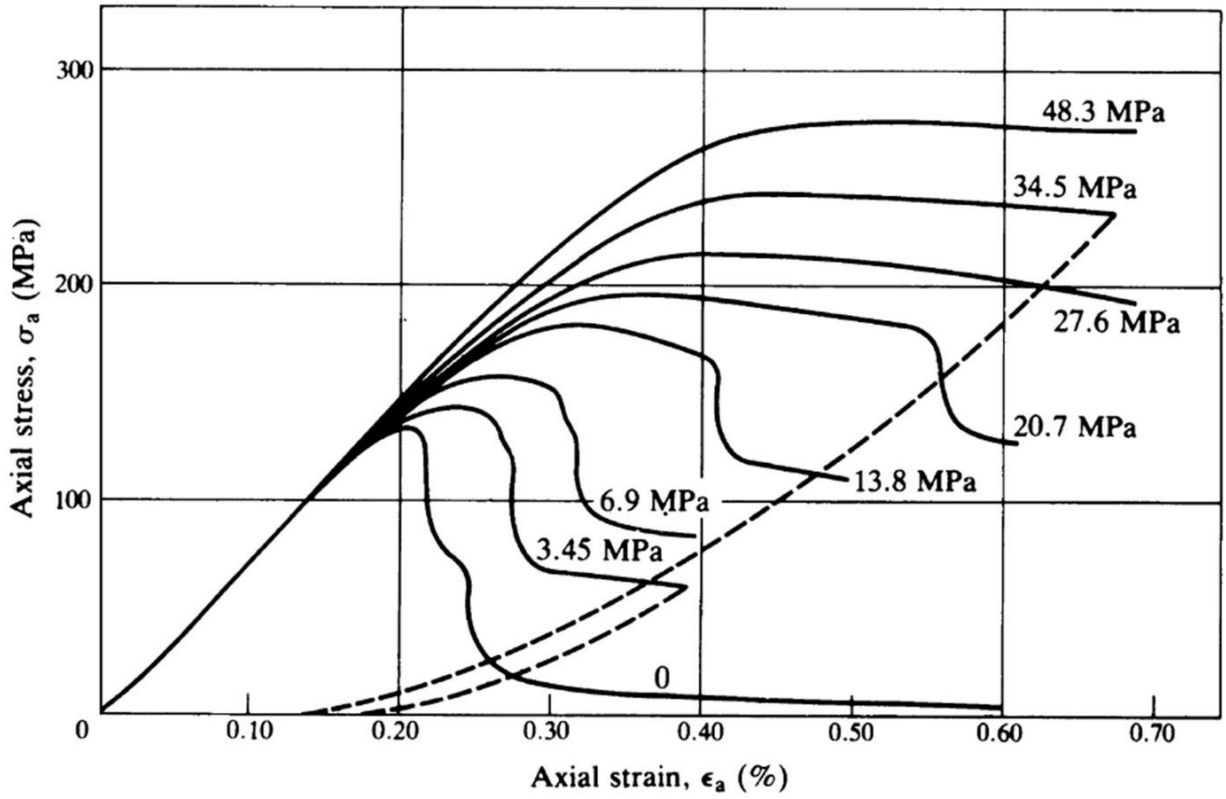

Figure 5 - Axial stress-strain relations for Tennessee Marble using varying confining pressures (Wawersik & Fairhurst, 1970), converted to metric units (Brady & Brown, 2006)

At low strains, the relation between stress and strain are practically linear, with a given sample of rock deforming elastically. This is evidenced in Figure 5 in the near-linear section common to all confining stresses. At the point in which the stress-strain relation is no longer linear, the stress will increase more slowly per unit of strain, and the slope of the stress-strain curve will flatten (Brady and Brown, 2006). This is the rock yield point. At this point, the stress will decrease after peak strength is reached.

The yield point will be impacted by the confining pressure. As confining pressure increases, so does the yield point. The confinement will also impact the manner in which the rock will fail. Figure 5 shows this relation.

With less confinement the rock will fail in a brittle fashion and with greater confinement will fail in a strain-softening manner (Carusone, 2018). It is also possible for a rock with relatively high hardness to exhibit an increasingly brittle behaviour with confinement (Tarasov and Randolph, 2011).

2.1.4.2.1 Seismicity and Yielded Regions

As discussed in Section 2.1.1, changes in stress and strain over time impact the response of the rock mass. The figure in that section will be reproduced here in order to identify the seismic responses proposed by Andrieux *et al*. (2008), shown in Figure 6.

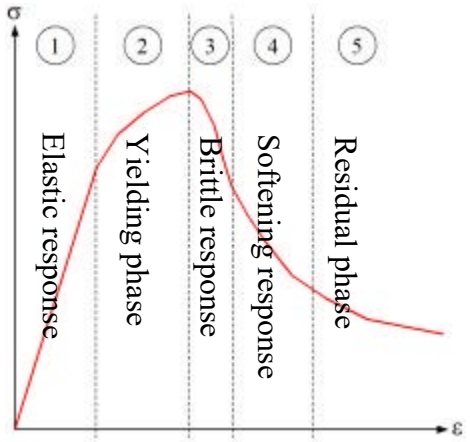

Figure 6 – Stress-strain curve and seismic response of a typical moderately jointed hard rock under a given level of confinement (Figure modified from Andrieux *et al*., 2008)

During the first region, the elastic response is described by Andrieux *et al*. as being "comparatively aseismic" and would generally include low levels of microseismic activity.

The second region is described as the "yielding phase" as largely microseismic responses with generally low amplitude and high frequency characteristics, useful for identifying areas of stress increase or plastic rock deformation.

The third region is described as the brittle response, where much of the strain energy is released at failure. This would generally include both the largest seismic events and those with either high energy or high moment.

The fourth region is described as including large seismic events, generally with large moment or large volumes of rock. These events would typically have lower energy than those in the third region.

The fifth and final region is described as the residual phase, where despite failure of the rock mass, it will continue to retain some load-bearing capacity. Generally seismic events will be limited in number, low amplitude, and low energy.

As previously discussed, the confinement of a rock mass will impact the manner in which yielding will occur. Figure 7 by Coulson (2009) attempts to describe different stress-strain curves for theoretical rock samples and/or rock masses under different levels of confinement. The figure shows the onset of microseismicity at the yield point for unconfined rock, which can result in brittle failure, strain-softening, and ultimately an aseismic response after yielding. Once a micro-fractured mass has been achieved, sufficient strain cannot accumulate to result in a detectable microseismic response.

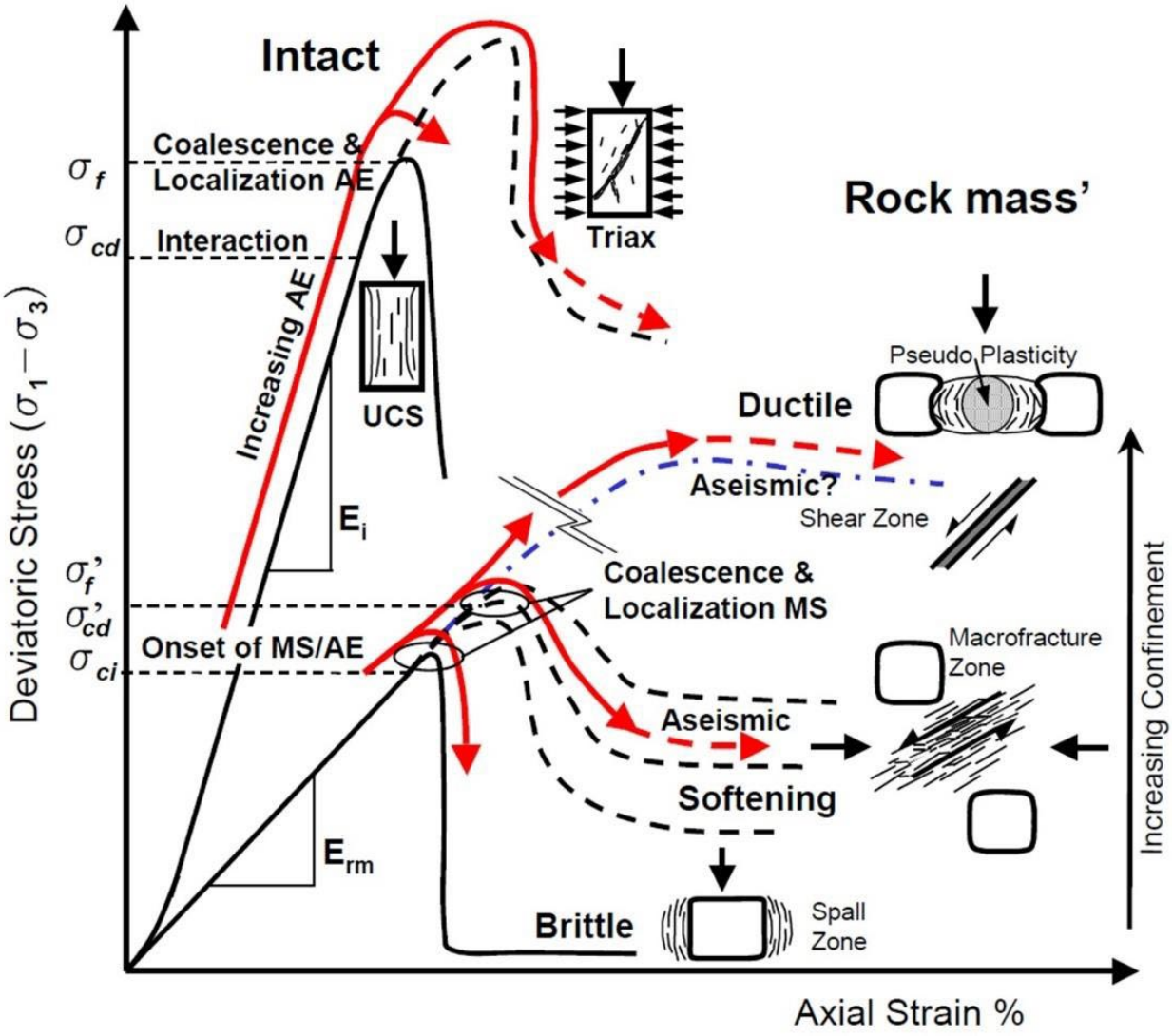

Figure 7 - Hypothetical stress-strain curves for intact rock samples and rock masses in Hemlo, Ontario (Coulson, 2009)

This type of response has been observed in stope-level observations, resulting in a three-region model to describe the zones by Bawden and Mercer (1994), shown in Figure 8 below. The closest region was referred to as the failed zone, analogous to the yielded region discussed in Section 2.1.4.2 above. This region is characterized by low stress, no seismic events, and is thus referred to as the aseismic zone. The second region is described as the zone of active failure,

corresponding to the definition of seismogenic zone (the period post yield point yet prior to a micro-fractured rock mass) in Figure 7 above.

Bawden and Mercer's (1994) model describes spatially the different types of zones around an opening, and goes further to describe potential seismic source parameters which may identify those zones. They go on to note that the hanging wall of the stope (Figure 8a) is in a low stress condition with little or no seismicity. Understanding this low stress/low seismicity area compared to the failed zone will be dependent on understanding the stress path over time.

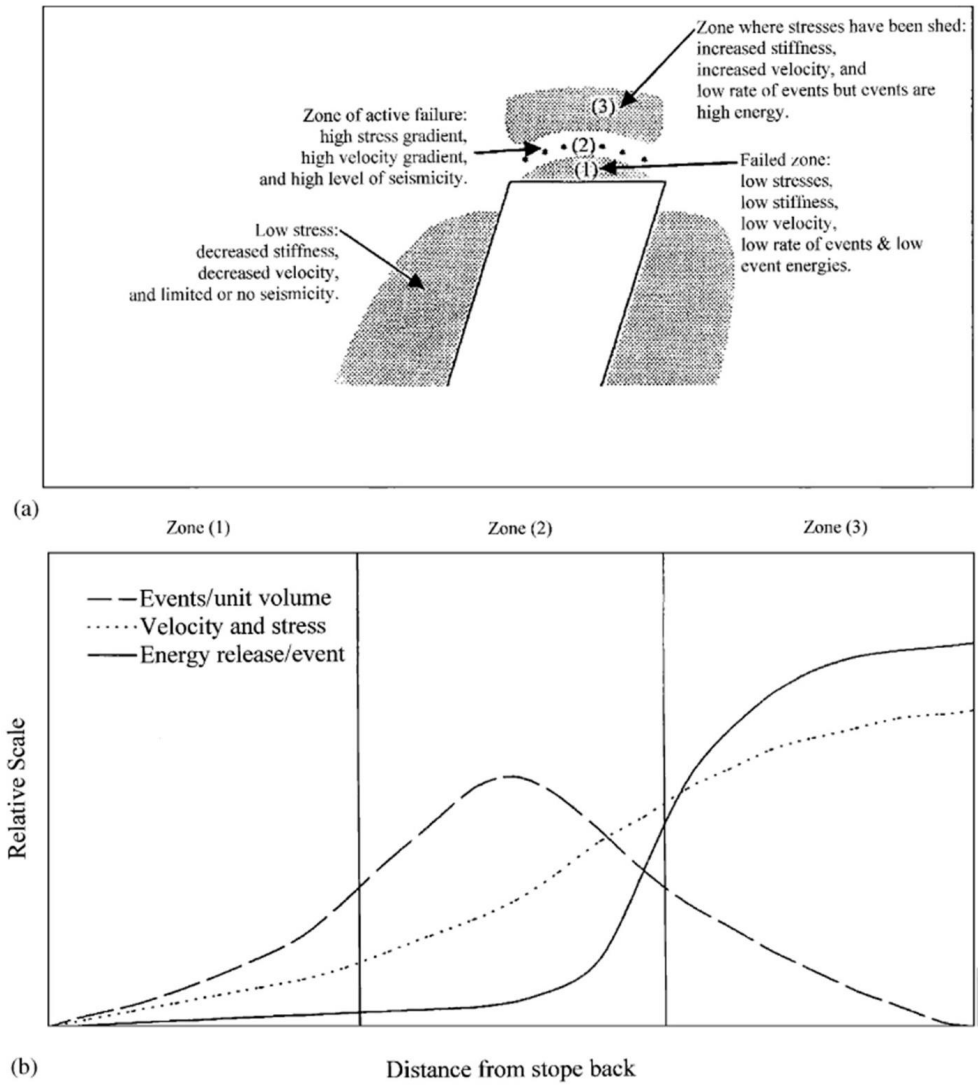

Figure 8 - Conceptual model of spatial variation in seismicity near an open stope (Mercer and Bawden, 2005; after Bawden and Mercer, 1994)

An additional model of the stope-level exhibition of aseismic and seismogenic zones has been suggested by Carusone (2018). Figure 9 below shows the four step process of the proposed redistribution of stresses after blasting of a stylized theoretical stope excavation represented as a black circle. Carusone's work focused on apparent stress. Apparent stress is defined as the seismic energy released for a given seismic deformation. Higher apparent stress implies a relatively high stress condition in the rock mass at the time of rock mass failure. Apparent stress will be discussed further in Section 2.2.5.

Carusone portrayed high and low apparent stress events as red triangles and green circles, respectively. He hypothesized that the four stages were as follows:

1. Creation of a new opening resulting in an increase in stress within minutes of blasting.
2. As the boundaries of the excavation begin to be exposed to stress in the hours after blasting, they begin to yield. This area around the opening is referred to by Carusone as the Excavation Damage Zone (EDZ), portrayed as a dashed circular line. It is not a defined boundary as shown in the schematic, and may be an irregular undulating shape depending on stress or rock mass conditions. The result of the creation of the EDZ in stress being redistributed further out, increasing the stresses in that zone.
3. After step 2, and for up to several days, a slow redistribution of the stress to a more confined rock mass occurs. This once again brings events closer to the stope boundaries.
4. The EDZ moves outwards from the excavation as the rock yields to a point where it can no longer support stresses sufficient to create seismic conditions. This is the creation of the aseismic zone, with an apparent spatial boundary where seismic events begin to occur

– the seismogenic zone. In Carusone's work, this process took up to several weeks to occur around a given stope.

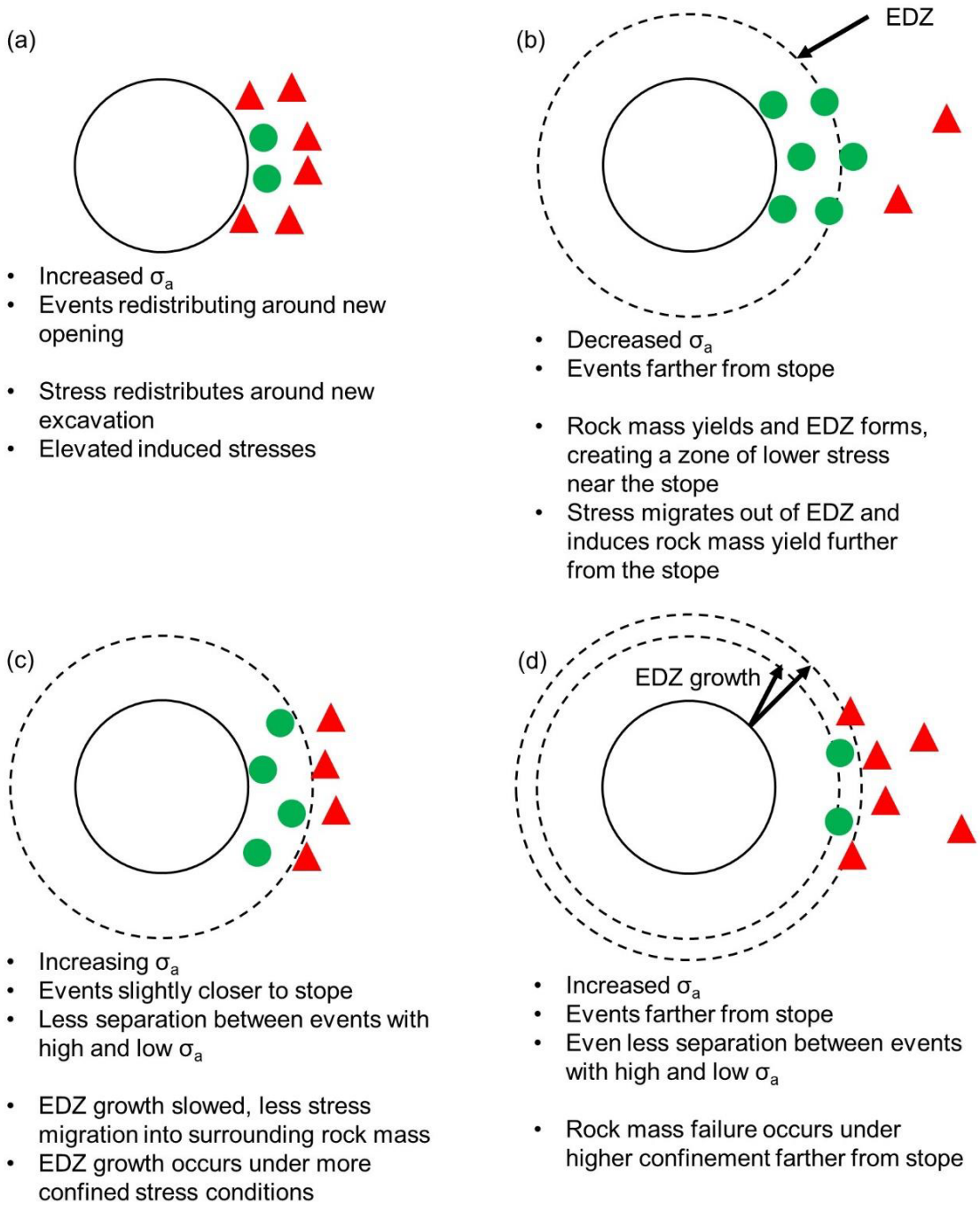

Figure 9 - Schematic of interpreted typical behaviour and inferred rock mass response, focused on apparent stress (σ_a) changes (Carusone, 2018)

Aseismic behaviour can also be exhibited on a larger scale, as was demonstrated by Cotesta *et al*. (2014). Figure 10, as proposed by Cotesta *et al*. (2014), shows on an orebody-level scale, how the plotting of seismic events can spatially indicate where both aseismic and seismogenic zones exist. For this figure, deviatoric stress (the difference between σ_1 and σ_3) was modelled, the results of which were overlain with the seismic event locations. This work postulates that the increases in stress around the mined-out stopes in this orebody have resulted in rock yielding in what is labelled by Cotesta *et al*. as the "Yielded Zone". This modelling corresponds directly to a lack of seismicity in that same area, with the boundaries of this zone being characterized by significant seismicity – resulting in a seismogenic zone.

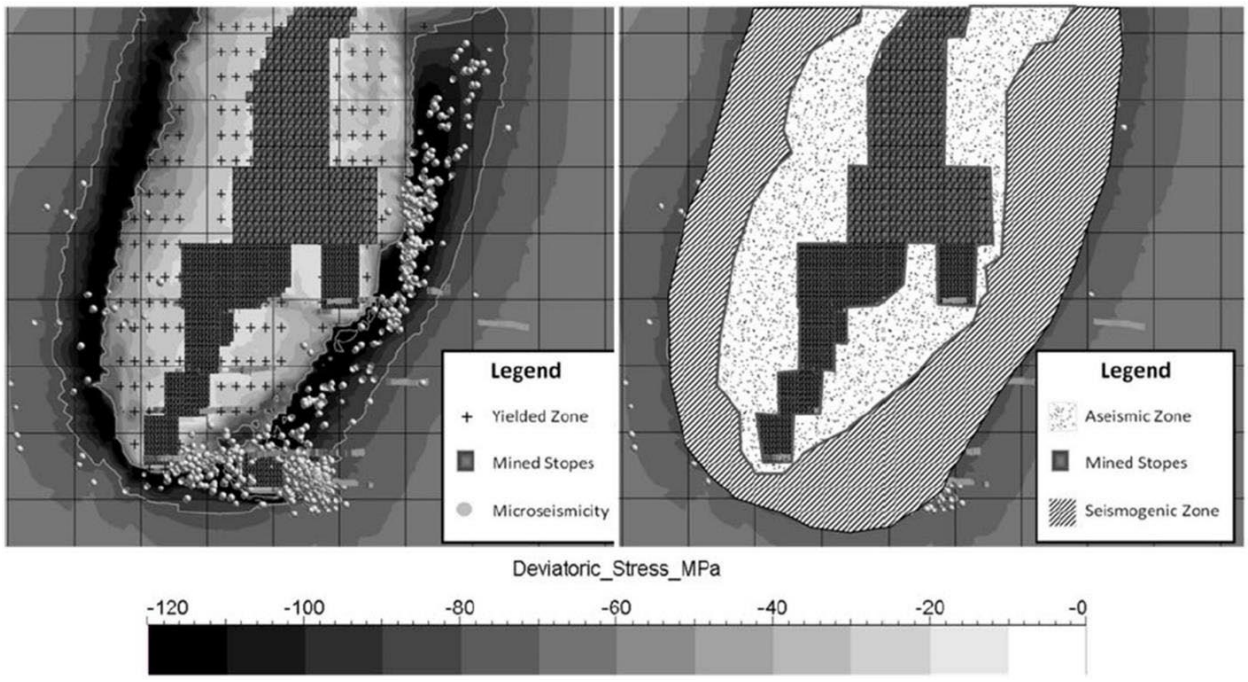

Figure 10 - Contours of deviatoric stress overlain with seismic event locations (left) and interpreted zones of yielded and yielding ground (right) at Creighton Mine, Sudbury, Ontario (Cotesta *et al.*, 2014)

2.1.5 Seismic Source Mechanisms

The seismic source mechanism is the mode of failure of the rock mass that results in seismic energy being released. Gibowicz (1990) states that "two broad types of mine tremors are almost universally observed: (a) those directly connected with mining operations, i.e. those associated with the formation of fractures at stope faces; and (b) those that are not, i.e. those associated with movement on major geological discontinuities." Although this crucial distinction does broadly separate the significant types of seismicity, it does not specifically identify the mechanisms themselves.

Six basic mechanisms were proposed by Hasegawa *et al*. (1989), which can be seen in Figure 11 below.

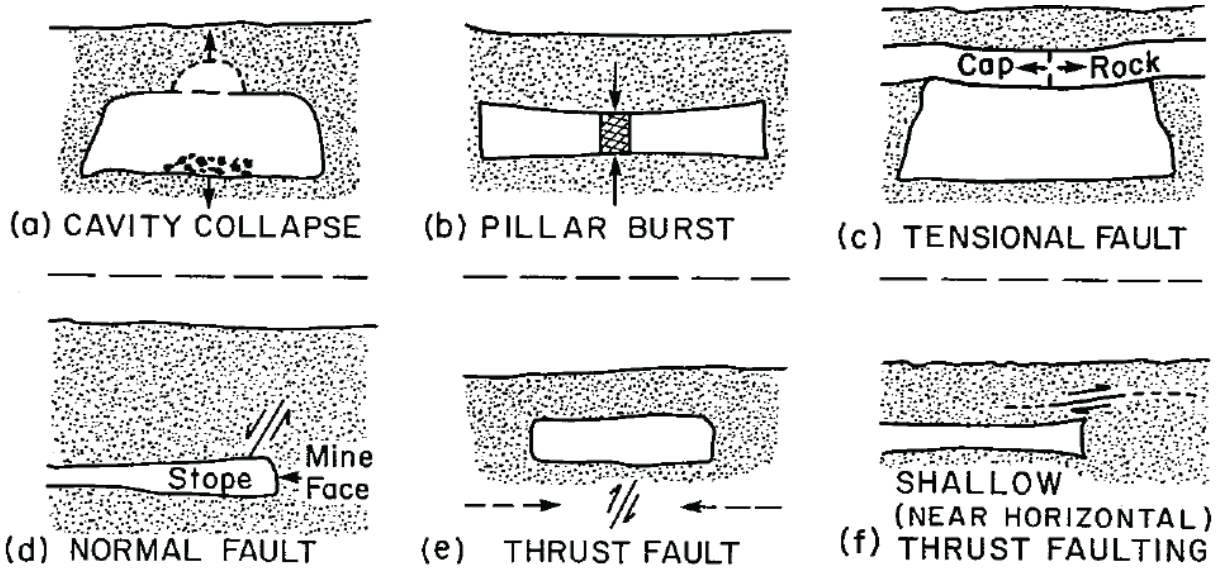

Figure 11 - Six basic mechanisms of tremors related to mining operations in Canadian mines (Hasegawa *et al.*, 1989)

Ortlepp (1992) proposed a more details around six proposed mechanisms related to isolated, rock mass failures on a large-scale, and are listed in Table 1.

Table 1 - Six mechanisms, their seismic event types, and magnitudes (after Ortlepp, 1992)

Seismic Event	Source Mechanism	Magnitude Range (M_L)
Stress-induced fracture	Energy dissipation through the creation of new fractures	-3.0 to -1.0
Strain-bursting	Superficial spalling with violent ejection of fragments	-0.2 to 0
Buckling	Outward expulsion of larger slabs parallel to opening	0 to +1.5
Pillar or face crush	Sudden collapse of stope pillar, or violent expulsion of rock from tunnel face	+1.0 to +2.5
Shear rupture	Violent propagation of shear fracture through intact rock mass	+2.0 to +3.5
Fault-slip	Violent renewed movement on existing fault	+2.5 to +5.0

Some variance in the magnitude ranges have been observed, however they are useful on a relative scale.

A more illustrative example of proposed mechanisms can be seen in Figure 12. Suggested by Hudyma *et al.* (2003), the left side of this illustration shows seismic events occurring at locations where rock mass failure is occurring. The presence of seismic events in these locations produces a seismogenic zone. In the figure, the symbols circle, square, triangle and asterisk represent increasing magnitudes of events that were unquantified in the original work as it was meant to be a hypothetical illustration.

On the right side of Figure 12, the various suggested seismic sources around typical underground mine workings is shown. Although the seismic response is a reflection of the source mechanism

(Brown, 2018), depending on the distance from the opening and the stresses involved there are potentially different mechanisms at each source.

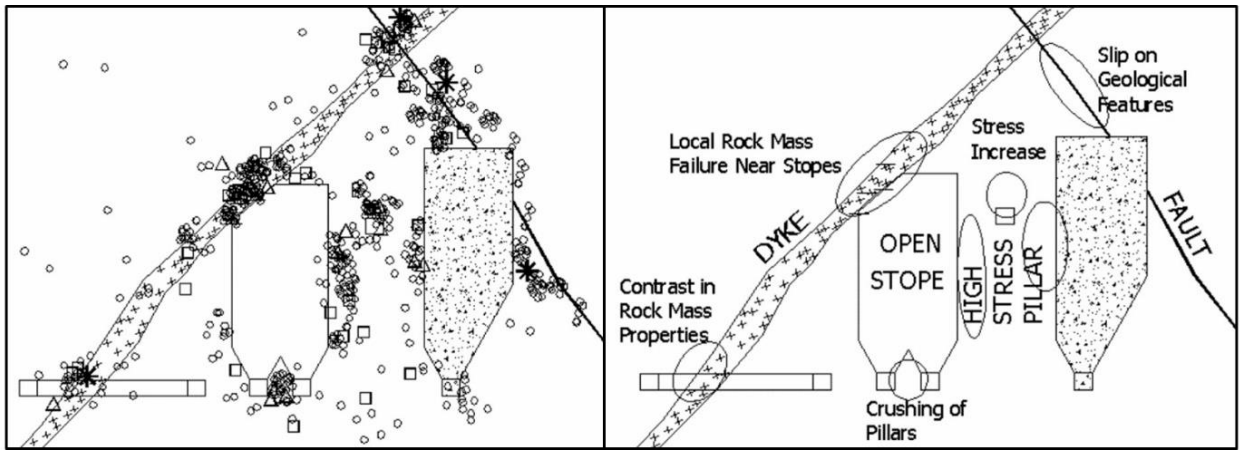

Figure 12 - Hypothetical seismic events in a typical underground mine (left) and seismic sources associated with those events (right) (Hudyma *et al.*, 2003)

2.2 Seismic Monitoring

Modern underground hard rock mines use an array of sensors located throughout the mining environment to detect seismic events occurring in the vicinity of the mine. The data collected from these sensors is digitized and conveyed to a seismic monitoring software system hosted on a computer where seismic source parameters can be both determined and evaluated. A typical layout of the sensors (shown as small cylinders) around the orebody (shown as a shaded "cloud" around mine development workings) can be seen in Figure 13 below. A schematic of the general components can be seen below in Figure 14.

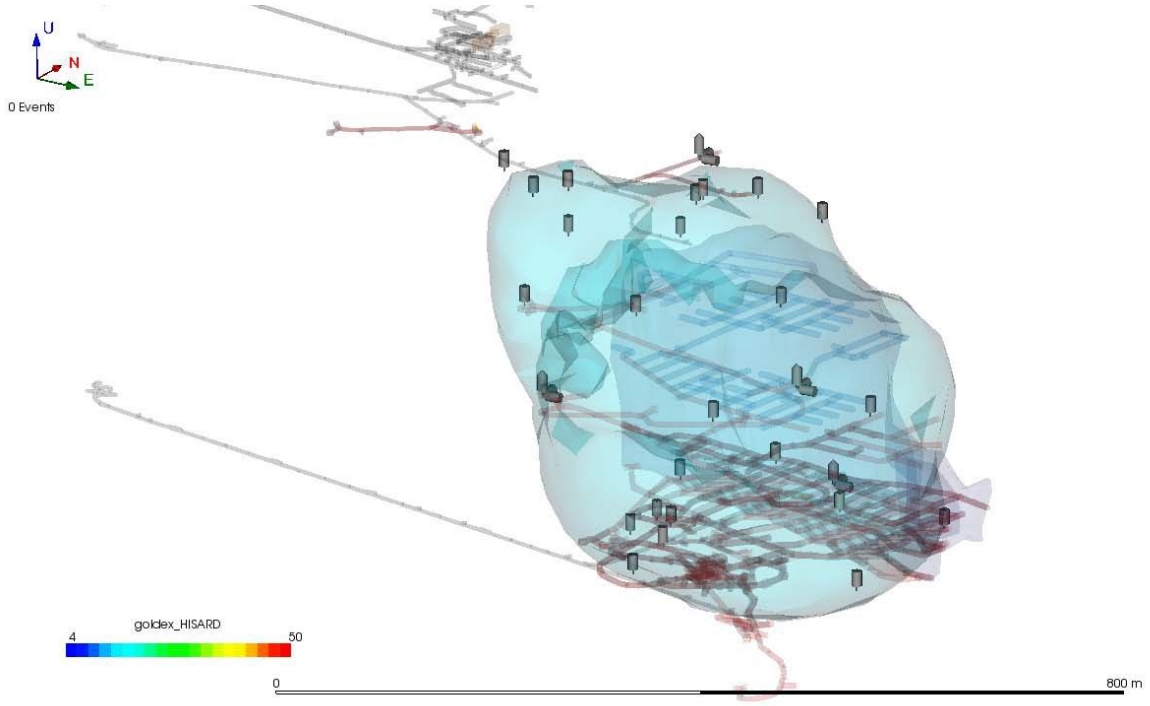

Figure 13 - General microseismic sensor array surrounding an orebody (Hudyma *et al.*, 2010)

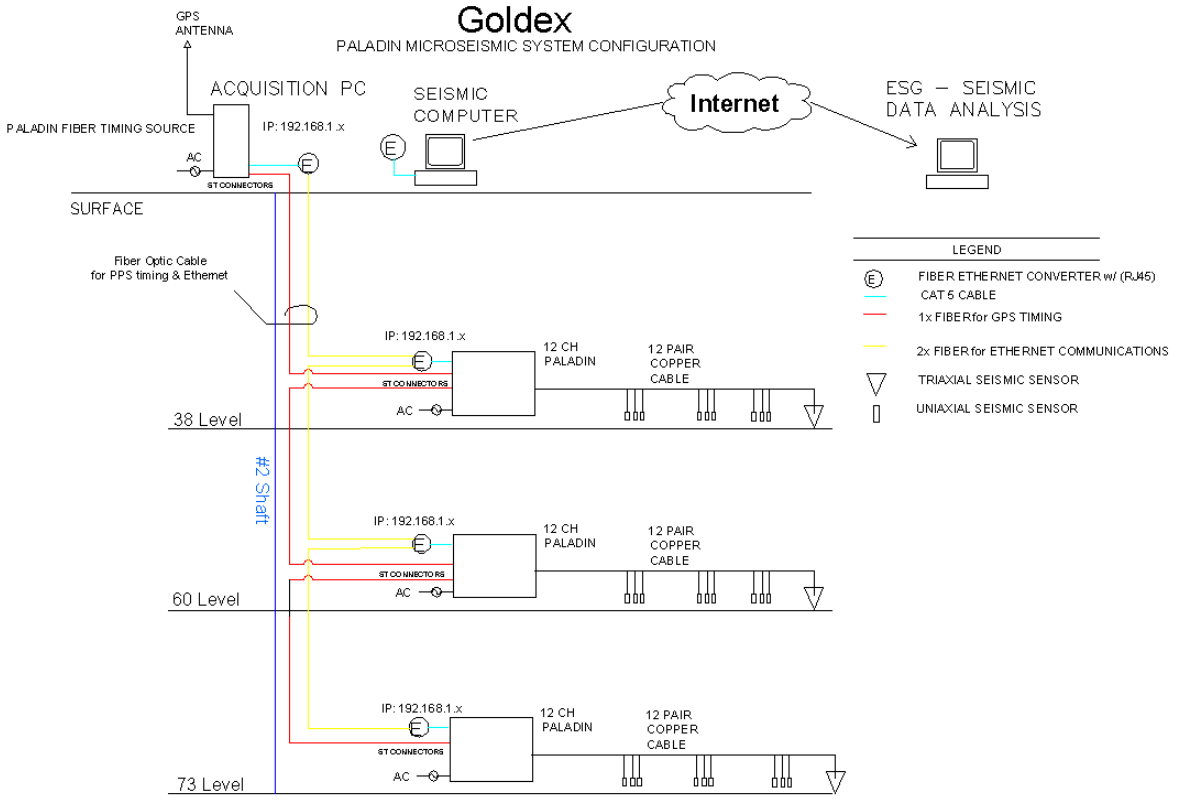

Figure 14 - Typical schematic of underground microseismic monitoring system (Hudyma *et al.*, 2010)

2.2.1 Seismic Sensors

Different types of sensors are used to detect and record different amplitude and frequency ranges of seismic events. In order to capture as much information as possible, a given seismic system will generally use a combination of sensors. In Canada, a combination of piezoelectric accelerometers and geophones are commonly used (Brown and Hudyma, 2018).

Piezoelectric accelerometers are typically used for the detection of high frequency (up to 15,000 Hz), small magnitude events through converting the ground motion pressure to an electrical signal which is then digitized and sent to a computerized system. They function by a piezoelectric crystal being sandwiched between two metal plates. As ground motion compresses or dilates the crystal, charges in the attached metal plates will change. A wire between the plates will produce voltage based on the different charges in the plates. This wire requires a baseline voltage for the accelerometer to function, which results in some background noise on the sensor readings.

Geophones, although many different frequency ranges exist, are typically used for larger, low magnitude seismic event monitoring. Geophones consist of a mass, suspended by a spring, with wire coiled around it. This mass is normally suspended over, inside, or around a magnet. Movement of the mass from ground motion causes the magnet to induce electron movement through the wire coil, creating voltage in the wire. The fluctuations in voltage can be read by the seismic system.

In both piezoelectric accelerometers and geophones, the sensors can be either uniaxial or triaxial configurations. Uniaxial sensors are a single sensor oriented in a given position, which only makes them capable of recording the ground motion in that single axis. This can limit the accuracy of the information received in cases where the uniaxial sensor is not directly aligned

with the oncoming ground motion waves. To reduce uncertainty, large arrays of uniaxial sensors facing in many different directions can be used.

Triaxial sensors include three sensors oriented orthogonally. The combination of three orthogonal sensors allows for a more true reading of the total ground motion experienced at the sensor site. Combining some triaxial sensors with more uniaxial sensors is a common method of balancing data accuracy and equipment cost constraints.

Each sensor can only accurately evaluate a range of motion in which it is designed. Mendecki *et al.* (1999) defined the maximum signal to background noise ratio of seismic sensors as the dynamic range, and argued that the minimum dynamic range should be 120 dB in a mining seismic system. Figure 15 shows the useful frequencies at which typical mine seismic sensors are effective, and why a combination of sensor ranges are preferred (Mendecki *et al*., 1999). The clip limits, the amount of motion at which the sensor capabilities to record are exceeded, shows where a given sensor's data may not be complete with large amplitude ground motion. This potential issue can be resolved through the introduction of far-field sensors, so that clip limits are not exceeded.

The figure also shows that accelerometers have higher clip limits compared to geophones, while geophones have lower noise limits. When background noise matches or exceeds the amplitude of the ground motion, the noise limit has been reached. The lower noise limit of geophones allows them to detect smaller events compared to accelerometers.

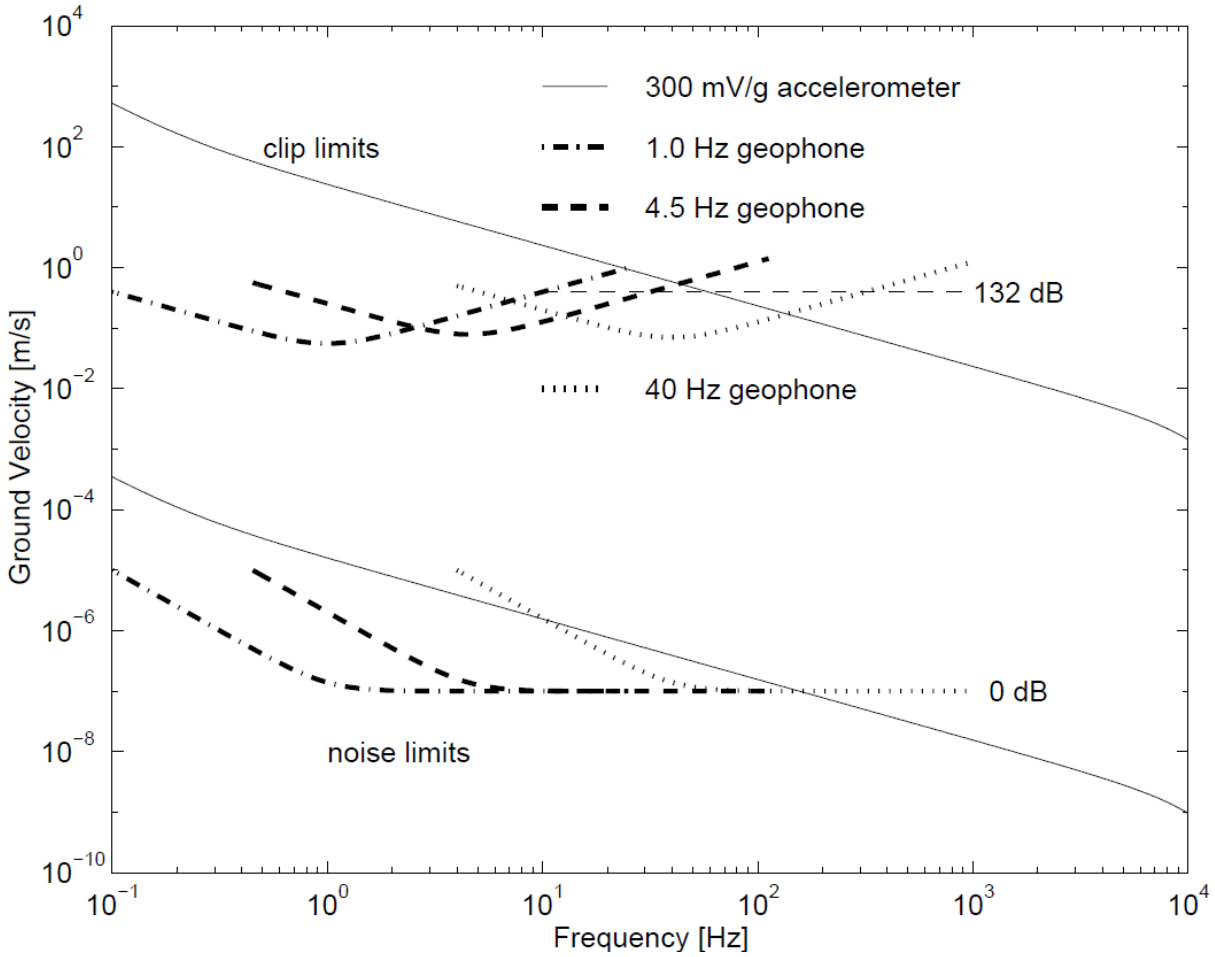

Figure 15 - Dynamic ranges and sensitivities of geophones and accelerometers commonly used in mine seismic systems (Mendecki *et al.*, 1999)

2.2.2 Ground Motion Phases

During a seismic event, four separate waves can be produced. Two of these waves, called the compression wave (p-wave) and the shear wave (s-wave), are typically recorded by seismic systems in mines. The other two waves, named the Love wave and the Rayleigh waves, are waves that travel along the crustal surface. Although these are significant in the context of earthquakes, due to the relatively limited surface areas exposed in underground mining, these last two waves are not considered in the field of mining-induces seismicity, and are not considered in this thesis.

Initially after an event, a smaller, higher frequency p-wave is recorded by a seismic system. This recording is generated by elastic compressions and dilations of the rock in the longitudinal direction of propagation. This wave arrives first, as it typically travels five to seven kilometres per second (Hudyma, 2008).

Shortly thereafter, a larger, lower frequency s-wave is recorded via transverse motion. This wave contains roughly 10 or more times the energy of the p-wave and travels three to four kilometres per second (Hudyma, 2008). Figure 16 shows a typical example of a seismic system recording a p-wave and an s-wave.

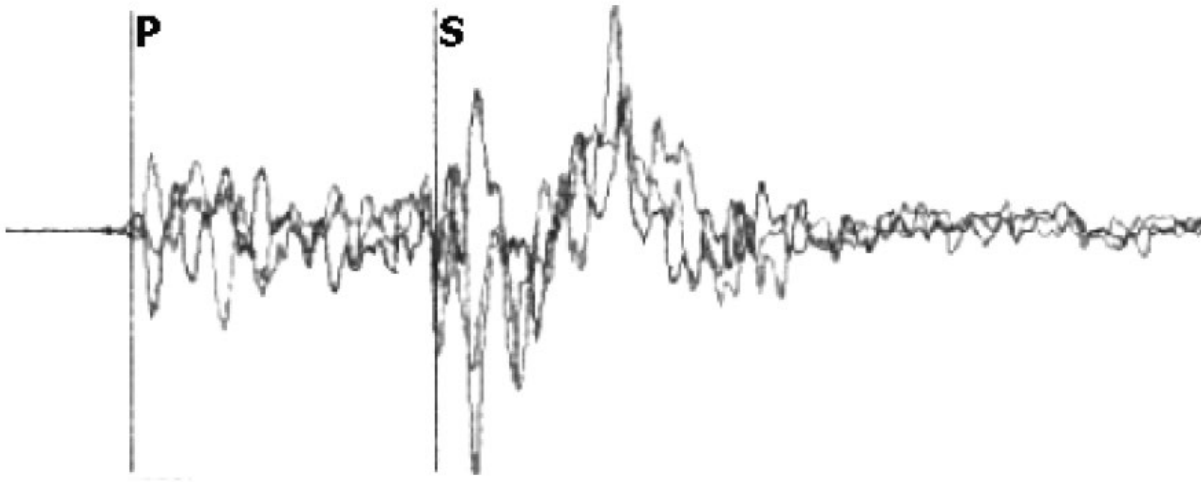

Figure 16 - Typical waveform example of a seismic event recorded by a seismic monitoring system in an underground mine with both p-wave and s-wave are identified (Hudyma, 2008)

2.2.3 Seismic Source Parameters

Seismic source parameters are the detectable parameters from the seismic event which can be recorded and analysed by a seismic system. Originally, Mendecki *et al.*(1999) proposed that to provide a meaningful description of a seismic event that time, location, and two additional source

parameters would be required. Three such additional source parameters have been established, creating a list of five primary source parameters:

- Time
- Location
- Radiated Seismic Energy
- Seismic Moment
- Source size

Although these are the only five independent source parameters, a significant number of other secondary parameters have been derived from these parameters. The independent source parameters relevant to this thesis are described below.

2.2.3.1 Time

Based on the relative times that a series of sensors received their first motions from a seismic event, with the inclusion of the location, the absolute time of the occurrence can be determined with good accuracy (Gibowicz and Kijko, 1994). Time of occurrence of an event is commonly compared to the time of other events, as well as causal factors.

Time can be used to:

- Observe the interval between seismic events and mine blasts,
- Observe the interval between seismic events themselves, and
- Identify potential seismic source mechanisms.

2.2.3.2 Location

A seismic system can determine location of a seismic event through the use of sonic velocities of the p-waves and s-waves of a seismic event. A well oriented mine-wide seismic sensor array can use the relative times at which various sensors have been triggered by a given event to estimate the likely source location of a seismic event. Location techniques may suffer in accuracy in cases where: seismic velocities vary (primarily through geological inconsistencies); where voids occur between the sensor and the event (such as a mined out stope); or where reflection of waves take place off of underground surfaces.

In mine seismology, there are two important ground motion phases – a compressional wave (also called a p-wave), and a shear wave (also called an s-wave). The compressional wave will arrive prior to the shear wave. Evaluation of the relative time between the two waves, when a sonic seismic velocity model is in place, can be used to determine the distance from a given sensor to the source location.

2.2.3.3 Radiated Seismic Energy

Seismic energy is a good indicator of event strength (Gibowicz and Kijko, 1994), and can be defined as the total elastic energy radiated from a seismic source. This includes the sum total of both compressional and shear waves, and can be represented by the following formula (Gibowicz and Kijko, 1994):

$$E = 4\pi\rho c R^2 \frac{J_C}{F c^2}$$

Where,

E = Radiated Energy (Joules)
ρ = Rock Density (kg/m^3)
c = Velocity of the Wave in Rock (m/s)

R = Distance from the Seismic Source (m)
J_c = Integral of the Square of the Ground Velocity
Fc = Empirical Radiation Pattern Coefficient

The ratio of energy of compressional to shear waves is a derived parameter from seismic energy, and has been related to seismic event source mechanism. This will be discussed in further detail in Section 0 below.

2.2.3.4 Seismic Moment

Seismic moment is an independent means of estimating the strength of the seismic source, and is often discussed in terms of size for seismic events with a slip mechanism. It is represented by the following formula (Gibowicz and Kijko, 1994):

$$Mo = 4\pi\rho c^3 R \frac{\Omega_o}{Fc}$$

Where,

Mo = Seismic Moment (Nm)
P= Rock Density (kg/m^3)
c = Velocity of the Wave in Rock (m/s)
R = Distance from the Seismic Source (m)
Ωo = Low Frequency Plateau of the Frequency Spectrum of a Seismic Waveform
Fc = Empirical Radiation Pattern Coefficient

The Ωo parameter requires additional introduction. A chart called a waveform frequency spectrum can, through a Fourier transform, determine the value of Ωo. This plateau is a level of spectral density (mm·s) where long period of displacement of the waveform occurs, and ends with a high frequency decay. The decay point was described by Mendecki (2013) as the corner

frequency (f_o). An example of a waveform frequency spectrum (Hedley 1992), with a labelled Ωo, can be seen in Figure 17.

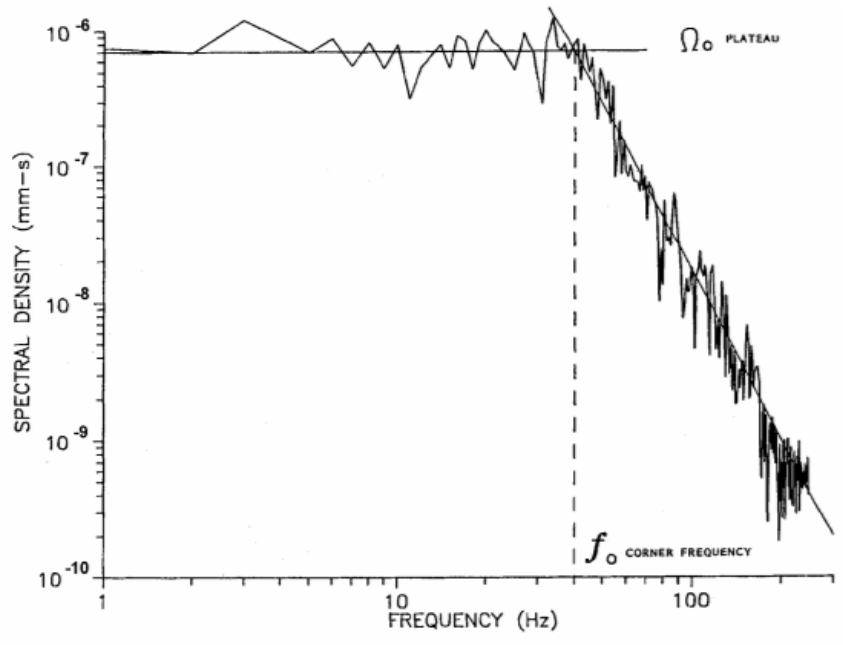

Figure 17 - Waveform frequency spectrum chart (Hedley 1992)

2.2.3.4.1 Moment Magnitude

Using spectral domain parameters, Hanks and Kanamori (1979) proposed the following equation to calculate the moment magnitude of a seismic event:

$$M_W = \frac{2}{3} \cdot logMo - 6.0$$

Where,

M_W = Moment Magnitude
Mo = Seismic Moment (Nm)

This scale has gained popularity as a measure of strength of earthquakes, especially those above a Richter 7.0, which would not be appropriately represented by the Richter magnitude scale.

Inclusion of the rock density, seismic velocity, and the amount of movement of rock allows for values to be compared across dissimilar conditions.

2.2.3.4.2 Energy Moment Relation

The relation between energy and moment can be graphed using a logarithmic scale to visually represent the relation between them. From van Aswegen and Mendecki (1999), the scaling relation is:

$$\log E = c + d \log Mo$$

Where,

E = Seismic energy (Joules)
c = Vertical axis intercept
d = Slope of line
Mo = Seismic moment (Nm)

An example of an energy-moment graph is shown in Figure 18, which shows that higher energy events correlate with higher moment events. The amount of energy is typically within two orders of magnitude of a given seismic moment (van Aswegen and Butler, 1993). There is also a correlation between variability in rock mass properties and variability in the energy-moment relation (Mendecki, 1993).

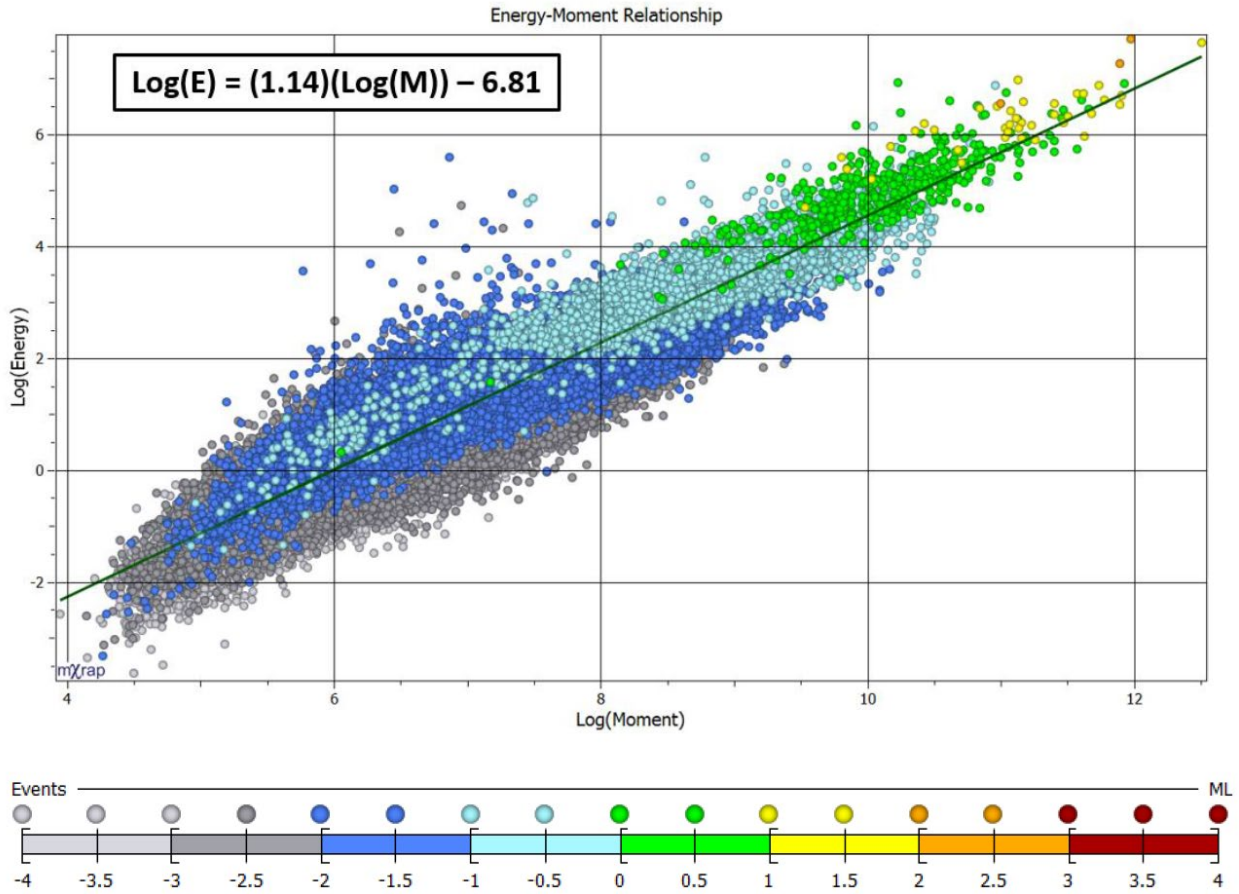

Figure 18 - Energy moment relation for a large population of seismic events (Brown, 2015)

2.2.3.5 Source Size

Source size is an assumed circular shaped approximate dimension of failure surface of a seismic event. It is represented as either a source radius or source diameter, model dependent, and inversely proportional to the corner frequency. Gibowicz and Kijko (1994) calculated source radius using the following formula:

$$r_0 = \frac{K_c \beta_0}{2\pi f_0}$$

Where,

r_0 = Source Size (m)

K_c = Source Model Constant (Hz)

β_0 = S-Wave Velocity in the Source Area (m/s)

f_0 = Corner Frequency (see Figure 17)

2.2.4 Other Magnitude Scales

Event magnitude is not an independent source parameter, however it is often strongly related to radiated seismic energy. Due to its frequent use in describing the size of seismic events, it has been included as a secondary source parameter.

Magnitude is an attempt to measure in a single value the intensity or strength of a given seismic event. Various magnitude scales have been proposed to represent the seismic response. Duplancic (2001), described magnitude scales as being generally based on amplitudes with either time domain parameters (such as with Richter and Nuttli scales) or use of spectral parameters (the use of Fourier transformation of seismic waveform from time domain into frequency domain for the determination of low frequency far-field displacement).

Three typical magnitude scales relevant to this thesis and their conventional uses are:

- Richter magnitude – a measure of the strength of an earthquake intensity based on crustal conditions within the Southern California region of the United States of America (Richter, 1935).
- Nuttli magnitude – a measure of the strength of an earthquake or large seismic events based on crustal conditions in Central and Eastern North America (Nuttli, 1973). This is the primary scale used by Earthquakes Canada to assess event strength in Eastern Canada.
- Moment magnitude – a measure of the size of a seismic event based on the measured seismic moment from a local seismic system (Hanks and Kanamori, 1979).

Despite being considered a poorer scale for describing the size of a seismic event (Gibowicz and Kijko, 1994; Mendecki, 1993), most mines have calibrated their local magnitude scale using their seismic system date to approximate Richter magnitude (Hudyma, 2008). However, application of moment magnitude is increasing. In this thesis, moment magnitude for the mine in question has been used as the magnitude scale.

2.2.5 Apparent Stress

Apparent stress is a model independent quantification of a seismic source's stress change. Although not a direct measure of the change, it is proportional to the change (Madariaga, 1976). Apparent stress was initially defined by Wyss and Brune (1968) as:

$$\sigma_a = \mu \frac{E}{M_0}$$

Where,

σ_a = Apparent Stress (Pa)
μ = Shear modulus of the rock mass (Pa)
E = Seismic energy (J)
M_0 = Moment (Nm)

Mendecki (1993) suggested that apparent stress is a practical indication of local stress conditions, a suggestion further supported by Simser *et al*. (2003) that high apparent stress events indicate a higher release of seismic energy.

2.3 Seismic Analysis Techniques

Over time, a significant number of techniques have been used to perform various analyses of collected seismic data. This section will discuss the relevant techniques used within this thesis work.

2.3.1 Gutenberg-Richter Frequency-Magnitude Relation

The Gutenberg-Richter Frequency-Magnitude Relation (Gutenberg and Richter, 1944), often referred to as a F-M Relation, is a chart which uses large quantities of seismic data over time, spatial location, or both, to assist in determining long term hazard. Due to the generally self-similar behaviour nature of seismic events, the events often follow or at least approximate a power law. Given that, the slope of the F-M Relation line (b) should be close to one if enough data and time is included.

Various magnitude scales can be used to plot the Gutenberg-Richter Frequency-Magnitude Relation chart. Varying the magnitude used can often show which magnitude scale might be more appropriate for a given selection of seismic data.

The F-M Relation can also indicate the maximum sensitivity of the seismic system around the population of events, as well as an estimate of what the maximum expected magnitude event might be in a given population.

Finally, the F-M Relation can assist in performing a data quality test. When the slope of the line is not linear, specifically when there are an abundance of significant or larger events, this can indicate that mine blasts may be included in the seismic record.

Some information about source mechanism can also be obtained from the slope of the line, once the data quality is better understood. The slope of the line decreases as stress increases (Gibowicz and Kijko, 1994). A steeper b-value (>1.0) would indicate a more likely stress-fracturing response in the dataset, whereas a shallower b-value (<1.0) would indicate a fault-slip mechanism (Hudyma, 2008).

A contrasting two datasets, comparing a flatter sloped fault related dataset to a steeper slope stress-fracturing dataset, can be seen below in Figure 19.

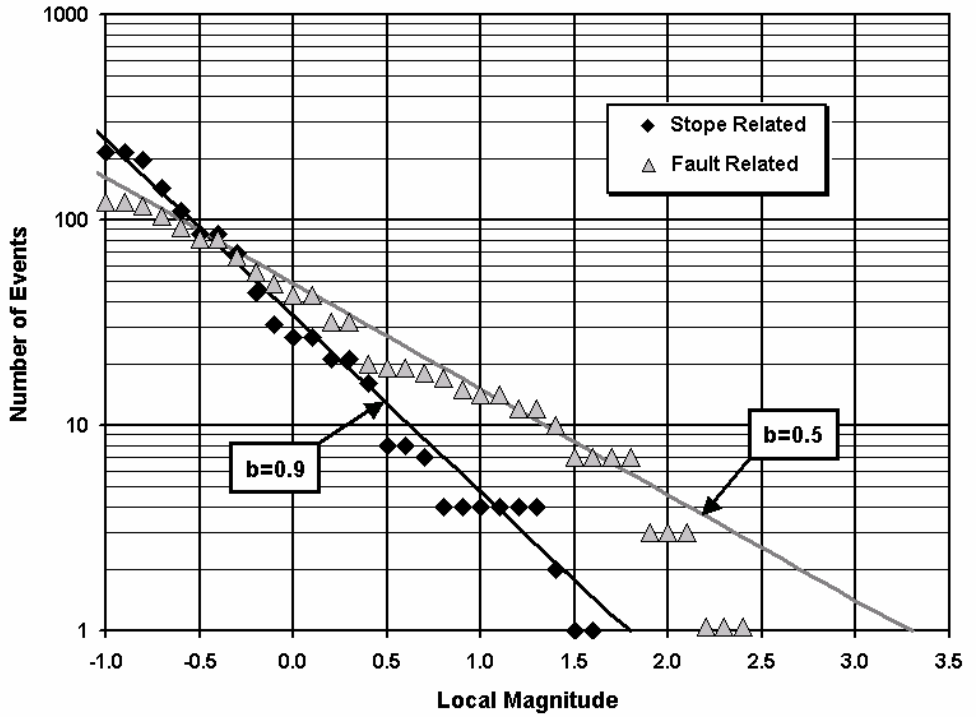

Figure 19 - Gutenberg-Richter frequency-magnitude relations for two contrasting data populations (Hudyma, 2008)

2.3.2 Magnitude-Time History

A Magnitude Time History (MTH) chart is a method of displaying time, local magnitude, and cumulative magnitude on an individual chart (Hudyma, 2008). This allows for observation of seismic response, though the magnitude variance over time. It will show the largest events, all significant events, the rate of events at any given point in time, and the timing of events in relation to mine blasting (Figure 20).

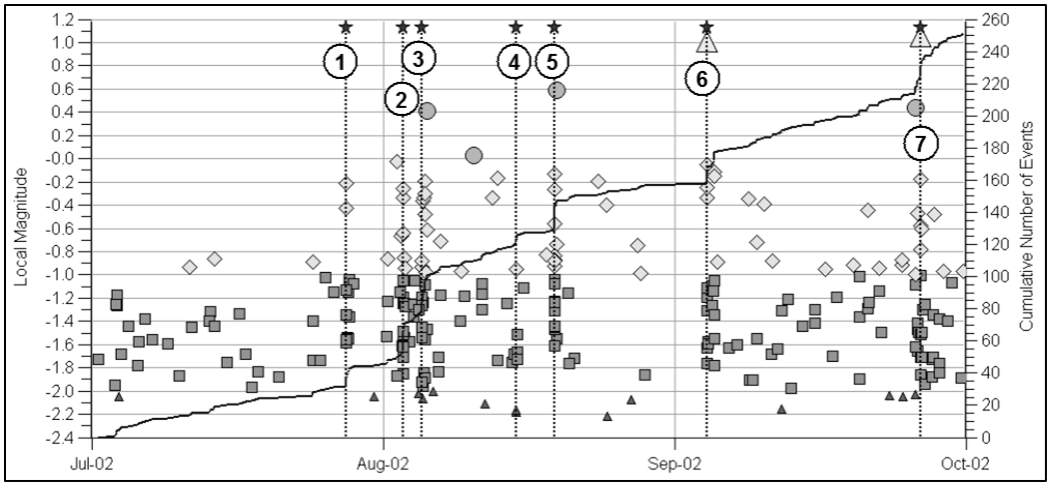

Figure 20 - Magnitude Time History chart showing rates and potential mechanism (Hudyma 2008). Triangles, circles, diamonds, squares and triangles represent decreasing magnitudes in units of 1.0 local magnitudes.

The chart above shows a series of vertical lines, which represent individual blasts taken during this time period. It can be observed that the cumulative number of events line makes significant jumps during these blasts times, indicating a stress-driven response. Between these periods, relatively constant rates of events are observed, with at least one significant event apparently unrelated to blasting. This may indicate a more fault-slip response.

The MTH chart can also function as a data quality test, through observations of the data. An absence of data at any point can suggest either an issue in collection of the data, or an abnormal event that had delayed production. The chart can also show the minimum and maximum sensitivities of the seismic system.

2.3.3 S-Wave to P-Wave Energy Ratio (Es:Ep)

Es:Ep is the ratio of the shear wave energy to the compressional wave energy. It can be used as an indicator of mechanism. When the ratio is low (typically below three), the typical mechanism is stress driven crushing events. Whereas, when the ratio is high (typically above 10), the typical mechanism of the event is often shear, such as along a structure.

This ratio is often presented as a cumulative distribution. Similar to the F-M Relation discussed above, rules of thumb have been applied to the Es:Ep ratio can be a proxy for the mechanism of an event. Generally speaking, an Es:Ep ratio with a value of less than three is indicative of stress-fracturing events (Urbancic *et al.*, 1992) and a value greater than 10 suggests shear events (Boatwright and Fletcher, 1984; Gibowicz and Kijko, 1994; Simser 2006). An example of a typical Es:Ep chart is shown below.

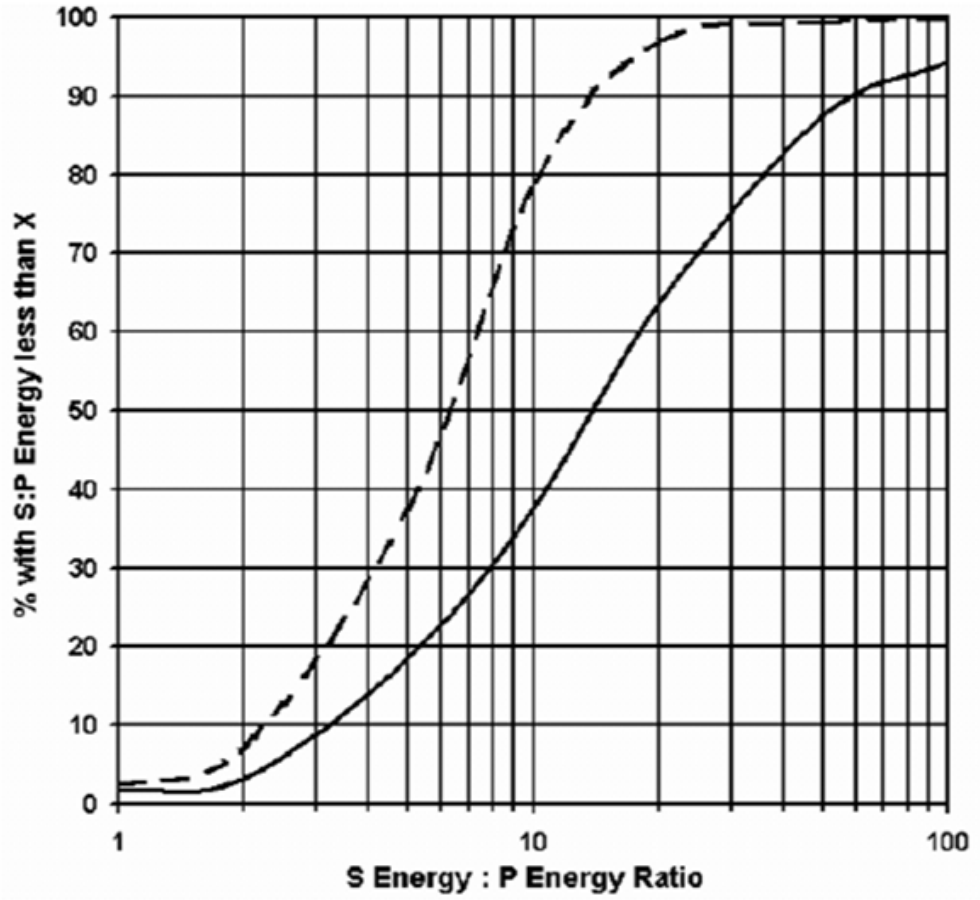

Figure 21 - Typical Es:Ep Ratio chart showing the cumulative ratio in a selected group (solid line) contrasted against the total population (dotted line) (Hudyma, 2008)

An additional relation between high Es:Ep and mining-induced large moment magnitude events has been identified by McGarr (1984) and Gibowicz and Kijko (1994), further supporting the concept that the value can assist in determining mechanism.

2.3.4 Seismic Source Mechanism Evaluation

Typically, two different methods are used to determine the source mechanism of seismic events: waveform techniques and inferred techniques. As described by Hudyma (2008), waveform techniques analyze the waveforms recorded at seismic monitoring stations for a specific seismic event. First motion analysis and seismic moment tensor inversion were discussed by Hudyma (2008). A particular weakness of this analysis method is its reliance on high quality digital data from triaxial sensors providing full coverage of the seismically active areas.

Inferred techniques can be more easily used in a wider variety of typical underground conditions and seismic systems, as they can integrate knowledge of both geometry and geology with data collected by the system. This spatial component is often useful from an operational point of view. For example, if the ratio of S-wave to P-wave energy is recorded as being very high, the event magnitude is high, with the seismic system spatially plotting the specific event in a known geological feature, it can be inferred that this particular event is more likely to be a shear/slip mechanism.

2.4 Literature Review: Summary

Seismic events, particularly those of larger magnitude, can pose significant hazards to operating mines. Seismic monitoring tools exist to inform the operators of where, when and by what mechanism past events have occurred. Meaningful trends in the seismic source parameters can

also be evaluated. Using analysis techniques described, those evaluations can also assist in future forecasting of seismic events.

Chapter 3

3 Goldex Mine

Goldex mine is an underground gold mine owned by Agnico Eagle Mines Limited, located in Dubuisson Township, Quebec, near Val d'Or. It is a large, low grade gold orebody hosted by a steeply dipping granodiorite or quartz-diorite. It contains over 1.1 million ounces of gold in proven and probable reserves, and is currently increasing production from 127,000 ounces of gold annually to 140,000 by the end of 2020 (Agnico Eagle Mines Limited, 2021).

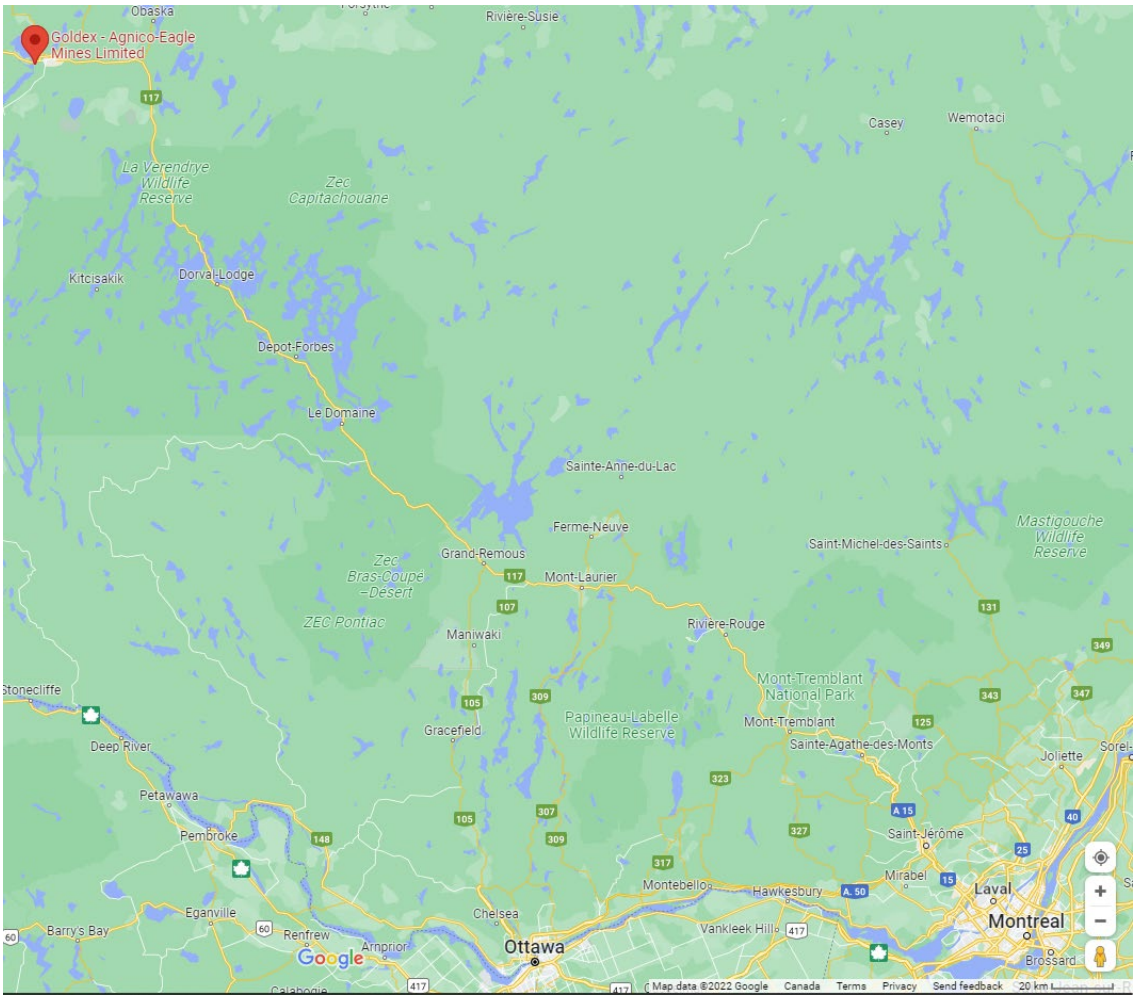

Figure 22 - Partial map of Quebec, Canada with Goldex mine identified by a red marker (Google Maps, 2022)

3.1 Mine Design

3.1.1 Mining Method

Goldex employs a longhole open stoping bulk mining method in the Deep 1, or D1 Zone, with delayed cemented paste backfill (Figure 23). This method was selected to effectively mine the thick orebody while enabling multiple mining horizons. Multiple mining horizons are useful in both scheduling and maintaining the required production targets of ~350 ounces of gold per day ramping up to almost 400 ounces per day. The use of backfill is important in both productivity (by allowing mining right up to previously mined areas) and strategically managing geomechanical hazards related to stress and seismicity (through supporting adjacent ground).

Due to the proximity of the mine to the town of Val d'Or, considerable efforts at the mine design level are made to reduce production-related blast vibration to an absolute minimum pounds per delay.

3.1.2 Mining Layout and Sequence

In order to facilitate production from various areas of the mine, primary mining horizons and various levels and distances from one another were established and mining sequences progressed vertically upwards from these primary horizons until they mined up underneath another primary horizon.

With respect to the D1-Zone at Goldex, the 120 level was established as the primary mining horizon, mining upwards towards 115, 110, 105, 100, 95, and finally 90. Over the time period of data gathered for this thesis, mining largely occurred on 120, 115, and 110 levels, with a small amount of mining done on the 105, 100 and 95 horizons. Figure 23, below, shows a visual of

these levels in a longitudinal projection of the mine. With respect to this thesis, the D1 Zone is the area of ore extraction in which the seismic response over time is being evaluated.

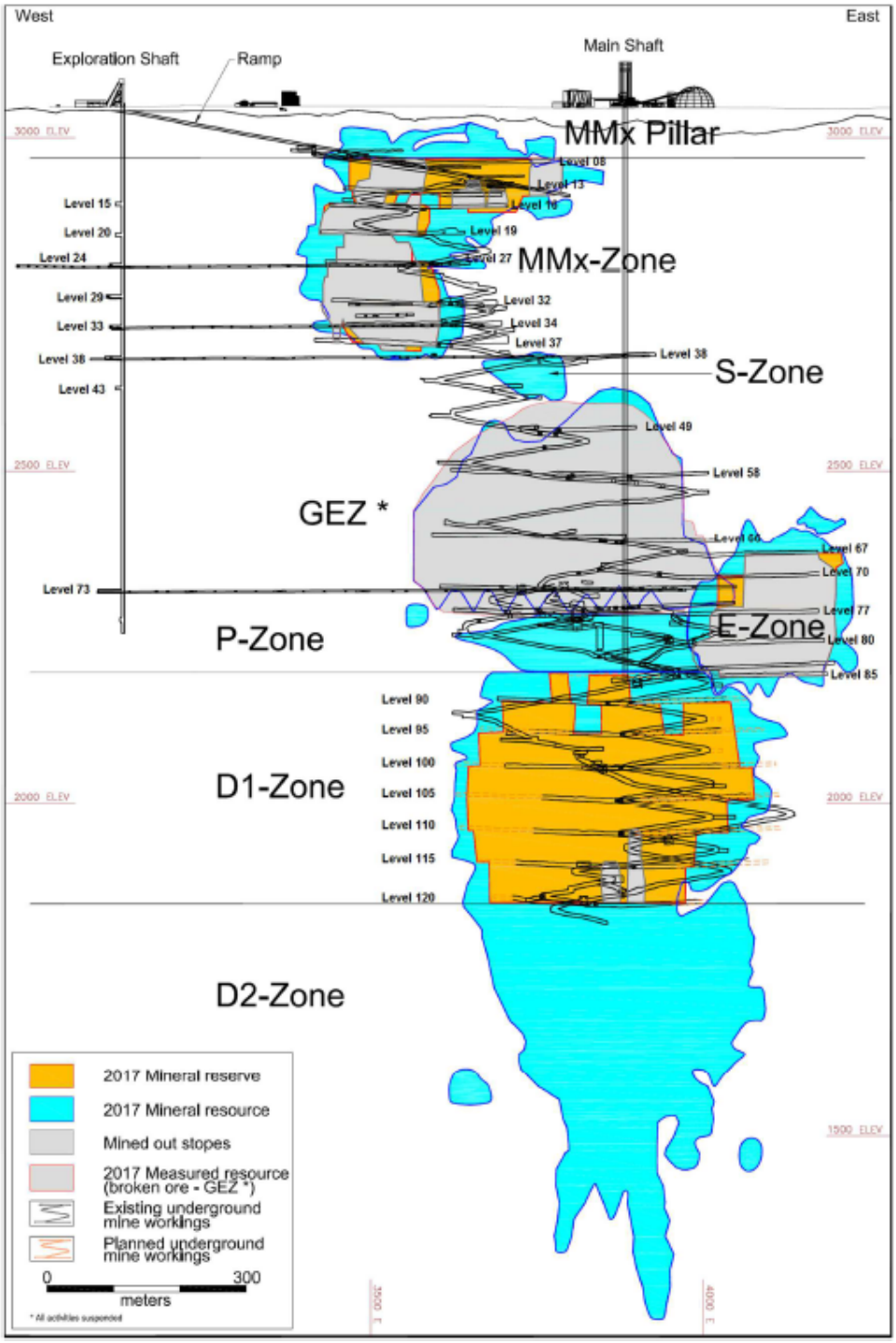

Figure 23 - Long section of Goldex Mine showing D1-Zone extraction (Doucet, 2018)

On each level, the general sequence was primary-secondary mining, from the hanging wall (North side of the orebody) to the footwall (South side of the orebody). This style of mining comprises of mining a stope, a block of ore with an approximate width of 25m and varying lengths from 20-30m depending on the geological information in the block. Stope height is dictated by level height, which is nominally 50m. Extraction on each level begins in the middle of the orebody at the northernmost extent, then after filling it with backfill, removal of the next southernmost stope with similar dimensions.

Each width of ore removed is referred to as a panel. Although the West-East extents of the ore varies from level to level, the panels involved in the D-Zone generally range from 120 (the westernmost panel) to 136 (easternmost panel).

Once the primary panel has been mined a distance towards the footwall determined by engineering through design and observation of the rock mass responses, then two panels away (East, West or both depending on production needs) can begin mining at the hanging wall similar to the lead panel. These panels too are referred to as primary panels. The adjacent panel on both the east and west side of the lead panel is left behind, until such time as the primary panels have been advanced enough on both sides that engineering determines the secondary panels can be extracted.

Figure 24 shows a typical level with five primary stopes removed from the level and filled with cemented backfill. The numbers on the figure indicate the order in which those stopes had their ore extracted.

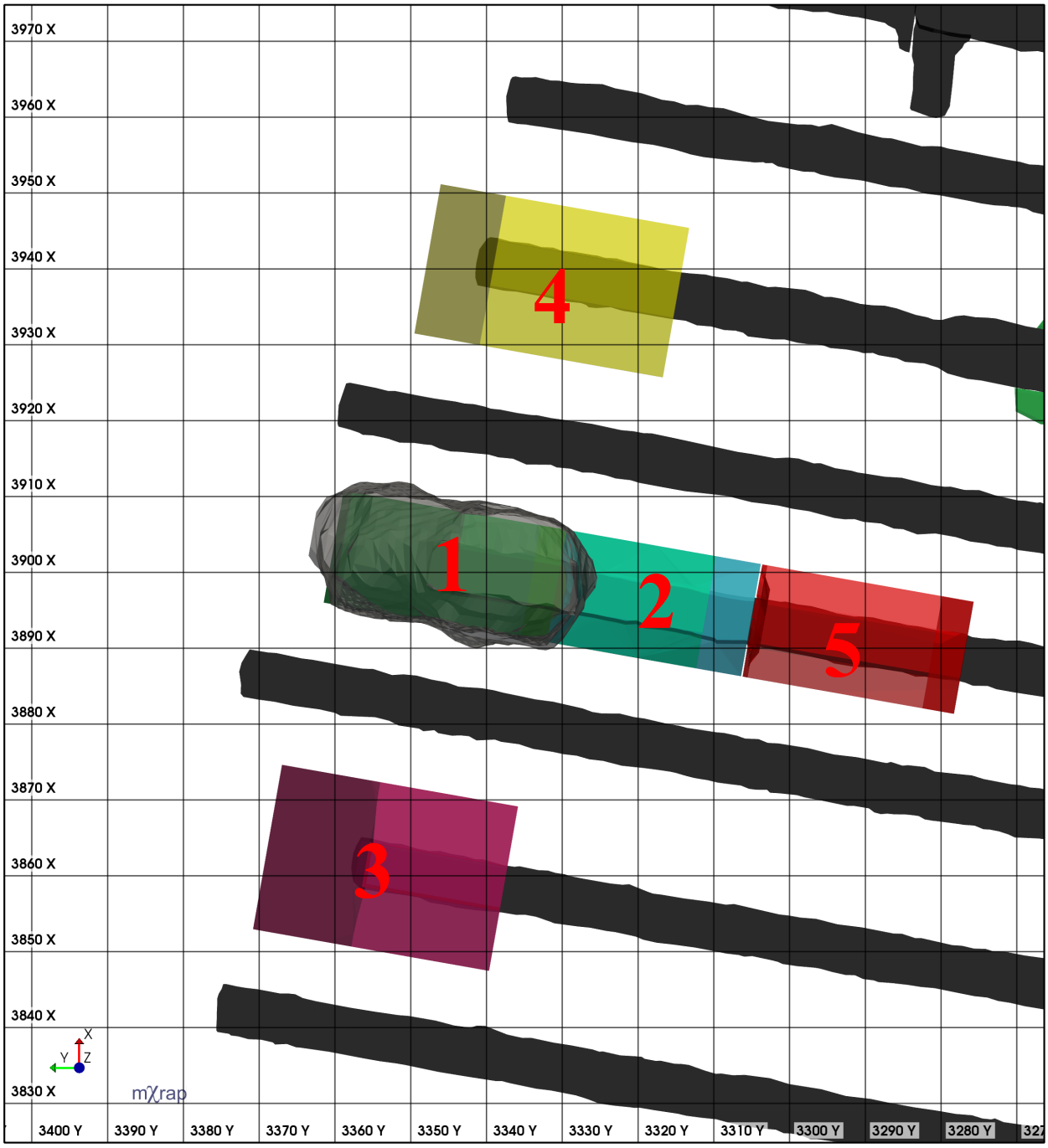

Figure 24 - Typical primary stope extraction in preparation of secondary extraction

Figure 25 shows a much later extraction of the same typical geometry. In this case, all grey stopes have been mined and backfilled prior, with the numbers on the coloured stopes indicating

the order in which those stopes had their ore extracted. Stopes numbered 3, 4, 6, and 7 are the first stopes taken out of the secondary panels.

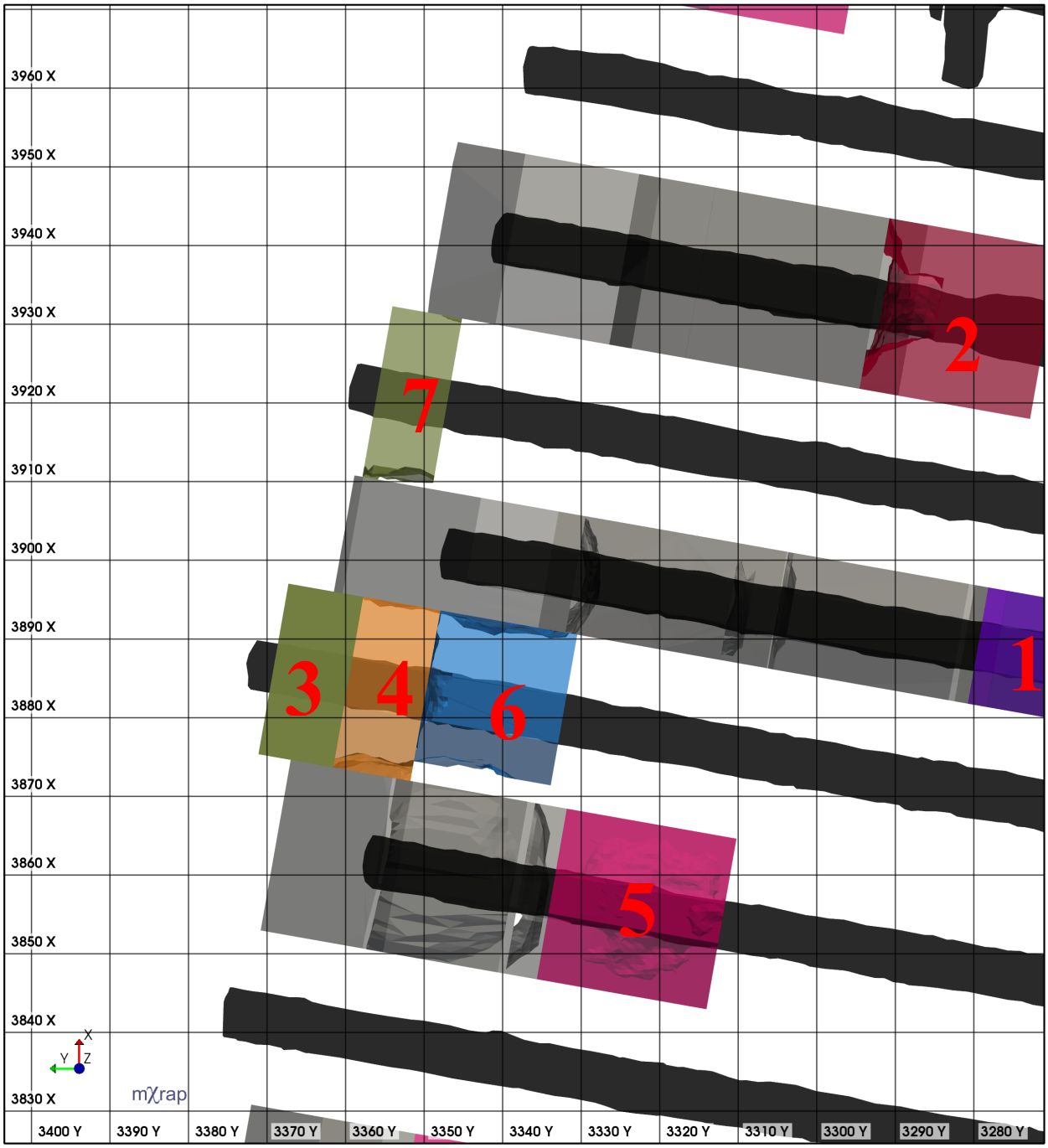

Figure 25 - Typical mid-stage primary-secondary stope extraction

The intent of this primary-secondary panel mining is twofold – increase in production of primary stopes as backfill is not immediately required in one panel to mine another primary panel on the same level; and the reduction of seismic risk by concentrating stresses re-distributed after mining the primaries into the secondary panels, with the intent of them yielding over time and not producing high-risk seismic events.

The theory progresses that through exposure of the secondary panels on both sides to openings, unless the rock itself is both very strong and massive, there is limited opportunity for the remaining secondary pillars to accumulate stress. Accumulation of stress can lead to higher risk seismic events, whereas slow failure over time sheds the stress to other locations.

The design dimensions of both primary and secondary stopes are critical to ensuring that stresses do not accumulate, and geotechnical design combined with empirical evidence can lead to re-dimensioning of primary-secondary panels over time if required.

3.1.3 Horizonal mining progression within the D1-Zone

Conventional mining begins at the bottom of a given zone, removing ore from a level and then progressing upwards to the top of the zone over time. Since extraction of the entire length of the orebody can involve significant engineering complexities, the ore zone on a level is subdivided into manageable widths to be taken out one at a time across the level. These manageable widths are referred to as panels, and in this particular zone the panels are numbered sequentially starting at around 120 on the west side and ending around 136 on the east. Panels generally run the entire depth of the mine, so panel numbers above or below those values may exist at elevations either well above or below the D1 Zone. Two such panels can be observed in Figure 23 (above), one extending from the Level 120 to the Level 115, the other from Level 120 to Level 110, coloured in light tan.

Figure 26, below, shows a three dimensional isometric view of this same zone, with the level development indicated in salmon and the various ore stopes located across the panels in contrasting colours. The stopes are in most cases one panel wide, with some potential deviation at the edges of the orebody.

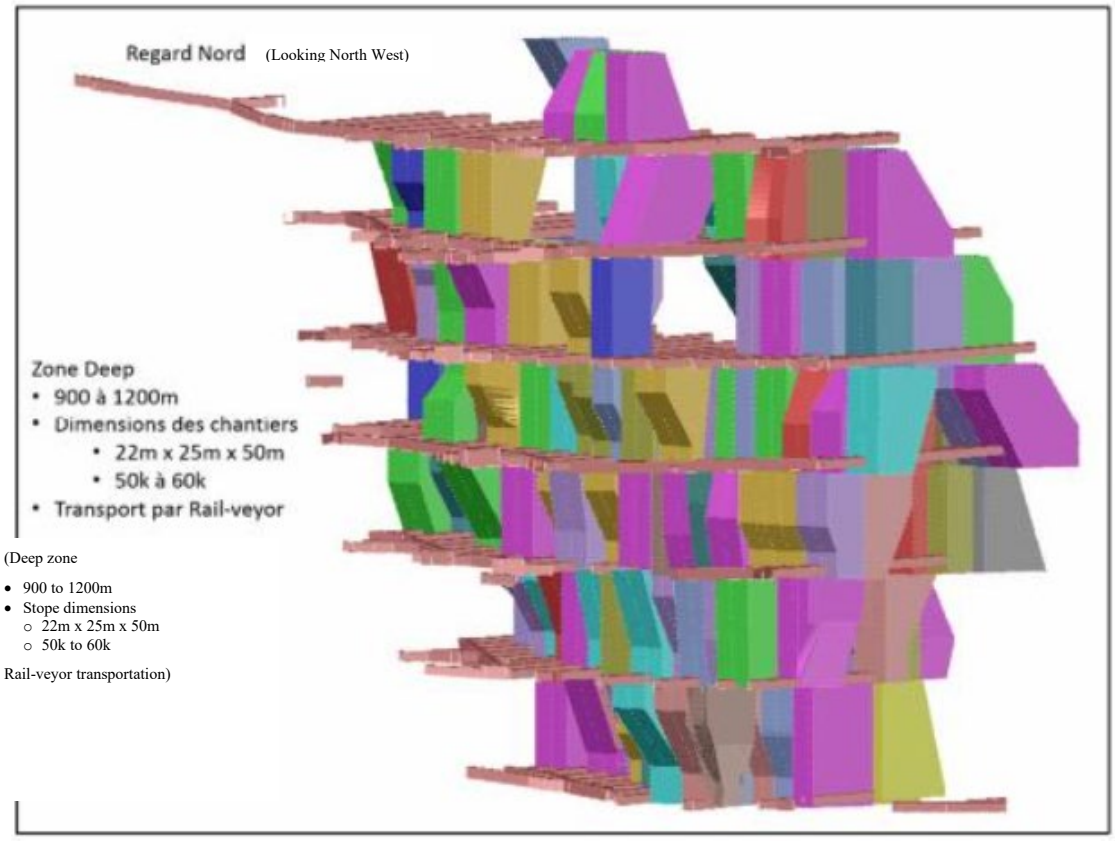

Figure 26 – 3D Isometric view of the D1-Zone orebody showing general stope dimensions and panel intersections (Doucet, 2018) (translations added by author)

One final view, taken looking South, shows various panels and levels in stages of excavation with the 3-d wireframes representing ore that has been previously removed and backfilled (**Figure 27**). It is apparent that every second panel is generally skipped during mining. Not only are secondary stope panels mined after primaries, as described in Section 3.1.2 above, but these secondaries are also carried vertically after the secondary stopes below are mined.

As previously discussed, this mining method is done to both increase production by mining multiple panels at once, while also managing the changes in stress during the extraction process. The design intends to concentrate the stresses from the removal of the primary panels into the secondary panels, which will yield those secondaries, and ultimately push the stresses to the extents of the orebody and outside of the active mining zones.

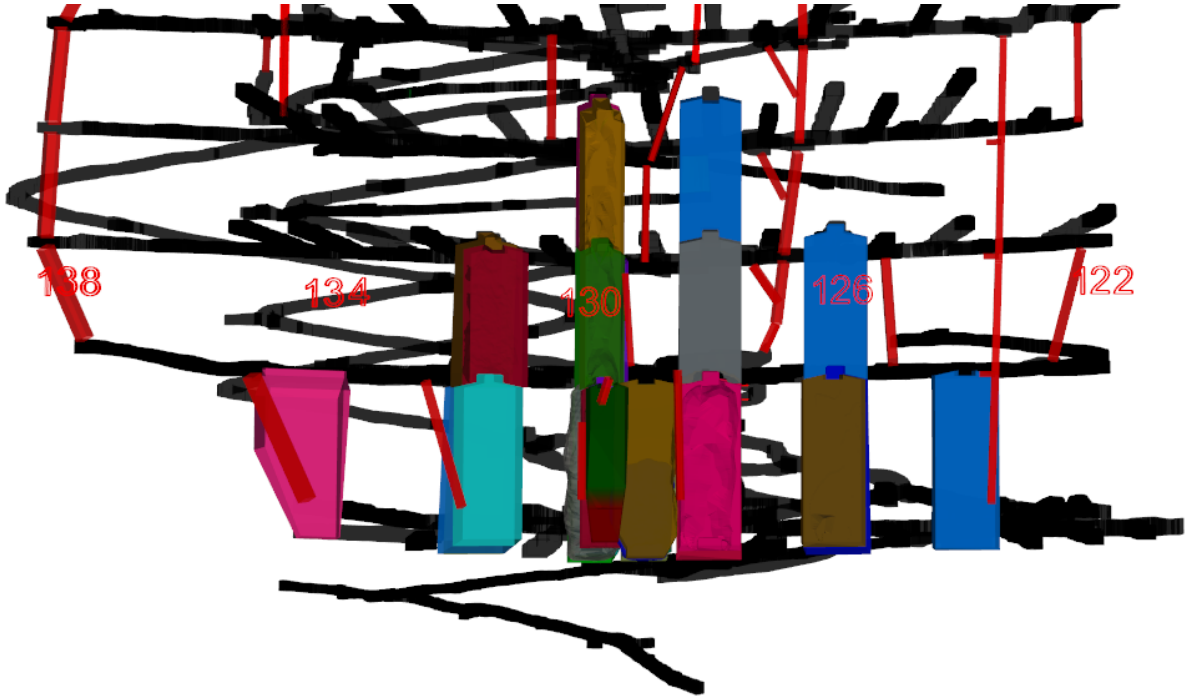

Figure 27 - Longitudinal section of D1-Zone in early extraction showing primary and secondary panels (facing south)

3.1.4 In-situ Stresses

Although outside of the scope of this work, an understanding of the in-situ stresses may assist in a more complete appreciation of the environment in which this study is based. To that end, in-situ stresses were originally determined through assumption and calculation based on Arjang (1996) for typical stress fields in the Val-d'Or region.

Over time, those calculated values underwent some verification through a measurement campaign (Corthesy, 2006) and ultimately numerical modelling assisted by a seismic activity records (Beck Engineering, 2013). The best understood general relations are detailed in Table 2, below.

Table 2 - In-situ stress relations at Goldex Mine (Doucet, 2018)

Parameter	Value
σ1 (MPa)	1.9 * σ3
σ1 azimuth/dip	160° / 0°
σ2 (MPa)	1.3 * σ3
σ2 azimuth/dip	250° / 0°
σ3 (MPa)	0.02649 * depth
σ3 azimuth/dip	000° / 90°

As can be seen in Table 2, the principal stress (σ_1) is horizontal and strikes at approximately 160 degrees. Although the magnitude of the principal stress is a function of depth, at depths experienced in the D1-Zone, it generally lies around 40-62 MPa.

The intermediate principal stress (σ_2) is again horizontal, striking roughly perpendicular to the principal stress (at 250 degrees), with a general value in the D1 zone of 27-32 MPa.

Finally, the minor principal stress is vertical, and primary representative of gravity loading. At the depths relevant to this work in the D1-Zone, would likely range from 21-33 MPa.

Work remains ongoing with a proposed borehole breakout study to be conducted in the deeper zones of the mine (Doucet, 2018).

3.2 Geology

3.2.1 Regional Geology

The Goldex mine is located in the southeastern area of the Abitibi region, approximately 4km west of the town of Val-d'Or, Quebec. This area is a typical Archean granite-greenstone belt,

part of the largest greenstone belt in the world (85,000 km2; Card, 1990). The Abitibi region extends from the Kapuskasing Structural Zone in Northeastern Ontario to the Grenville Province Front in northwestern Quebec, approximately 700km. Figure 28 shows the regional geology around the Goldex mine with a highlighted area of the Val-d'Or area.

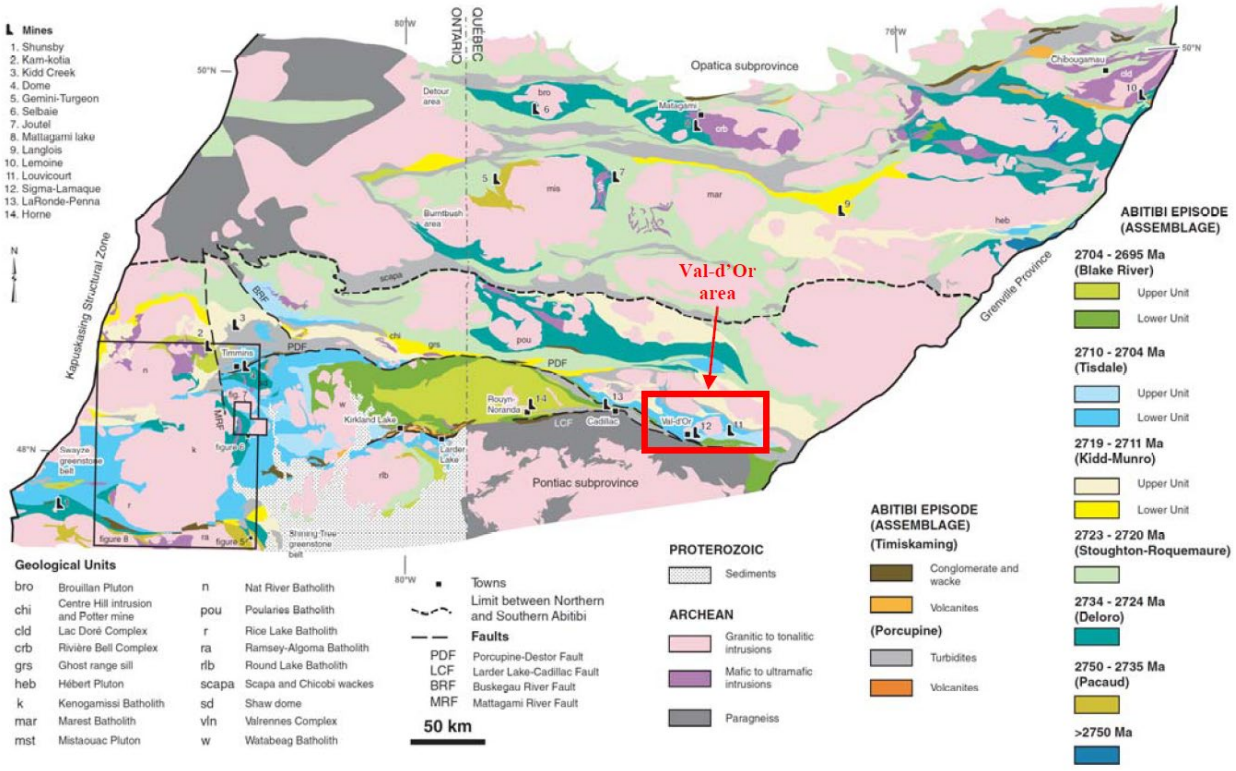

Figure 28 - Regional geology map including the Abitibi zone with location of the Val-d'Or area highlighted (Thurston *et al.*, 2008)

3.2.2 Mine Geology

According to the Ground Control Program (*Programme en contrôle de terrain)* (Doucet, 2018), the Goldex D1-Zone lies 1200 metres below surface and is a large, low grade gold orebody hosted by a steeply dipping granodiorite or quartz-diorite. The ore consists of both a structurally driven lode gold-type deposit which changes with depth to what is surmised to be a more disseminated pyrite near the bottom of the current mining. The structures above include gold-

bearing quartz-tourmaline-pyrite veinlets, typically under 50 cm in width. In the deeper areas, the structurally driven ore makes up less than 10% of all ore, with disseminated sulfides making up the remaining portion. Despite geological changes, no observed changes to overall grade has been observed. Any potential structural related links to grade are still under internal study.

3.2.2.1 Diabase Dykes, Dylonite Zone and Branches

Two separate types of geological structures have relevance to the evolution of seismicity within this thesis:

Diabase dykes

Several diabase dykes have been observed in the western half of the D1-Zone and intersect known infrastructure (Doucet, 2018). The dominant family trends at N285º/40º and a secondary group at N300º/80º. These dykes are described as: observed in meter-scale thickness, black to brownish black, phanitic and strongly magnetic (Doucet, 2018). The dykes have sharp contacts that are weakly sheared.

Dylonite zone and branches

Additionally, a geological unit observed to be a strongly foliated, banded and folded diorite has been referred to locally as dylonite (Doucet, 2021). Figure 29 shows a typical core sample of this geological unit.

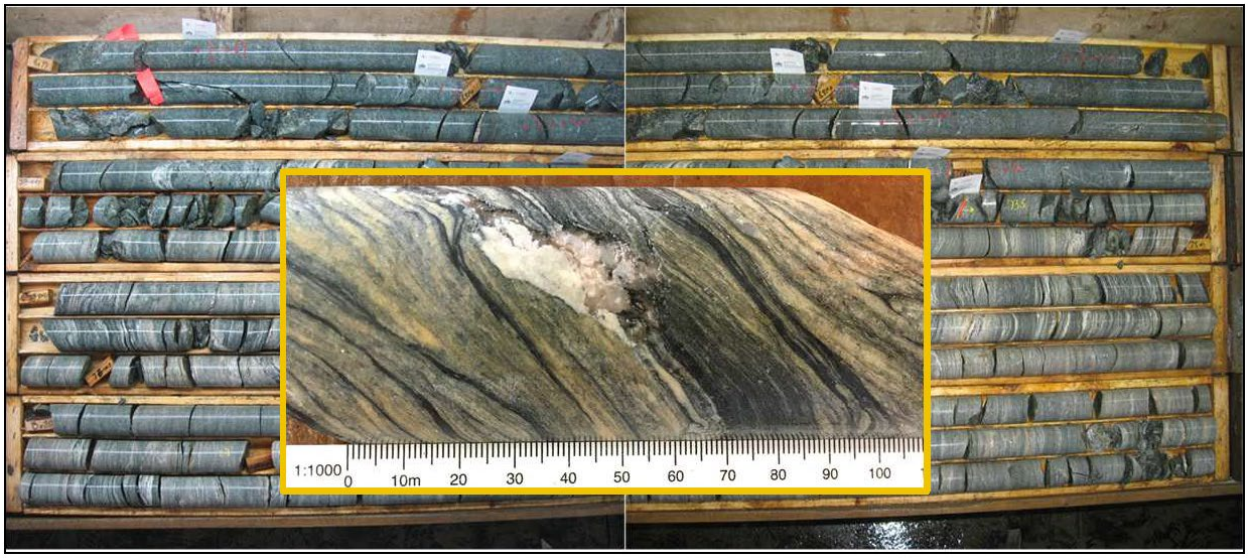

Figure 29 - Dylonite core and grain structure (Doucet, 2021)

This unit has several branches extending the entire height of the D1 zone down into the D2 zone in at least 3 branches in addition to the main zone.

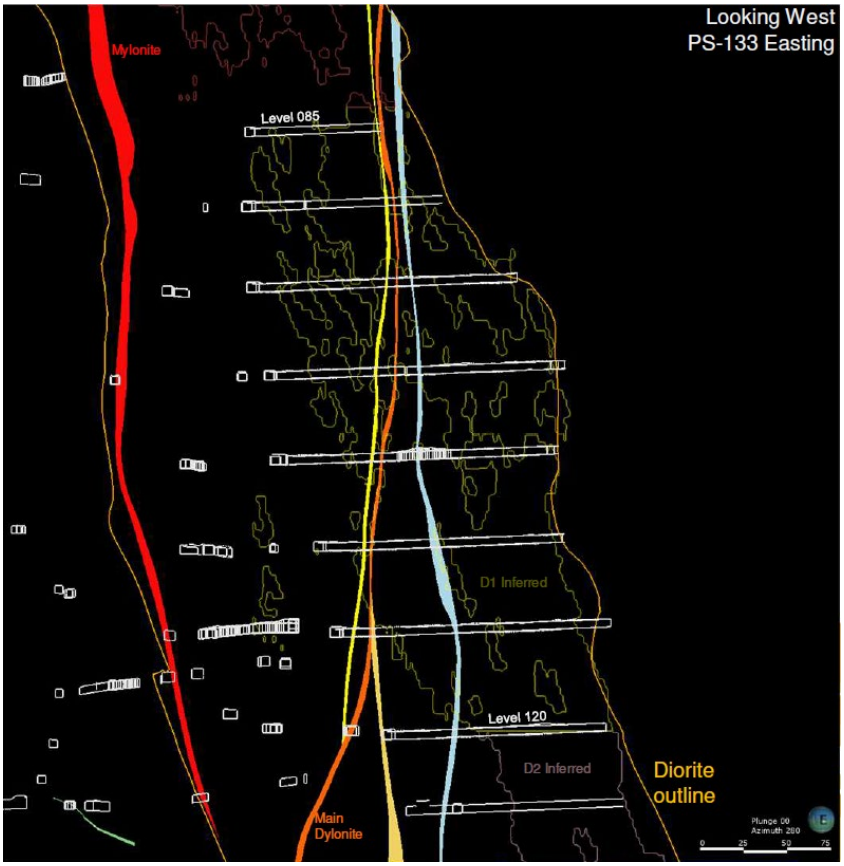

Figure 30 - Main dylonite (orange) and known branches (yellow, tan, light blue)

3.2.3 Rock Mass Classifications

Three separate rock mass classification systems have been used on site to determine the rock mass quality of the major geological units found on site at Goldex. This includes RQD (Deere *et al.*, 1967), RMR76' (Bieniawski, 1976), and Q'(Barton *et al.*, 1974). It is recognized that these systems are more commonly used in near-surface excavations and may not be as effective in representing the units under failure modes likely in high stress or high deformation environments. That being said, they do represent relative rock qualities. Table 3 (Doucet, 2018) shows the geological units and their respective quality through the classification systems.

Table 3 - Rock mass qualities for typical geological units at Goldex Mine (adapted from Doucet, 2018)

Rock Unit	RQD*/**	RMR76'	Q'	Quality
Diorite (M, E or GEZ Zone)	70-85	65	10	Good
Diorite (D1 or D2 Zone)	85-90	75	14	Good
Diabase dyke	60-75	45	7	Moderate
Mylonite	50-70	45	4	Moderate
Dylonite	50-70	50	6	Moderate
Basalt	75-85	55	6	Moderate
Silicified basalt	70-80	65	8	Moderate
Komatiite	50-70	40	3	Poor
Shear zone	30-40	30	1	Poor

*RQD estimated from the 30th to 5th percentile values

**RQD of shears estimated from visual observations

While determining the rock mass classification, uniaxial compressive testing was done on various core samples. The table below includes the summaries of the various tests completed during this phase.

Table 4 - Unconfined Compressive Strength (UCS) testing statistics per rock unit

Rock Unit	Minimum Value (MPa)	Maximum Value (MPa)	Mean Value (MPa)	Standard Deviation	Number of Tests
Basalt	48	291	127	66	34
Diorite	40	332	168	79	35
Komatiite	5	128	49	29	34
Mylonite	54	147	100	30	8

3.3 Seismic Monitoring at Goldex

In order to both locate and have a better understanding of the rock mass failure occurring at Goldex, a seismic monitoring system has been installed. During the data period of this thesis, the system consisted of 23 uniaxial and 6 triaxial sensors in an array covering the entire mining area. Of these, 12 uniaxial and 4 triaxial sensors are in the immediate vicinity of the D1-Zone, however even the sensors more distant would be capable of assisting in determining seismic source parameters. Figure 31 shows a schematic of the microseismic system at Goldex mine.

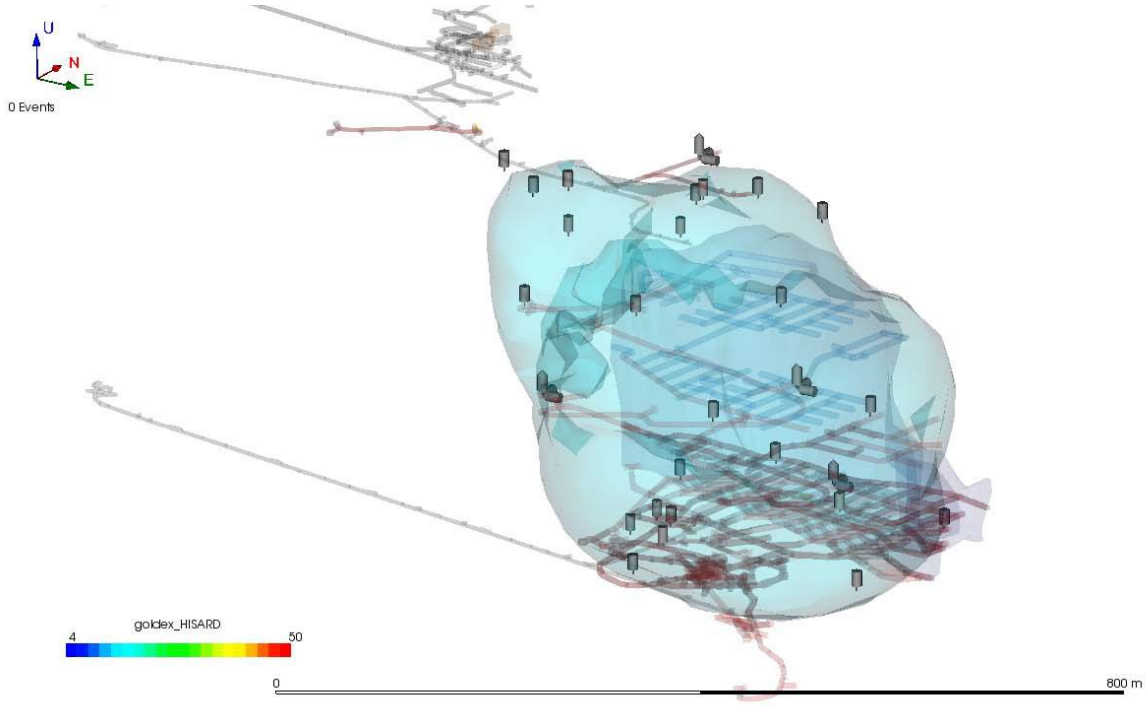

Figure 31 - Goldex microseismic system schematic (Hudyma *et al.*, 2010)

Additional to this local system, a macroseismic Regional Seismic Network consisting of a total of 13 geophones in the region is available to provide more information about large, low frequency events in the area. Five such geophones are located in very close proximity to Goldex (all <10km), and can be seen in Figure 32, below.

Figure 32 - Regional Seismic Network geophone locations shown as red markers for evaluation of large, low frequency seismic events at Goldex

3.4 Summary of Seismic Record

As mining at Goldex progressed into the D1 zone, changes to the seismic response can be observed. A Magnitude-Time History chart for all seismic events from the initial production blasting of the D1-Zone until the end of 2020 is shown in Figure 33.

In this cart, it can be observed that certain gaps in the data are present. This includes Q1 2020 where a reduced production period was observed due to a global pandemic, and several other smaller gaps which correspond to technical difficulties in either administration or service interruptions within the seismic system.

A significant upgrade to the seismic system sensitivity can also be observed occurring in Q3 2019. Prior to this, virtually no events with magnitudes less than -3.0 were recorded by the

system. Over time, the system sensitivity increased to such a point that magnitudes of -4.0 and below were recordable. A final observation is an ever increasing maximum magnitude value, with proportional increases in both the significant (green), large (yellow), and very large (orange) events.

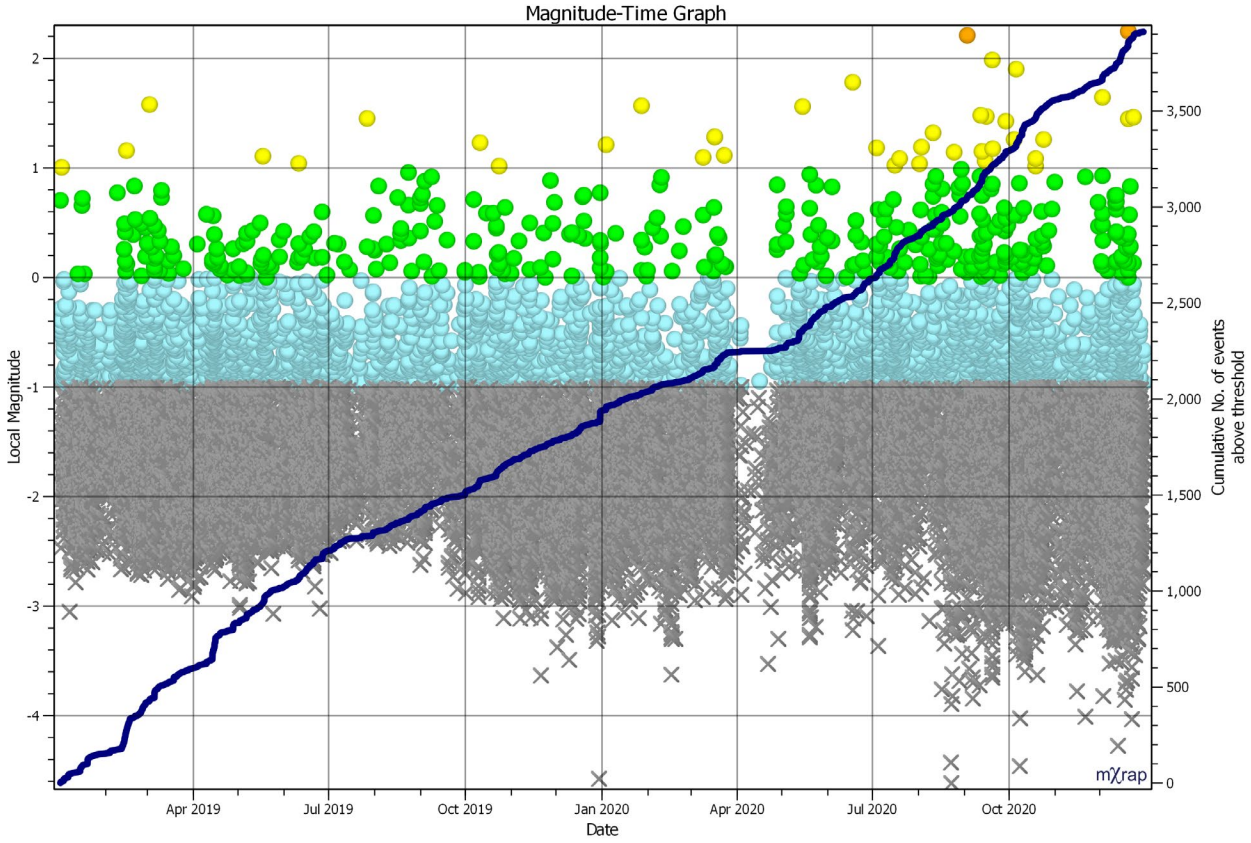

Figure 33 - Magnitude-Time History chart for all events occurring at Goldex mine between January 2019 and December 2020. Colours observed apply to increasing magnitude

As discussed in Section 2, Frequency-Magnitude charts also provide information regarding both the seismic hazard and the capacity of the seismic monitoring system.

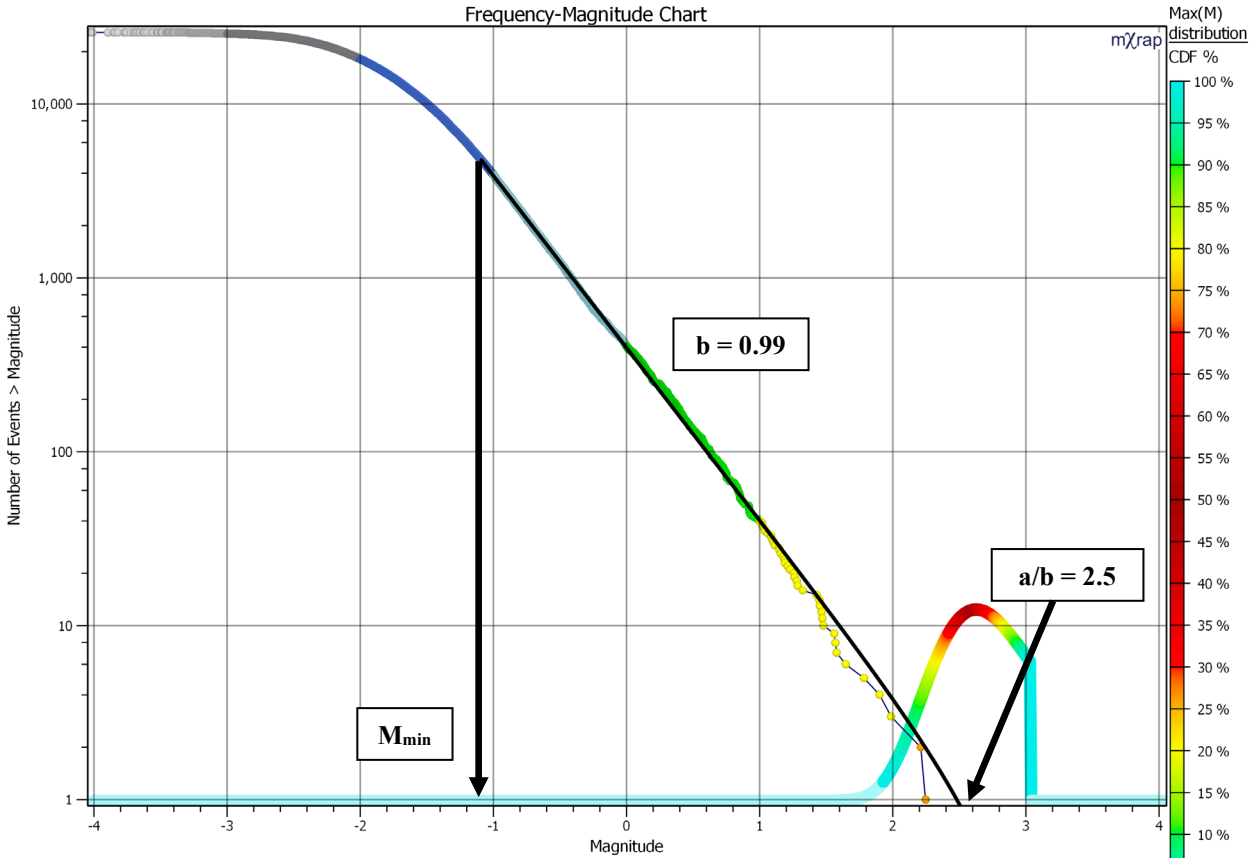

Figure 34 - Frequency-Magnitude relation for all seismic events at Goldex mine between January 2019 and December 2020. Colours observed apply to increasing magnitude

Despite the overall system sensitivity increase above, the minimum value which can assumed to include the entire seismic record, all of the events in any location, is a local magnitude of -1.1. The total of all events over this two year time period show a slope, or b-value, of 0.99. Large populations of seismic data are said to be consistent at values approaching one, so it can be inferred that this total population of data is both uniform and complete. At this time, the largest expected magnitude event would have been approximately a magnitude 2.5, slightly above the observed 2.25 magnitude event by the system during this time frame.

Chapter 4

4 Seismic Response to Mining

An abundance of seismic data was available spanning from the beginning development of the D1 Zone at Goldex right up until the end of 2020. Given the subject of this thesis, reduction of that data down to a usable amount which could accurately show the evolution of seismicity was required. Various criteria were used in order to reduce the data down to an applicable time period, and finally to a number of other factors. This section will describe both how those factors were important, and the observations made.

During the time period evaluated in this thesis, a global pandemic of coronavirus disease 2019 (COVID-19) occurred. On March 11, 2020, the World Health Organization declared the virus a Public Health Emergency of International Concern. Over the next couple of weeks, preventative measures were put in place worldwide, which included the temporary shutdown of many workplaces in which workers were exposed to potential risks that were not fully understood at the time.

With respect to the workplace in this thesis, despite the total shutdown lasting only a few weeks, there was a significant impact on all production activities for quite some time both before and after the shutdown itself. Supply shortages were seen in many industries, and many transportation networks were significantly impacted due to limitations placed on various manufacturing facilities around the world, as well as changes to both international and even interprovincial travel.

Due to a significant reduction in both production blasting and mucking rates, seismic responses over the relevant time period were observed to be considerably different than other periods. For

these reasons, the data record between March 17, 2020 and June, 2020 was not included in either the dataset or subsequent analyses.

Where applicable, the primary/secondary stope responses will be discussed separately. Additionally, macroseismic events defined as having a local seismic magnitude (M_L) greater than 0 will be discussed separately from the total seismic response.

4.1 Data Selection

Over the 15 month period spanning September 2019-December 2020, a total of 190 production blasts were recorded in the blast logs. In order to draw conclusions from the blasts and their associated seismic responses, a number of criteria were used to determine applicable blasts. These criteria were in addition to the removal of data during the COVID-19 pandemic production irregularities previously discussed. These are described below.

4.1.1 Evaluation of the 24 Hours Following the Blast

Due to the industrious nature of an underground production mine, production blasts are scheduled as frequently as reasonably possible. Due to a number of logistical or operational issues, this typically results in production blasts occurring once every 24 hours.

In order to determine the impact of a single blast on a given seismic response, evaluation of a period greater than 24 hours after the production blast typically introduced at least one other production blast into the general vicinity. At that point, separation of any given seismic response from one blast to another became impractical and would have required significant analysis while introducing subjectivity. Consequently, analysis of seismic data was limited to the 24 hour period after a production blast.

Over the time period of the data set, eleven large events occurred, all of which have been captured in the data set, with the appropriate analyses conducted. During that same time period, 31 of the 50 significant events were also analyzed.

4.1.2 Number of Events in the 24 Hours Following the Blast

Various production blasts had differing seismic responses following the blasts. Blasts with a greater number of events were selected over blasts with fewer events. The objective of this thesis is to quantitatively describe the seismic response to mining, in particular, the seismic response to production blasts. Blasts with minimal seismic responses were not investigated as there was limited data to describe the seismic response. The result was 29 total blasts selected that met the criteria. Preference was given to larger responses during the same general time frames. The median number of events in the 24 hours following the blasts selected was 74.

4.1.3 Only Single Production Blasts During a Blasting Window

Due to the dynamic environment within an active mine in production, blasts were chosen where more certainty existed that one particular blast had an influence on the following seismic response. In many cases, multiple production stopes were blasted in the same general blast window, at times within minutes of one-another. These blasts were omitted from the analysis to ensure that a given response was more likely to be related to one specific blast.

Although preference was given to no development blasting at the same time as the production blasts, removal of any production blast close in time to a development blast would have resulted in a very limited data set. For most development blasts at Goldex, development blast seismic responses are very limited or confined to the immediate area around the development blast. A typical example of a limited development blast response is shown below in Figure 35.

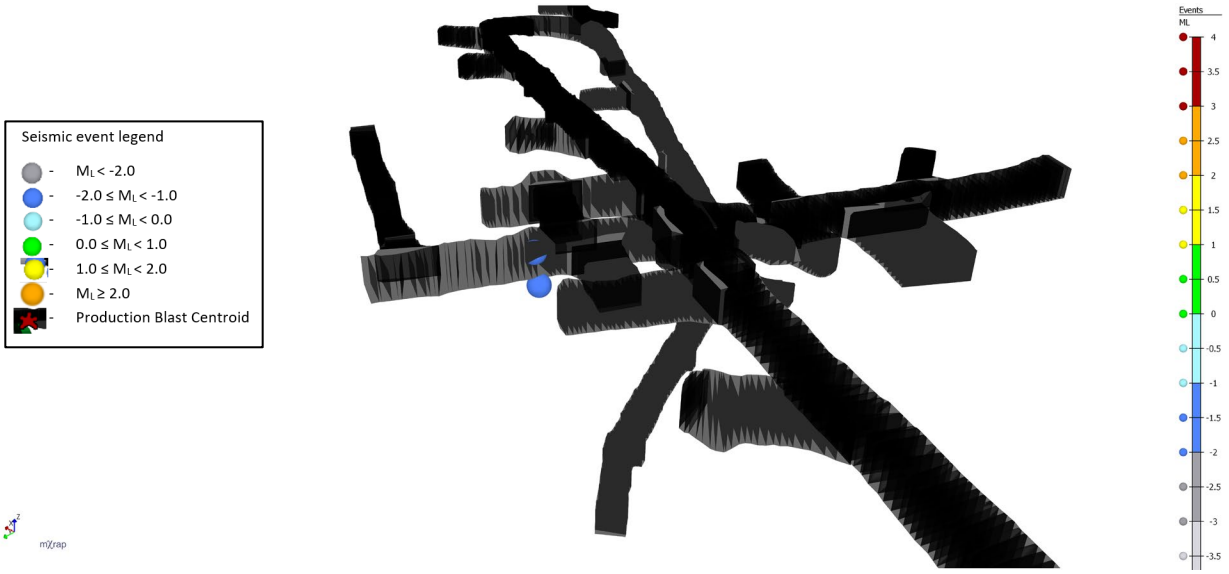

Figure 35 - Typical blast response following a development blast

As can be observed in Figure 35, a typical development blast response can consist of as few as only two events. In this particular instance, both of which were microseismic in nature (M_L -1.35 and -1.91) occurred after a development blast. In the year prior to production mining in the D1 Zone (April, 2017), approximately 109 seismic events were recorded, with all but a single M_L 0.32 event being microseismic in nature. During this time period, exclusively development mining was occurring in this zone. Over the thousands of development blasts, only 109 events were recorded.

In contrast, for the year spanning April 2017-April 2018 when production stoping had first started in the D1-Zone, approximately 5585 seismic events were recorded. Production stope mining has a dominant impact on the seismic response to mining.

Due to significant data filtering efforts described in section 4.1 Data Selection, many large events were not included in the total data set. Many instances of large events occurred after multiple blasts took place, or occurred at times greater than 24 hours after a preceding production blast. A case-by-case seismic analysis of all these large events would be required to understand the

most likely blast to have led to the large event, and even then considerable speculation may be required.

Over the time period of the data set, 37 large events occurred. Eleven of those events have been captured in the data set, with the detailed analyses conducted.

4.1.4 Larger Blasts Were Selected Over Smaller Blasts

With the same or similar densities of rock being blasted, larger blast tonnages correspond with larger openings being created in the underground mining environment. This larger opening will generally result in a more significant elastic stress change than a smaller opening. With all other influences being equal, this larger elastic stress change would lead to a greater seismic response. For this reason, a larger blast tonnage was selected in cases where several blasts met the other criteria discussed within the record.

Using the dataset which included all criteria set out in Section 4.1, Figure 36 demonstrates this general relation. It can be observed that overall, an increasing trend exists between the production blast tonnage size and the number of seismic events which occurred in the 24 hours following the blast. For that reason, larger blasts were selected over smaller blasts.

Due to the previously discussed proximity to municipal infrastructure, the blast tonnage has minimal impact on blast vibrations, which are limited using various blasting delay timing strategies.

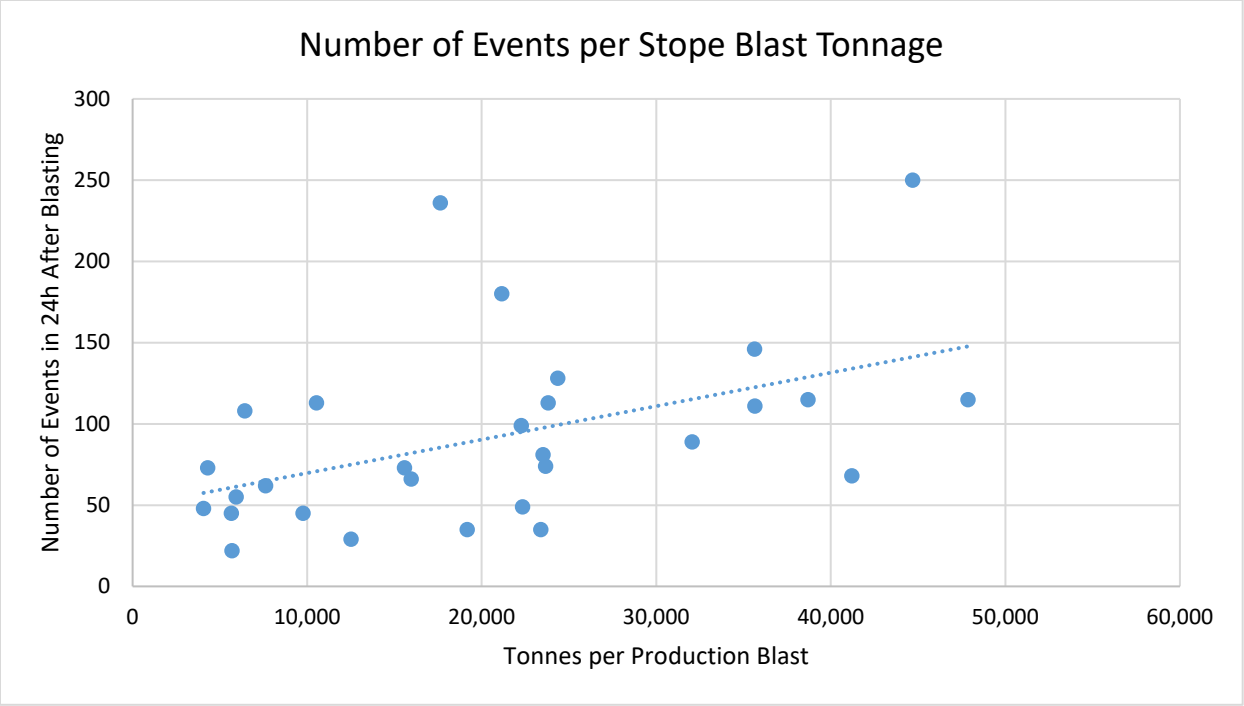

Figure 36 - Number of seismic events per stope blast tonnage for the complete dataset

4.1.5 Seismic Responses Greater Than 350 Metres from a Blast Were Not Considered

Previous work (Brown, 2018) has shown that in the context of Canadian Shield hard rock mines, a limited seismic response distance to underground blasting is observed. This response was observed by Brown in induced, complex and triggered seismic event, and are generally contained to within a few hundred metre radius of the original blast.

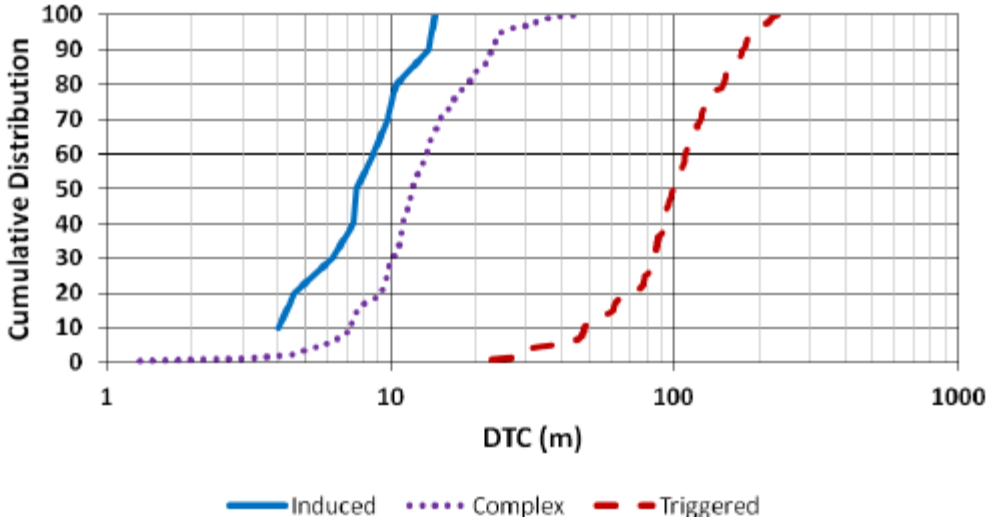

Figure 37 - Cumulative distributions of Distance to Centroid (DTC) in metres for an induced, complex and triggered response to mining (Brown, 2018)

Although excavations of significant size can alter the Distance to Centroid value, the stopes blasted related to this research would not be of great enough size to create a response greater than 350m distant. Figure 38 below gives a visual reference as to what a removal of events 350m from the blast itself would look like. This exclusion zone extends almost 100m below the active development mining front and above the D1-zone, including both the P-Zone and E-Zones and a small portion of the GEZ, all of which are above the D1-Zone.

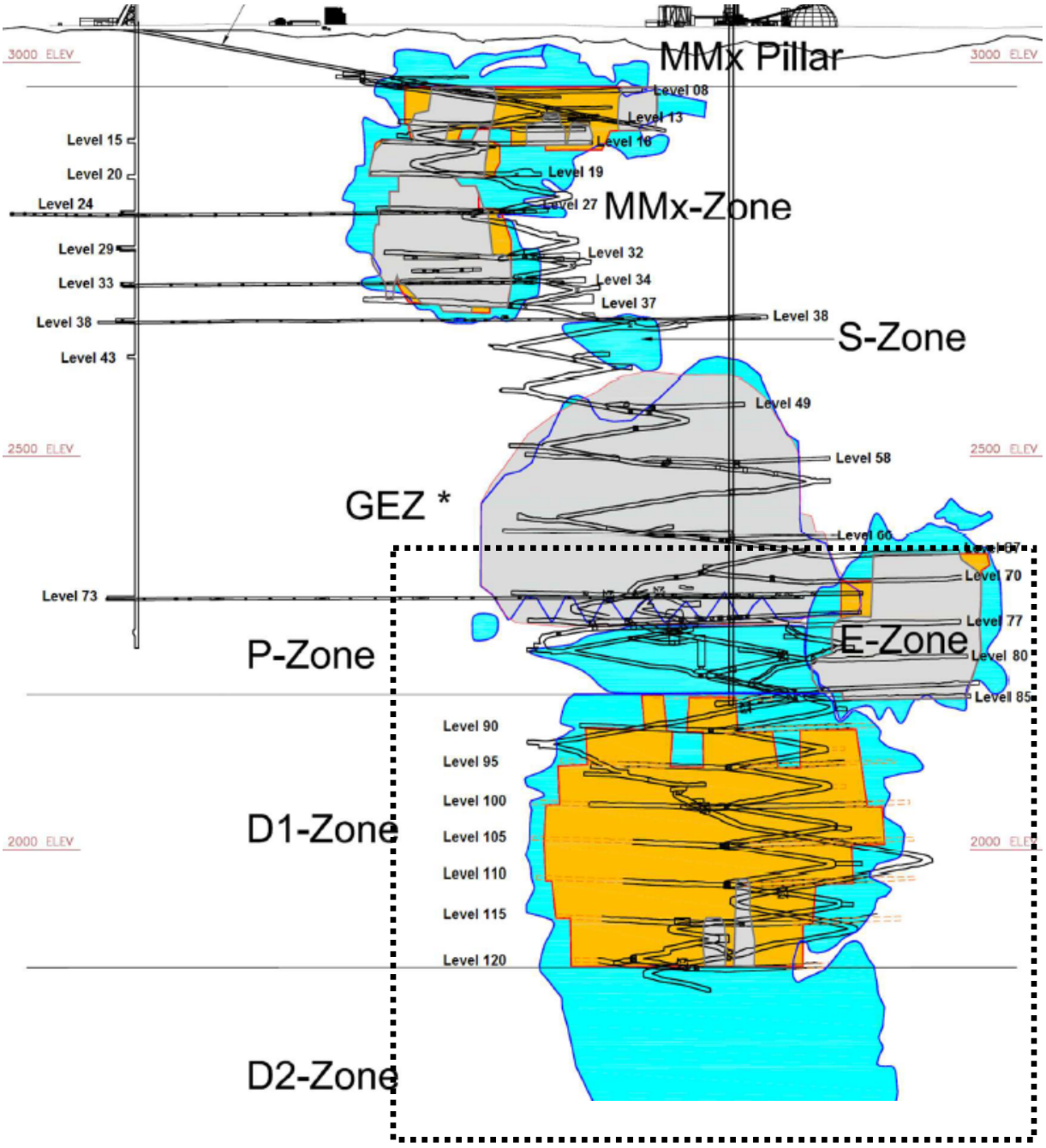

Figure 38 - 350m distance from the centroid of D1 Zone shown as dotted square. Figure modified from PROGRAMME EN CONTRÔLE DE TERRAIN, Mines Agnico Eagle, Mine Goldex, October 2018

4.1.6 Other Data Selection Considerations

Once the filters described in the preceding sections were observed, the next priority was to balance the numbers of primary and secondary stopes in the dataset. While doing so, efforts

were made to represent the mining panels equally within the D1 zone. Finally, an attempt to represent the stopes as evenly across the entire time period was applied to have as continuous a dataset as possible.

4.2 Distance of Seismic Event Response

To characterize a given seismic response, reduction of the total response after a blast to a minimum, maximum and median value distance to the blast is used. Prior use of median distances in mine seismicity is common in seismic research (e.g. Brown 2018, Kgarume *et al*. 2010). The purpose of applying these values to a population of data is to both simply quantify a given response, while minimizing the influence of outliers in that set of data. Inclusion of the minimum and maximum values will show the variances within each response.

4.2.1 Individual Stope Seismic Response

After a blast takes place, an opening is created in the underground mine which contains the blasted materials. The stresses acting on the excavated volume are redistributed to other areas of the mine, based on a host of factors including geometry, geology, any previously yielded ground, and other openings which may exist in the underground environment (Cook, 1976). This stress redistribution can result in rock mass failure, which can be identified by the resultant seismic events. These waves can be described as seismic events (Hedley, 1992). If damage to the excavation is experienced during these seismic events, this condition is referred to as a rockburst (Ortlepp, 1997).

Figure 39 shows a typical pre-2020 primary stope blasting response. In the figure below, the red star denotes the centroid of the stope being blasted, CH-115-132-D. A series of microseismic

events and a single macroseismic M_L 0.46 event (located on the boundary of the blasted out and filled yellow stope below) is visible, with the vast majority of the response taking place in close proximity to the newly generated opening.

In this same figure, the closest event has been labelled at 15m distant from the centroid of the blast. Twenty other events occur within 30m of the blasted centroid of the stope.

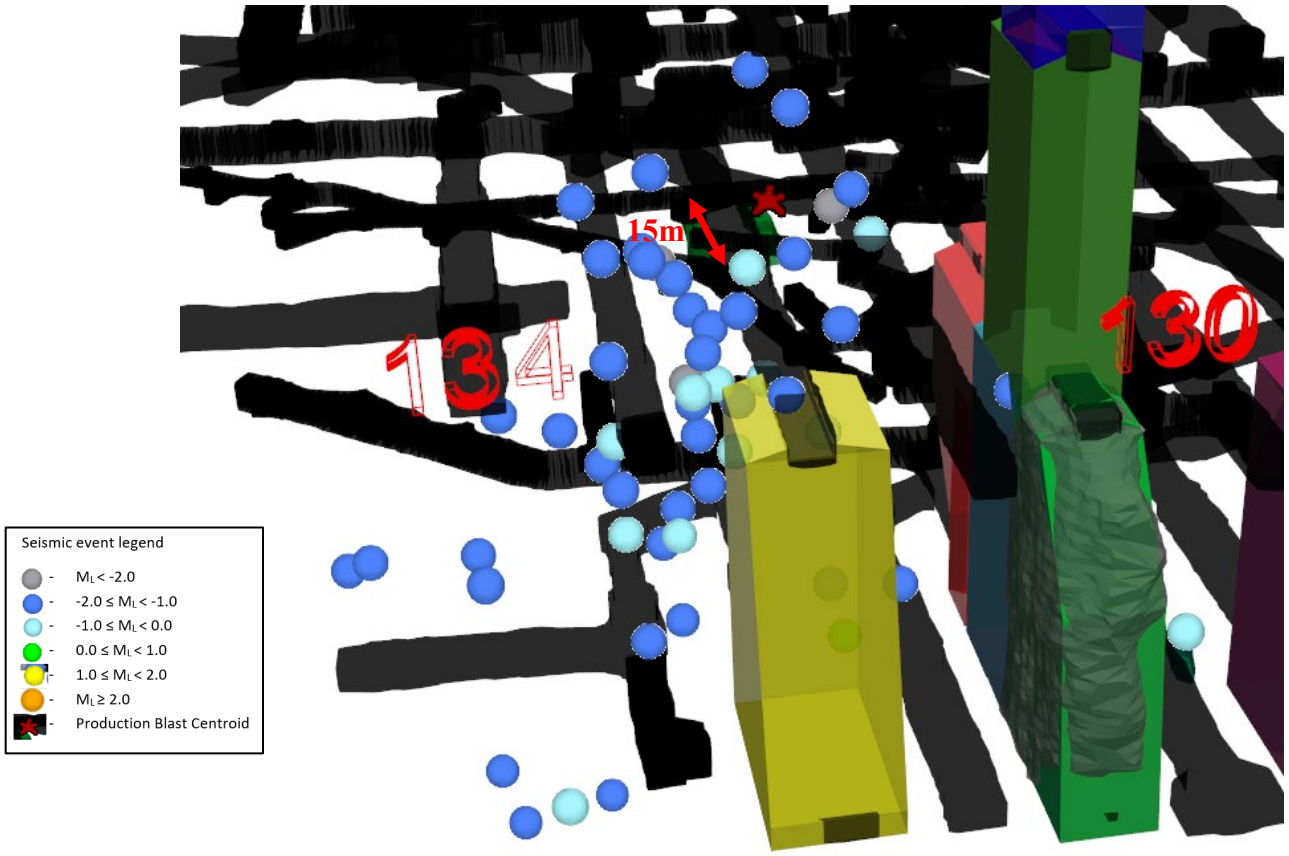

Figure 39 - Isometric view of the CH-115-132-D stope blast identified as a red star on September 5, 2018, and the resultant seismic response over the following 24 hours

In stark contrast to the previous figure, Figure 40 shows a typical late (late-2020) blast response of a primary stope. In the figure, not only is there an obvious lack of near-field seismic response visible, but also a stronger seismic response including three macroseimic events (M_L 0.35, 1.02 and 1.09) occur at some distance towards the footwall in the 24 hours following the blast. The

closest event has been labelled at 51m distant from the centroid of the blast. The two largest (yellow coloured) events are located 79m (below) and 106m (above).

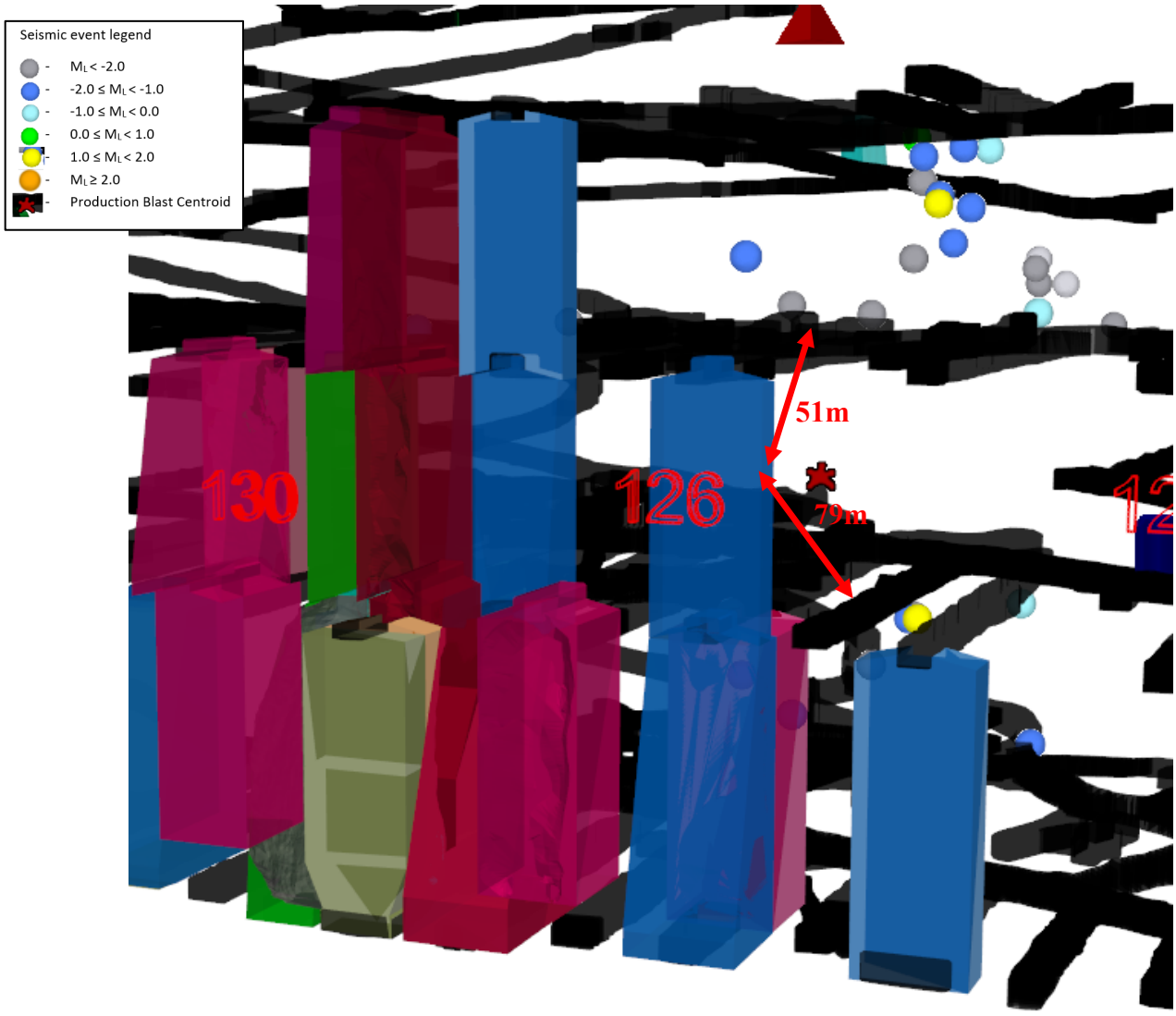

Figure 40 - Isometric view of the CH-115-126-G stope blast identified as a red star on October 18, 2020, and the resultant seismic response over the following 24 hours

Figure 41 shows a typical early (pre-2020) blast response of a secondary stope. Similar to early primary stope blasting, a large number of small magnitude events are visible in the near proximity to the blasted stope itself. In contrast to the primary stopes, blasting the secondary

stopes results in much of the small magnitude seismic response being either above or below the blasted stope. The closest event has been labelled at 31m distant from the centroid of the blast, however relatively few events occur at that distance. Instead, the majority occur approximately 50-60m above the centroid of the blast.

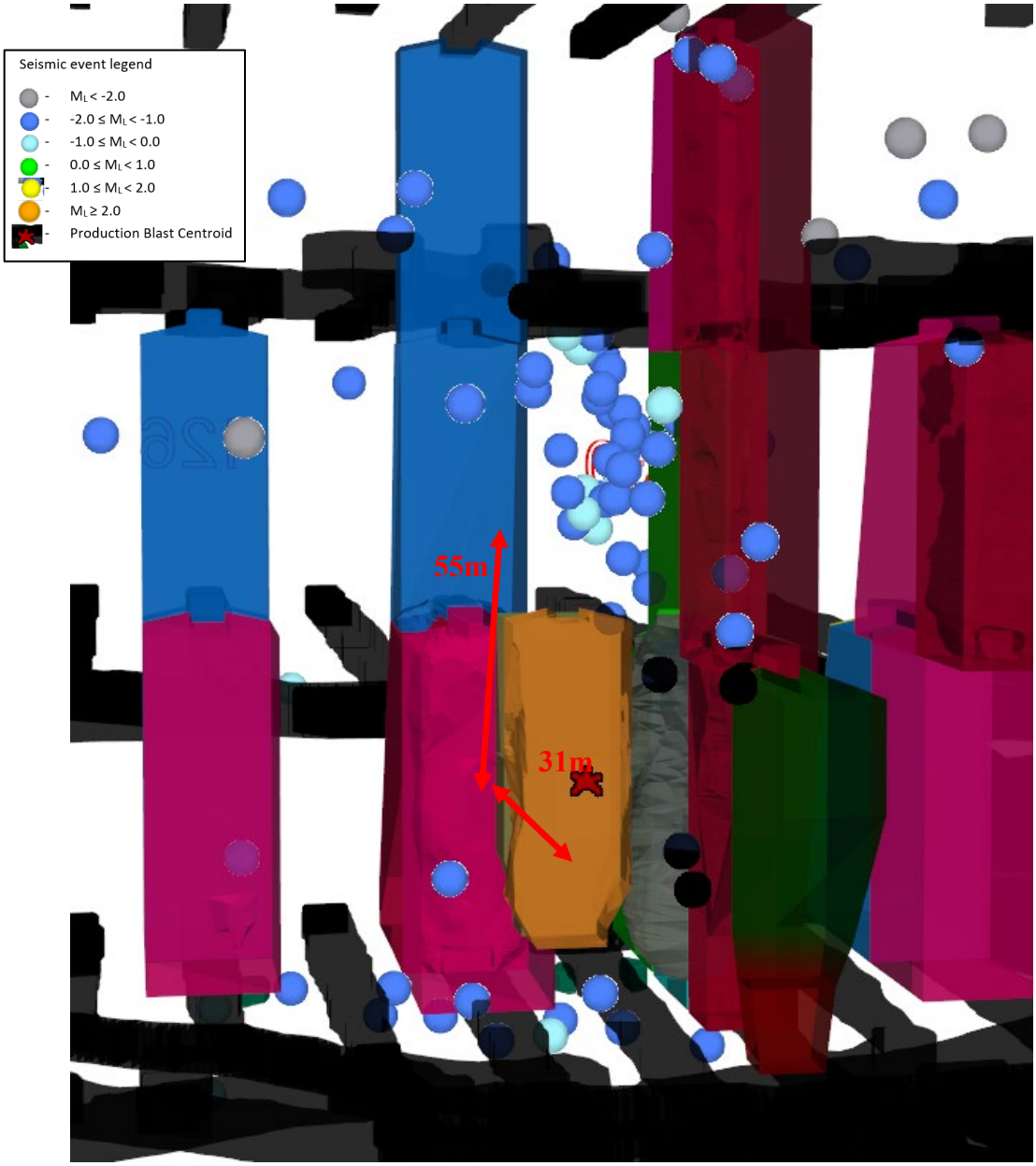

Figure 41 - Isometric view of the CH-120-129-C stope blast identified as a red star on February 27, 2019, and the resultant seismic response over the following 24 hours

Figure 42 shows a plan view of a secondary stope blasted in late 2020. As seen in the later primary stope blasting, the seismic response to the blast has moved a considerable distance away towards the footwall. Larger events are seen to occur, with this blast including six macroseismic events including an M_L 0.11, 0.11, 0.48, 0.58, 0.93 and 1.65. Through filtering of both the mine excavations and seismic response, only the level and seismic events within 25m of the level are shown. This more clearly illustrates the seismic response. A few events occurred on the level immediately to the footwall of the blast, with the closest approximately 39m distant. However, the bulk of the seismic events occur around 75m distant.

Figure 42 – A level plan of 12.5m above and below 120 level showing the CH120-129-F stope blast, identified as a red star, on December 2, 2020, and the resultant seismic response over the following 24 hours

4.2.2 Total Seismic Response

Throughout the data evaluated, the median response for distance from blasting was greater for secondary stopes compared to primary stope blasting. Median distance to the blast centroid was not consistent across all blasts, but some relation was observed. Figure 43 shows the median distance of seismic event response for the blasts taken over the filtered Goldex dataset.

Figure 43 shows how the seismic response after production blasting varies at Goldex. Twenty primary stope blasts and sixteen secondary stope blasts were investigated from August 2018 to October 2020. Each vertical line in Figure 43 refers to an individual blast, with the vertical line representing the closest event to the furthest event in the 24 hours after the blast. The symbol (dot for primary stope blast and square for secondary stope blast) refers to the median distance of seimsic response. In some cases, there are two or more spatially distinct clusters of events after a blast, with the symbol referring to the median distance for each of the blast responses.

Key observations from Figure 43:

- Primary stope blasts
  - Events following primary stope blasts vary from a distance of 10 metres to more than 300 metres
  - Half of the median blast responses are within 50 metres of the blast
  - Over time the median primary stope blasts become more variable, with some median blast responses between 150 and 200 metres from the blast

- Secondary stope blasts
  - There are very few events within 50 metres of stope blasts and no median stope blast responses between 150 and 200 metres from the blast

- Half of the secondary stope blast responses are between 50 and 100 metres from the blast
- Half of the secondary stope blast responses are between 100 metres and 250 metres from the blast
- Over time the median secondary stope blast responses increase in distance from the blast

Overall, the primary stope blast responses are clearly closer to the stope blasts than the secondary stope blast responses. There is a lack of seismic response close to the mine production blasts for secondary stope blasts. This lack of seismic response will be referred to as the “aseismic zone”.

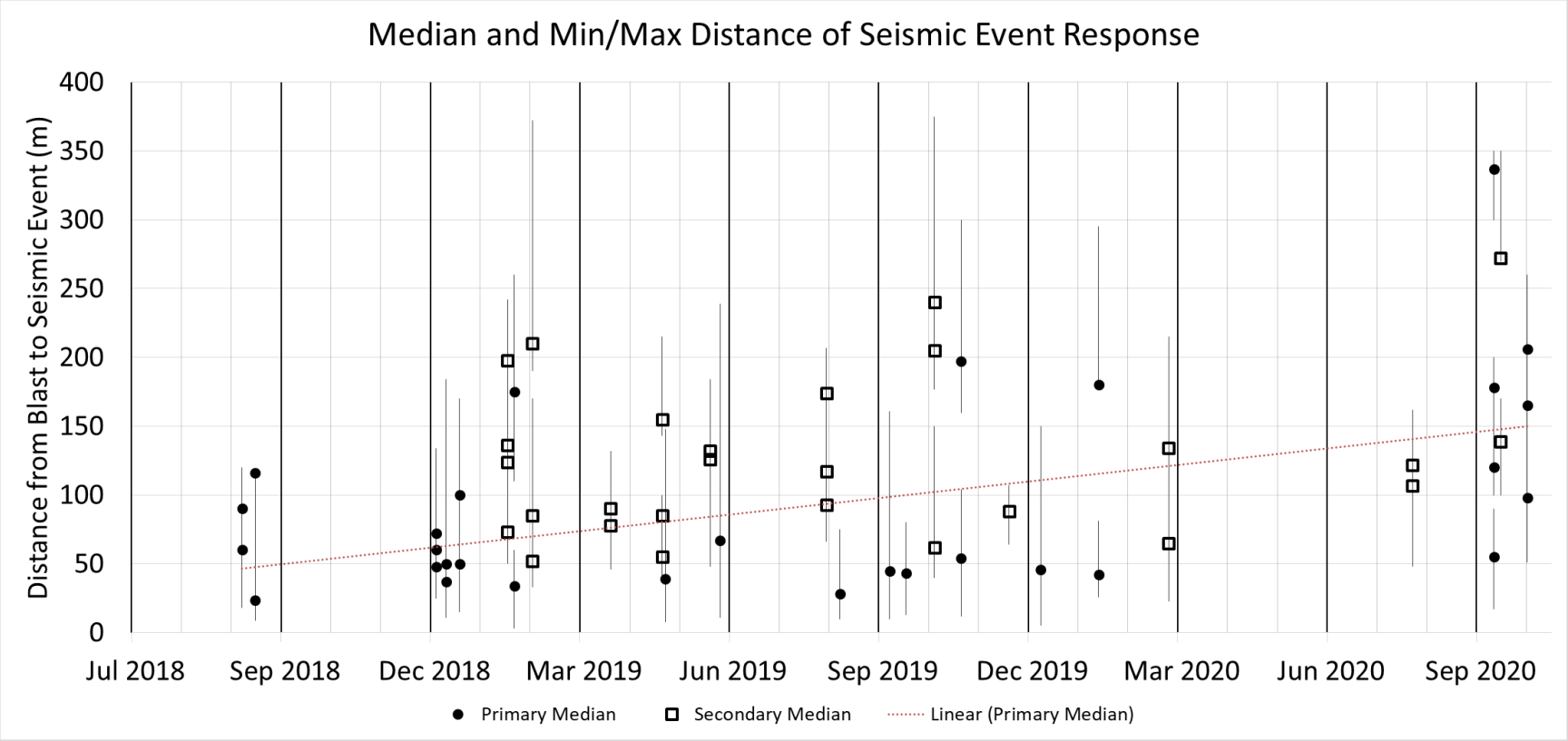

Figure 43 – Median, minimum and maximum distances for the complete seismic event response for all stopes in the filtered dataset

4.2.3 Primary Stope Median Response

As for the median responses for the primary stope blasts, although a general increasing trend was observed throughout the time period, a significant step change appears to have occurred sometime after September 2019. Prior to this date, the minimum median response was 28m, the average median response was approximately 72m, and only 14% of primary stope responses were greater than 100m. This is in a stark contrast to the medians observed later in 2020, which had a minimum median response of 55m, an average of approximately 166m, and 71% of the medians were located greater than 100m away from the blast.

Figure 44 below shows the plot of all median, minimum and maximum seismic responses from primary stope blasts throughout the dataset. It can be observed that the aseismic zone in primary stopes over the time period was generally minimal until the beginning of 2020. After 2020, the aseismic zone varied widely between 17m-300m, and averaged 117m. A generally increasing distance over time was observed.

Impact on, and spatial relations to infrastructure, will be discussed in Section 4.10.

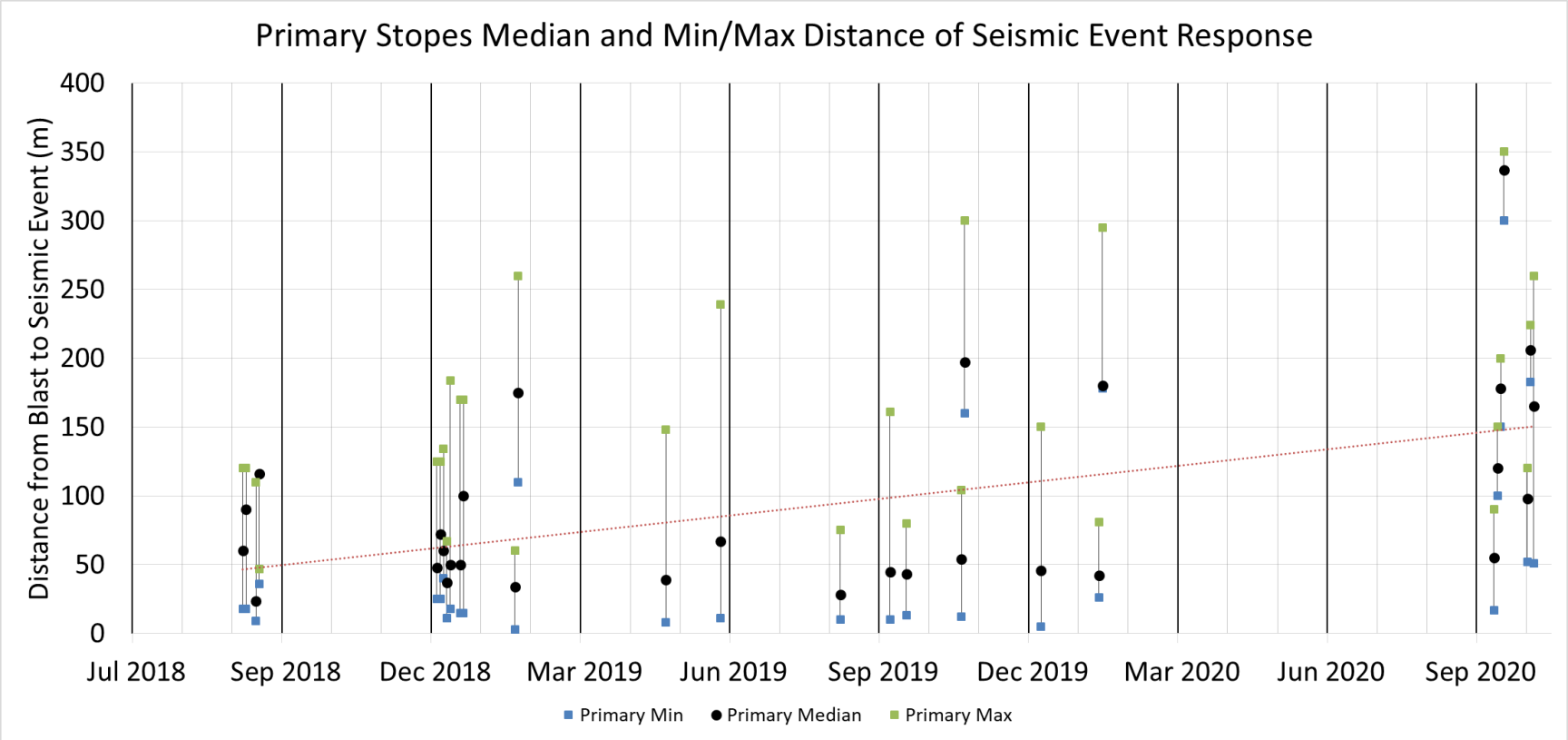

Figure 44 - Primary stope median, maximum and minimum seismic responses

4.2.4 Primary Stope Significant Events ($M_L \geq 0$) or Large ($M_L \geq 1.0$) Seismic Events After Blasts

Figure 45 below shows the plot of all median, minimum and maximum seismic responses from primary stope blasts throughout the dataset, overlaid with any significant or large events occurring directly attributable to the relevant primary stope production blasts.

Although in total, 50% of the significant events occurred at distances greater than the median, that number is considerably skewed between the early data and the later data. Prior to September 2019, 100% of all significant events occurred further than the median stope response. This reduced to 50% of significant events occurring greater than the median distance of stope response from the time period October 2019 – March 2020, and further reducing to 0% for the remainder of 2020.

In contrast, throughout the entire dataset, not a single large event occurred at a greater distance than the median. The large events ranged from 28%-75% of the median stope response distance, with no apparent trends.

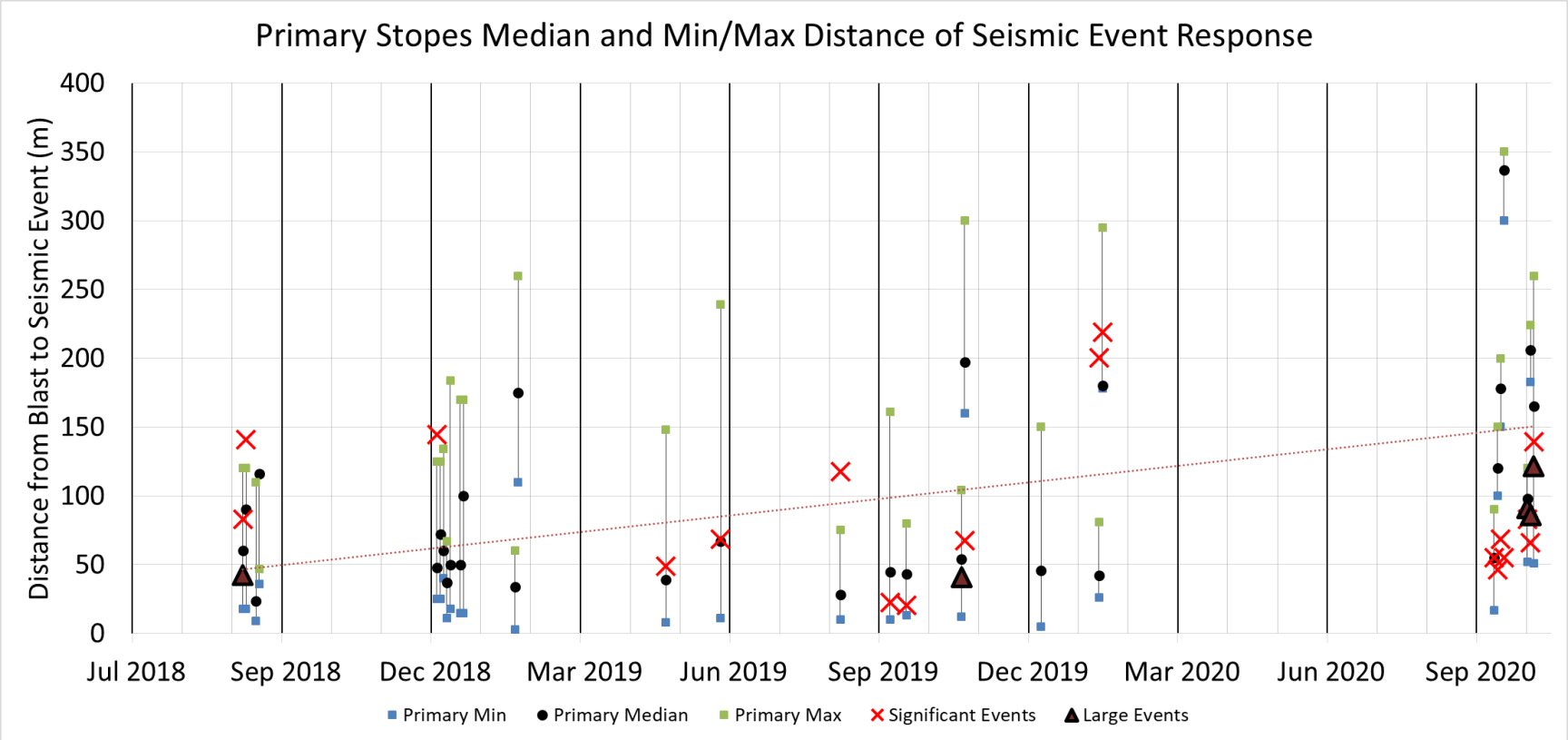

Figure 45 - Primary stope median, maximum and minimum seismic responses overlain with the significant and large events

4.2.5 Secondary Stope Median Response

Secondary stope response distances remained relatively stable throughout all time periods prior to 2020 with an average of 120m and a median of 117m response. A slight increase in response distance was observed in 2020, resulting in an average of 140m and a median of 128m.

It is notable that out of 27 responses, not a single median response over the entire timeframe was less than 50m, whereas in the primary stopes, the median response was averaging only 28m in earlier blasts which increased only to 55m over the time period. Similar patterns were observed in the minimum and maximum values within the total responses.

The minimum response distance, which indicates the aseismic zone, was at all times greater than the primary stope responses. The aseismic zone remained relatively constant throughout the entire time period for secondary stopes, with a range from 23m-270m, averaging 82m.

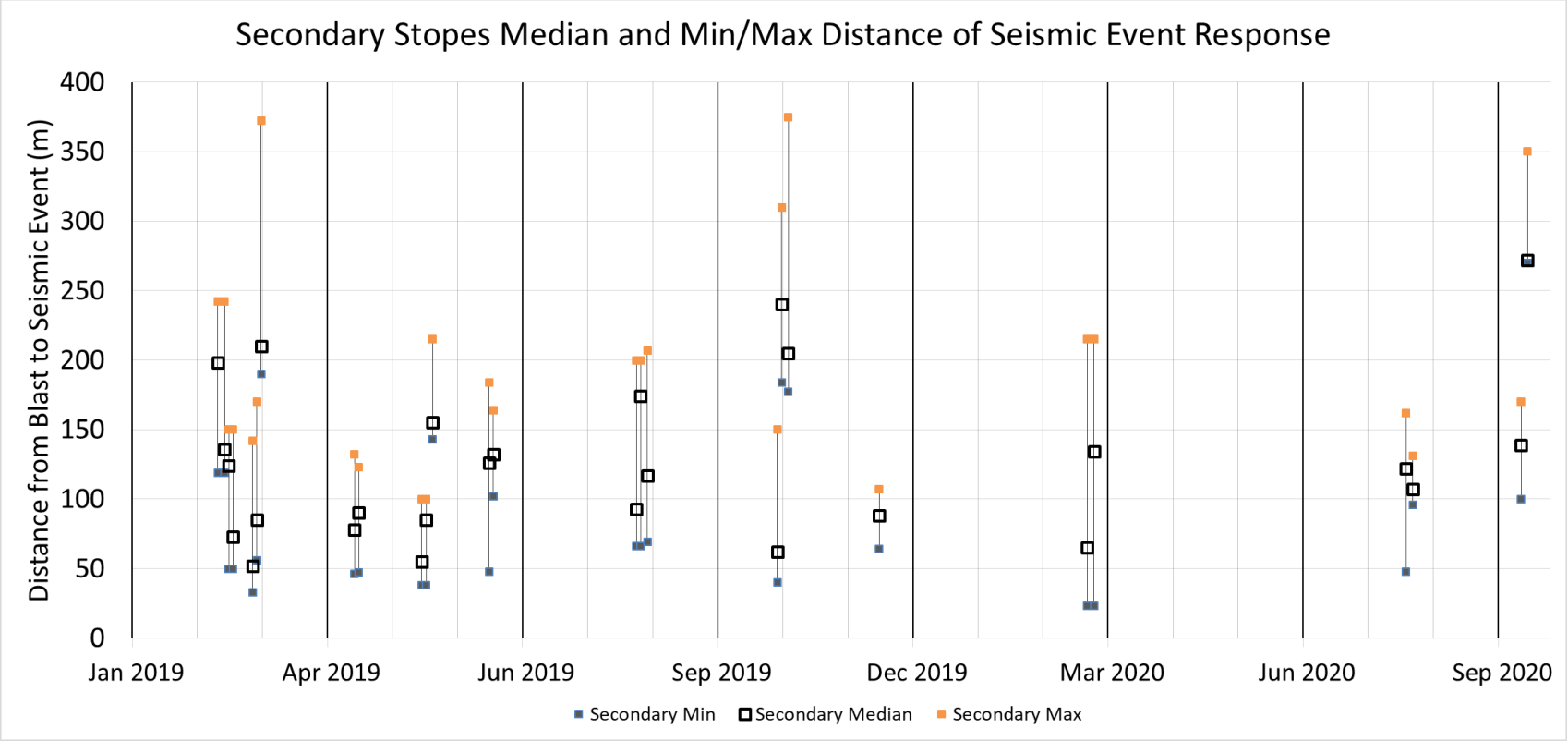

Figure 46 - Primary stope median, maximum and minimum seismic responses

4.2.6 Secondary Stope Significant ($M_L \geq 0.0$) or Large ($M_L \geq 1.0$) Seismic Events after Blasts

The secondary stope response can once again be observed to contrast with the primary stope response with respect to significant or larger seismic events. In the secondaries, there was more conformity between both the significant events and large events compared to the median stope response. Fifty-five percent of the significant or larger events occurred within one standard deviation of the mean stope response, and none of them occurred at distances greater than the overall stope response. Figure 47 shows this relation, below.

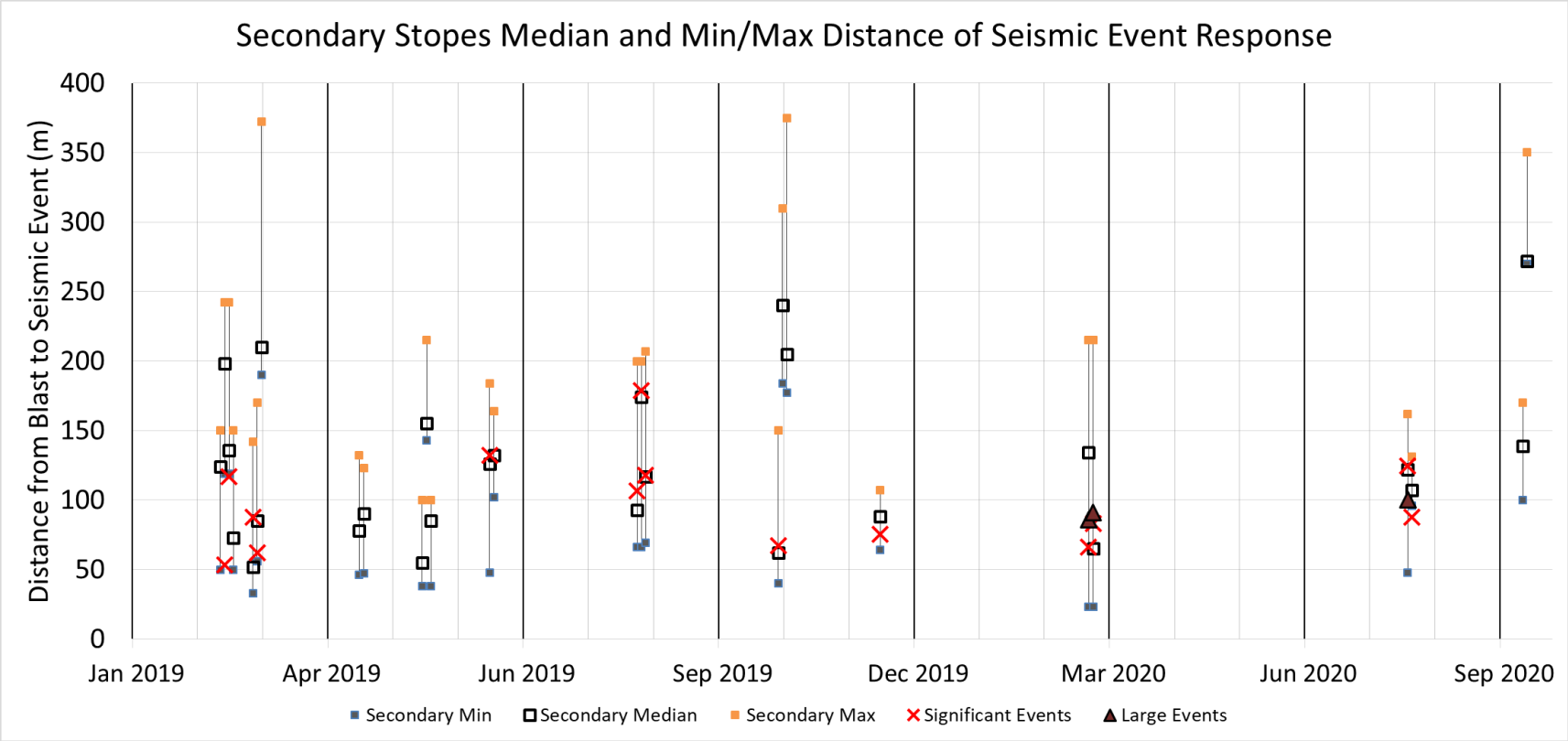

Figure 47 - Secondary stope median, maximum and minimum seismic responses overlain with the significant and large events

4.2.7 Conclusions

Secondary stope responses were almost entirely observed to have a response greater than the primary stope responses, in all categories: Minimum seismic event distance; maximum seismic event distance; and median seismic event distance.

Aseismic zones were not observed in early primary stope mining, but did appear in early 2020. Aseismic zones around secondary stopes remained relatively stable throughout the time period of investigation.

Large events are consistent across primaries and secondaries, with all 9/9 occurring within one standard deviation of the mean. The event locations found in this work contrast work done on caving mines, which has shown in the larger events at further distances within the seismogenic zones (Abolfazlzadeh, 2013). The large events show an increasing distance trend over time. This difference likely stems from the difference between blasting induced stress change and the kinematic driven response in caving mines.

Large events are known to occur at distances not normally expected based solely on stress change, but instead are a result of the combination of stress change and geological structures (Vallejos, 2010).

Although significant events involve a lot of scatter, over time their distance has not significantly changed. Interestingly, the stope median responses have changed, especially in the case of primary stopes, leading from significant events being primarily closer than the median response to exclusively further than the median response.

4.3 Median Seismic Response Time for 24h Post-Blast

Observing the median response time, for the 24 hours following any given blast, allows for an understanding of how quickly the seismic response occurs following a blast. Similar to the use of median distance in Section 4.2 above, use of a single value for median response time will allow for a straightforward value to quantify the response.

Figure 48 shows how the median blast time for a blast taken in the CH-110-134-E Stope on December 30, 2019 was derived. The time at which the 50th percentile event occurred can reduce a series of seismic events down to a single value. In Figure 48 there are 146 events in the 24 hour blast response. The median time after blast is 49 minutes and 13 seconds.

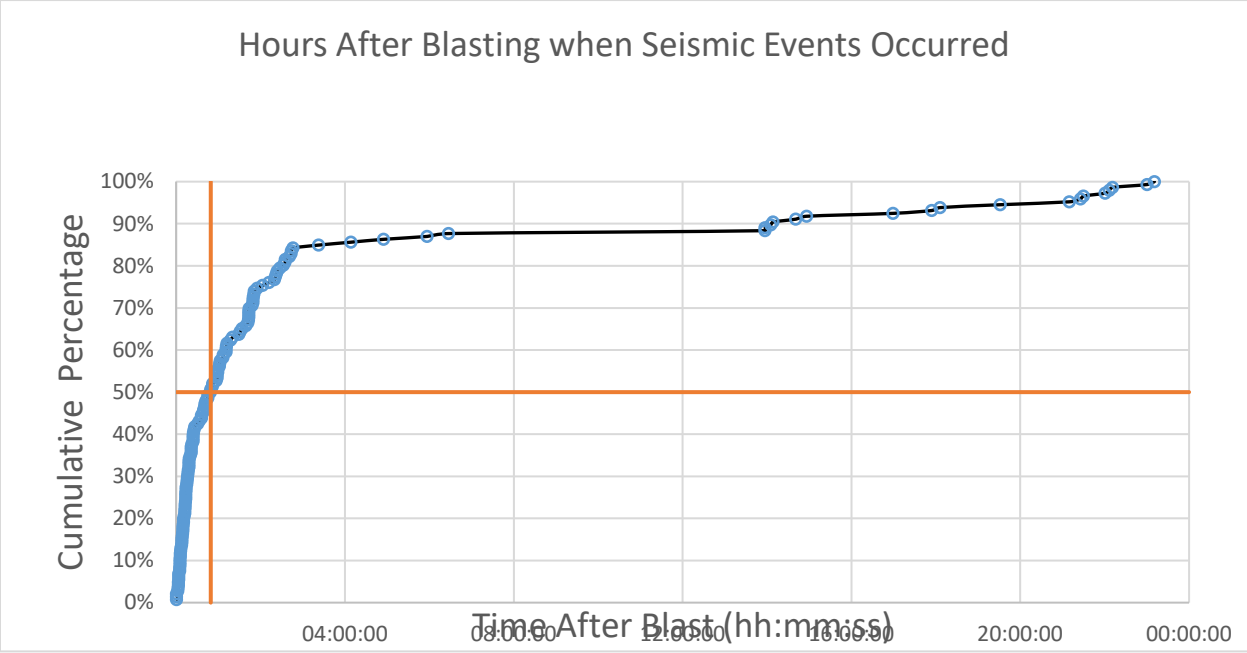

Figure 48 - Sample median seismic response calculation for 146 events from CH-110-134-E stope blasted on December 30, 2019

4.3.1 Total Seismic Response

For primary stopes, the median response time was from almost immediately up to about two hours, with 4/7 median responses greater than an hour. By mid-2019, all the remaining median responses for primary stopes were less than one hour. Over time, the median response time for primary stopes appeared to gradually decrease with less overall deviation. Figure 49 shows the median time of seismic event response for the blasts taken over the 16 month period.

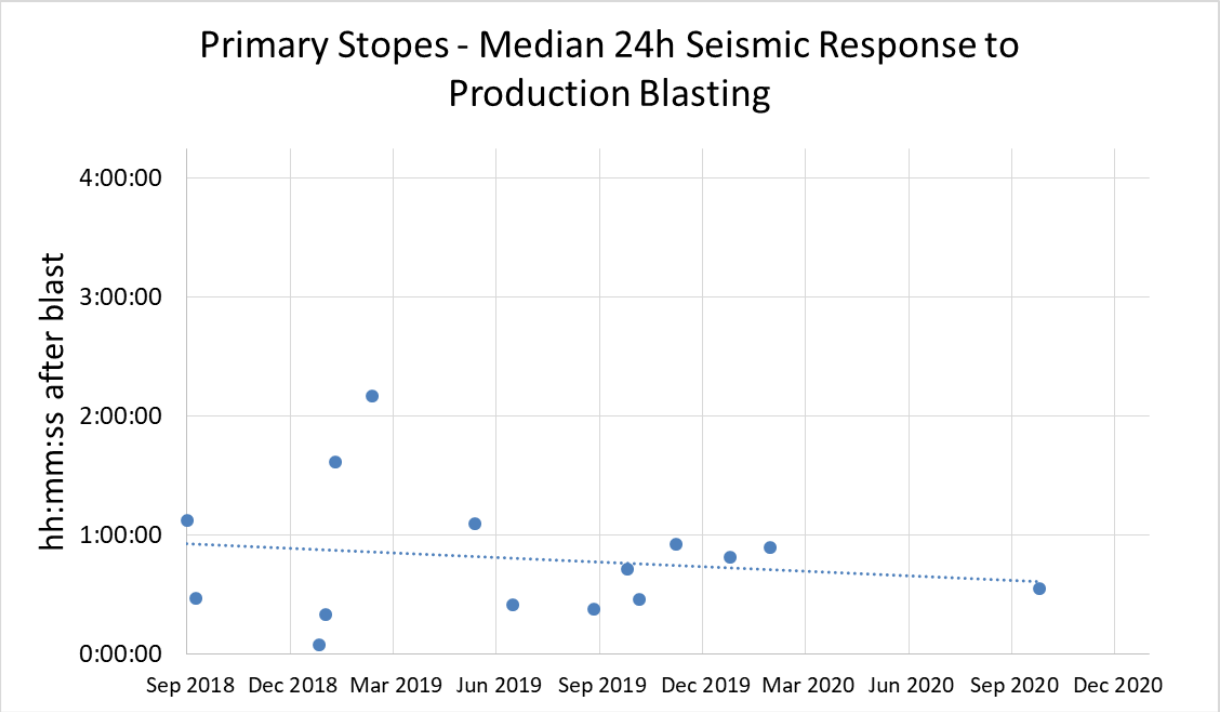

Figure 49 - Median seismic response time for 24h following production blasting for primary stopes

Figure 50 shows the median response time for the twelve secondary stope blast responses. Similar to the primary stopes, there is a gradual decrease in the median response time for the secondary blast responses. However, the secondary stope blast median response time is significantly greater than the primary stope blasts. Figure 50 shows only 4/12 secondary stope

blast responses to be less than an hour, in contrast to 11/15 primary stope blast responses occurring in less than one hour.

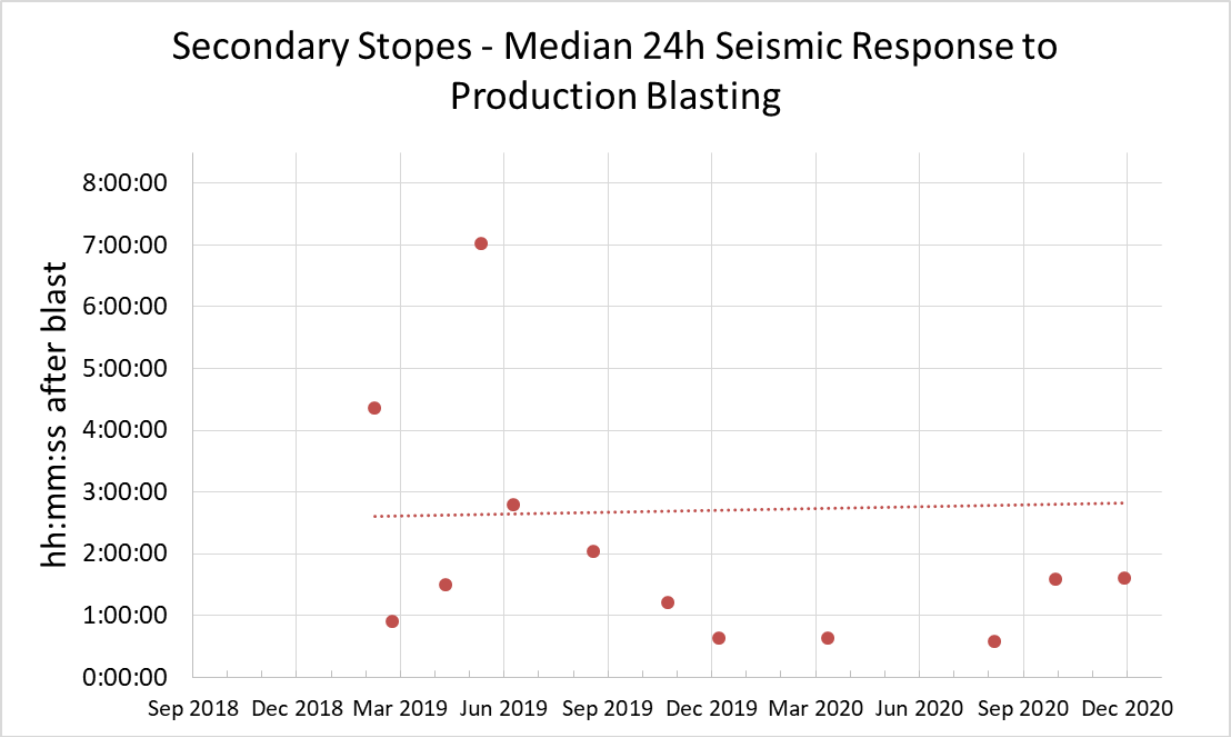

Figure 50 - Median seismic response time for 24h following production blasting for secondary stopes

4.3.2 Significant ($M_L \geq 0.0$) or Large ($M_L \geq 1.0$) Seismic Events After Blasts

Figure 51 below shows the median seismic response time for all events in the 24 hours after a blast, overlaid with any macroseismic events which occurred during that same time frame.

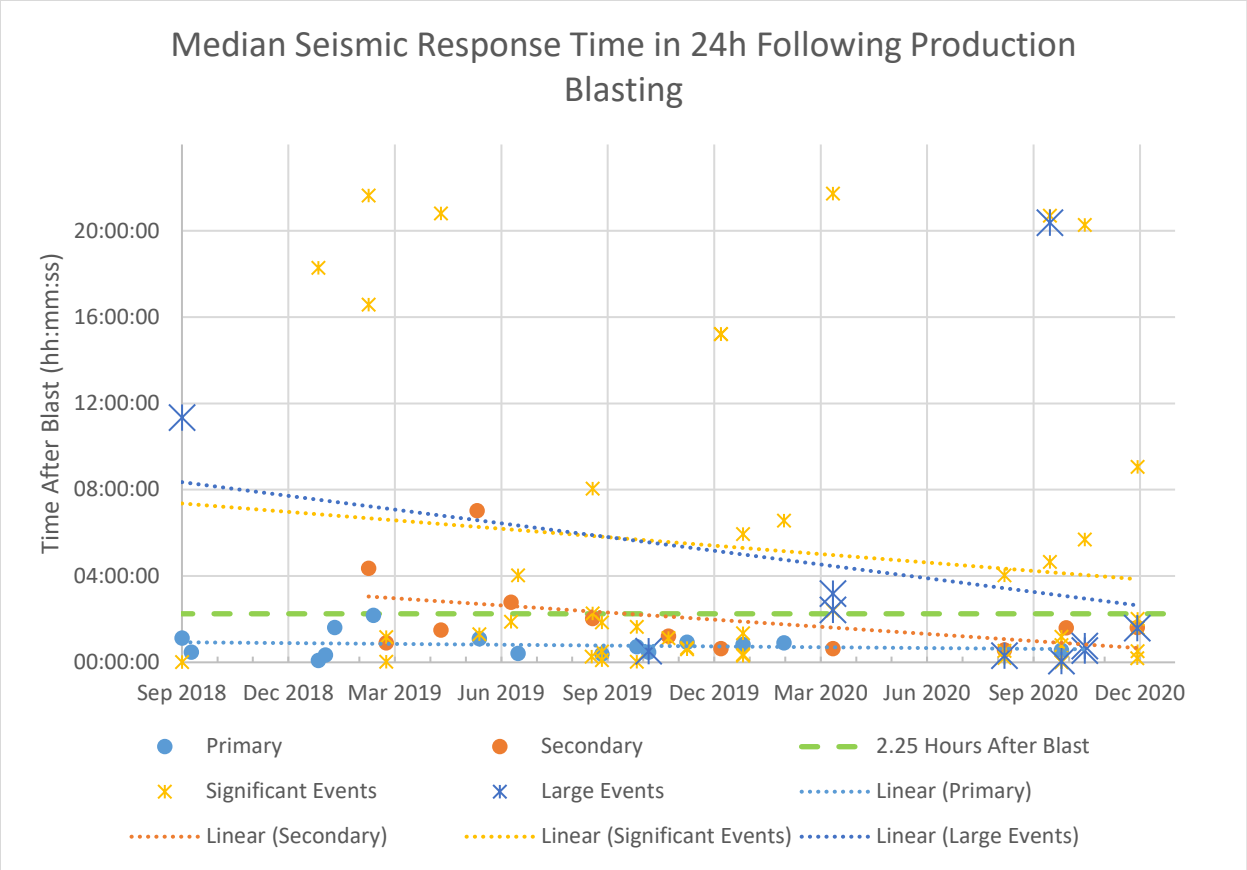

Figure 51 - Median seismic response time for 24h following production blasting for all stopes, overlain with the significant (M_L >0.0) and large (M_L > 1.0) events

As discussed in the previous sections, the median response time for both primary stopes and secondary stopes are relatively unchanged over time. This is in contrast to the macroseismic events, which show reducing trends in both significant and large events.

Over the entire dataset, the average response time for all significant events was 5h12m, with a standard deviation of 7h9m. This consisted of an average of 3h50m for primary stopes and an average of 6h21m for secondary stopes.

Different than the significant events, the average response time for all large events was 4h6m, with a standard deviation of 6h37m. This consisted of an average of 2h38m for primary stopes and an average of 5h34m for secondary stopes.

In both cases, the macroseismic events had shorter averages in the primary stopes than the secondary stopes.

Approximately half (14/27 or 52%) of primary stope macroseismic events are greater than the median stope response. A slightly higher percentage of secondary stope macroseismic events (16/27 or 59%) are greater than the median stope response.

Very few (4/27 or 15%) of primary stope macroseismic events occur more than 8 hours after a blast. This is in contrast to the secondary response, in which 9/26 (or 35%) occurred greater than 8 hours after a blast.

This indicates that secondary stopes have an increased likelihood of producing significant or large events at during a longer time frame.

Seventy eight percent (7/9) of all large (M_L >1.0) events occurred within 4h following a blast.

The majority of both significant and large events appear to occur shortly after blasting. When combined with the observations about the proximity to the median in Section 4.3 above, the implication of these large events happening close to the blast, but with a slightly higher propensity to be above the median response, once again suggests that the macroseismic events appear to be largely related to stress change.

Observing Figure 52 below, the median response time plotted against the times of the macroseismic events shows some interesting trends.

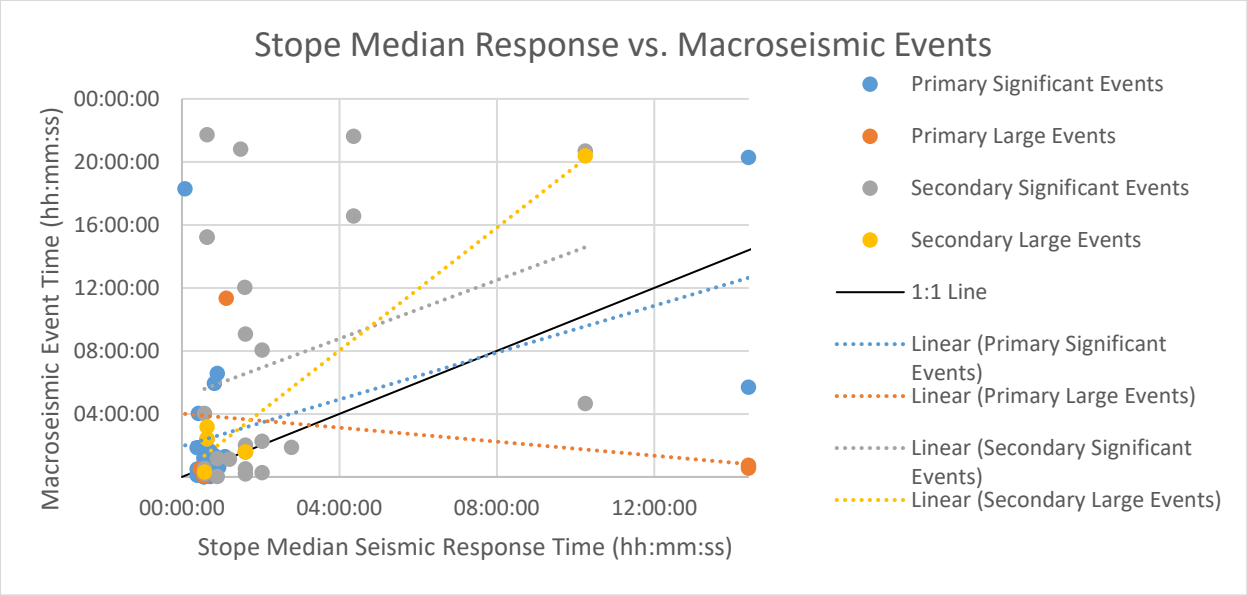

Figure 52 - Median total seismic response time compared to macroseismic event timing

Secondary stope blast triggered large events may be correlated to the median response time, however current sample size is limited. Some evidence of a trend between primary stope blast significant events and median response time also exists. With a limited sample size, more exact correlations cannot be achieved, however any relation between the macroseismic events and the median 24 hour response time of a stope may assist operations personnel in re-entry protocols. Also observable in the figure above, all primary stope blast related large events occur within twelve hours after a blast, however it is recognized that the sample size is quite small. The sample size following primary stope blasts was 22 significant and five large events. Following secondary stope blasts it was 24 significant and five large events.

In an attempt to understand mechanism better, Figure 53 and Figure 54 below show all macroseismic events and their time after the blast, scaled by their Es:Ep ratio. The use of S:P energy ratio (synonymous with Es:Ep) is a common method of evaluation of seismic source parameters as it relates strongly to the seismic source mechanism. Shear failure, typically

represented as shear failure mechanism events, generally have Es:Ep above 10 (Boatwright and Fletcher, 1984; Cichowicz *et al.*, 1990; Simser, 2006).

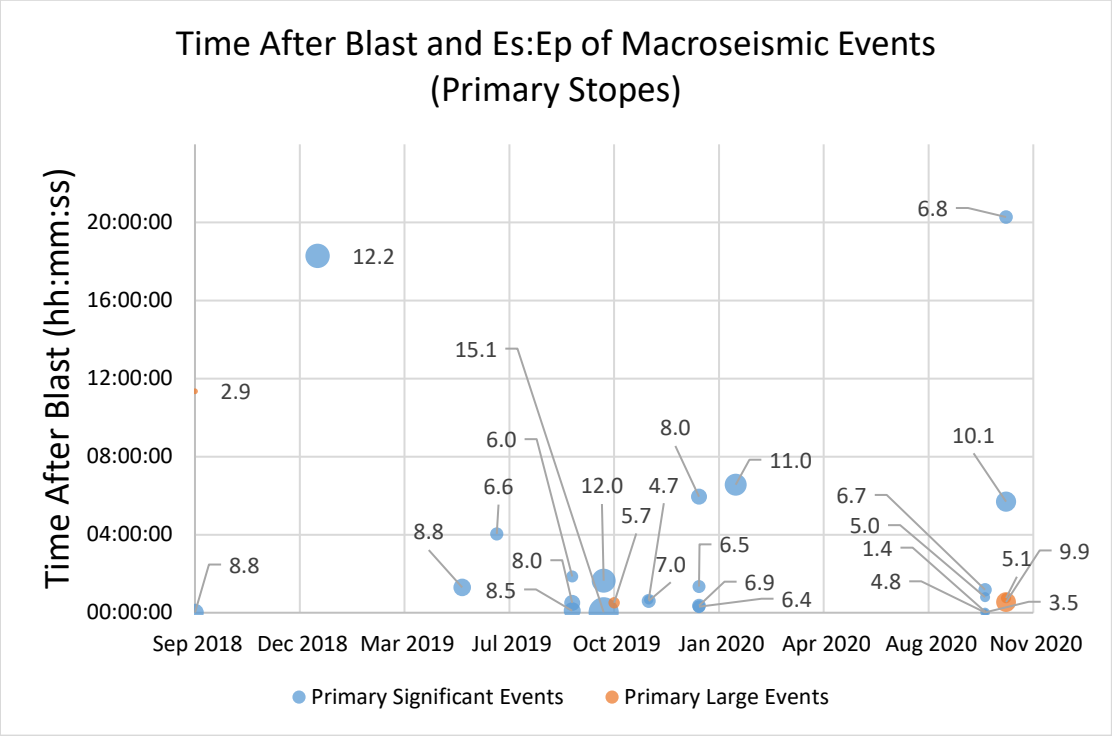

Figure 53 - Es:Ep ratios contrasted against time within the data set and time after blasting (primary stopes macroseismic events)

From this figure it can be observed that generally, the Es:Ep tends to be higher with events occurring greater than two hours after the blast. That being said, all large and the majority of significant events related to primary stope blasting are below 10 Es:Ep, and thus are unlikely to be shear events.

In contrast to the primary stope response, Figure 54 below shows the response of the secondary stope blasts over the same data set.

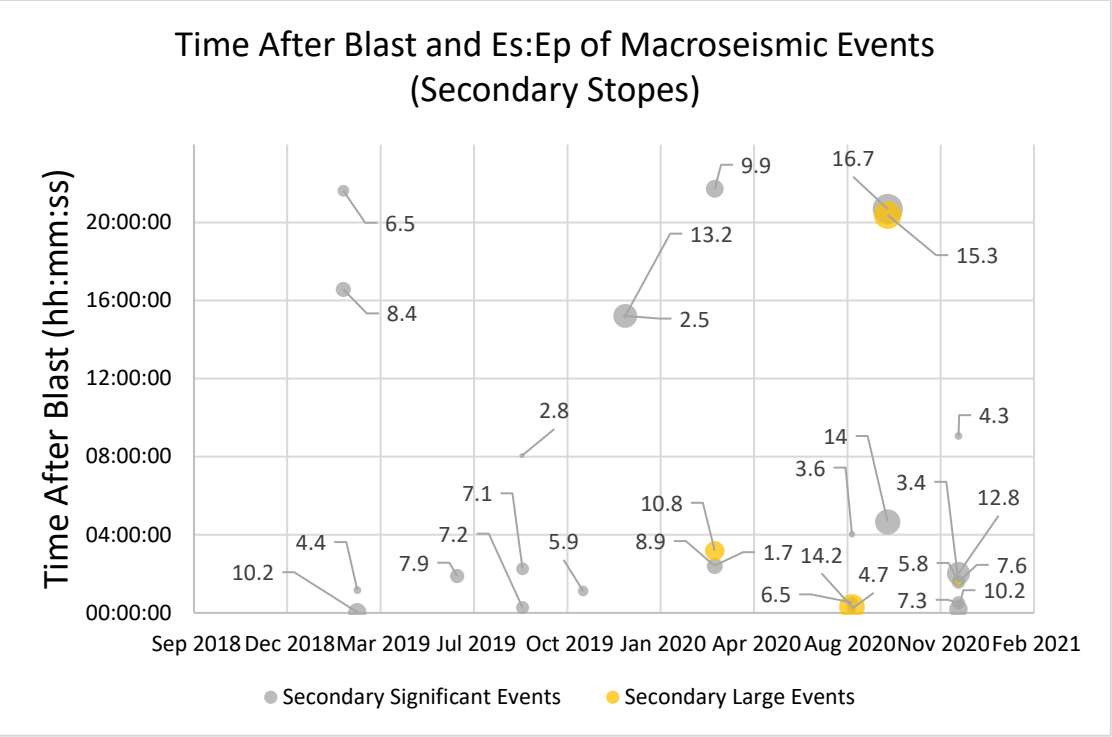

Figure 54 - Es:Ep ratios contrasted against time within the data set and time after blasting (secondary stopes macroseismic events)

This figure shows a higher proportion of shear events (28%), but they are concentrated over the time period from late 2019 to 2021 (35% of that portion of the set). When only the large events are observed, 60% are shear events.

Time of an event after the preceding blast may be an indicator of seismic source mechanism. The average time after blasting that a shear failure macroseismic event occurred after March 2020 was 8h18m. The non-shear events during that same time frame had an average time after blasting of 2h56m, with only two events exceeding five hours.

4.4 Number of Seismic Events in the 24 Hours Following a Blast

Observing the total number of seismic events following any given blast provides some understanding of how the stresses have been redistributed as well as an understanding of the seismic hazard.

4.4.1 Total Seismic Response

Figure 55 shows the number of events which occurred within 24 hours following production blasts within the dataset.

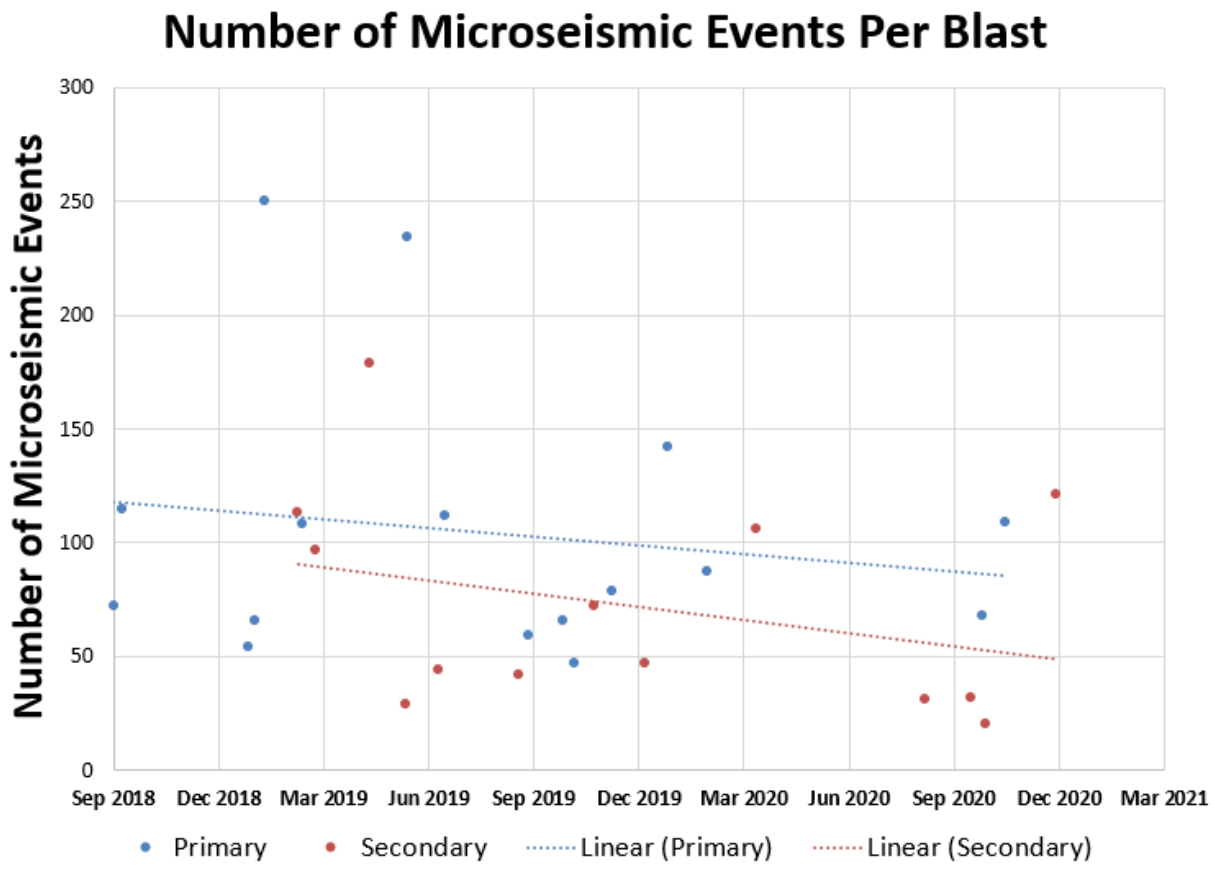

Figure 55 - Number of microseismic events after production blasting over time

Over the time period examined, aside from two primary responses and one secondary response which may be early outliers, the total number of events did not show any significant changes. Primary stopes show slightly higher averages than secondary stopes, but not to any significant degree.

Assuming the microseismic events are driven by elastic stress change, this shows a relatively stable response over time of total responses.

4.4.2 Significant (M_L > 0.0) or Large (M_L >1.0) Seismic Events After Blasts

The response of significant events showed a deviation from the microseismic event response. A clear increasing trend in all events greater than M_L 0.0 was observed. In general, large events began following primary stope blasts late 2019 (aside from a single outlier in 2018). Large events following secondary stope blasts began in very early Q2 2020, and have been occurring regularly since, within the dataset.

Figure 56 below shows the macroseismic responses to stope blasting.

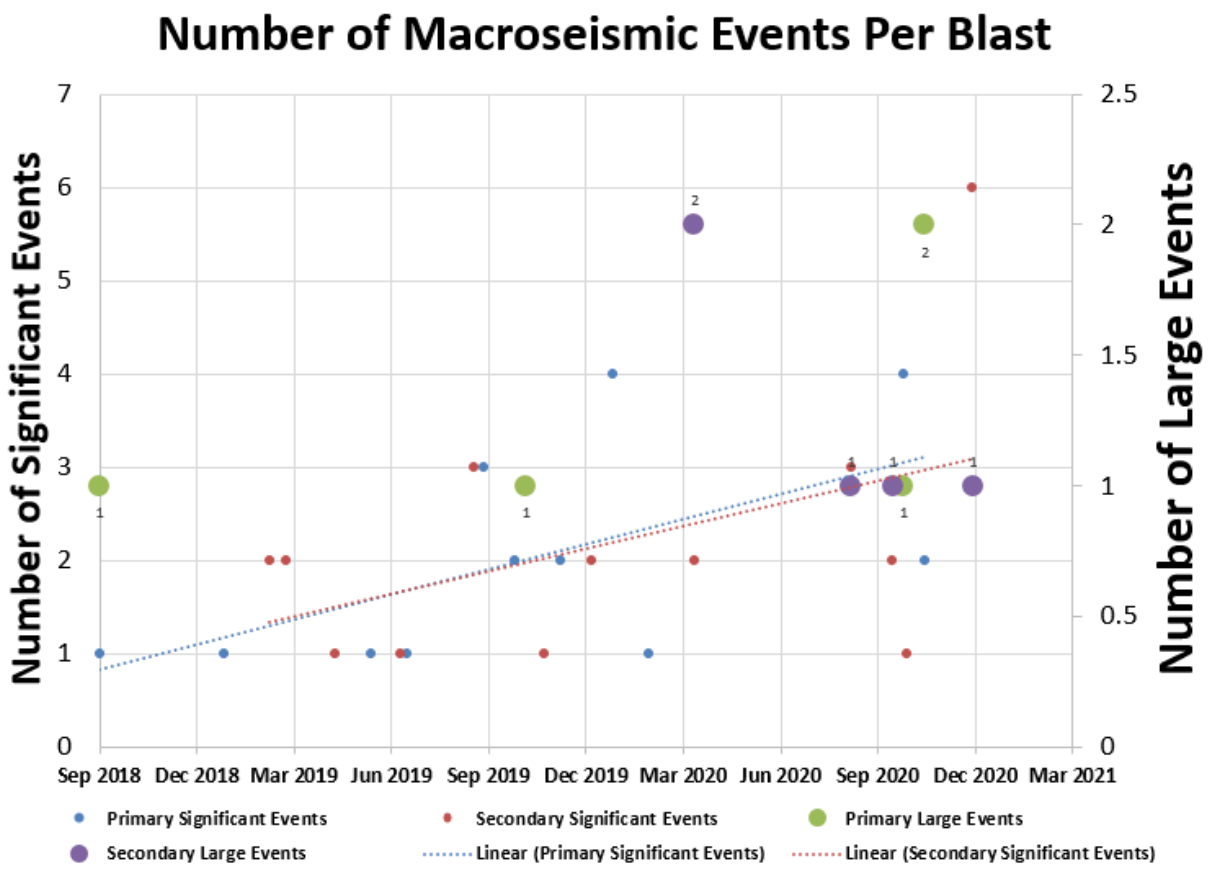

Figure 56 - Number of macroseismic events after production blasting over time

4.5 Events Per Tonnage of Blast

As seen in Figure 57, primary stope macroseismic events show no trend with respect to the blast size of the stope blast. However, for secondary stope blasting, both the significant events and the large events show strong trends. There has yet to be a secondary blast <18,000 tonnes which has resulted in a large seismic event in the 24h following. A trend may exist between blast size of secondary stopes and macroseismic response, checking this theory against future data may assist in quantifying that relation.

.

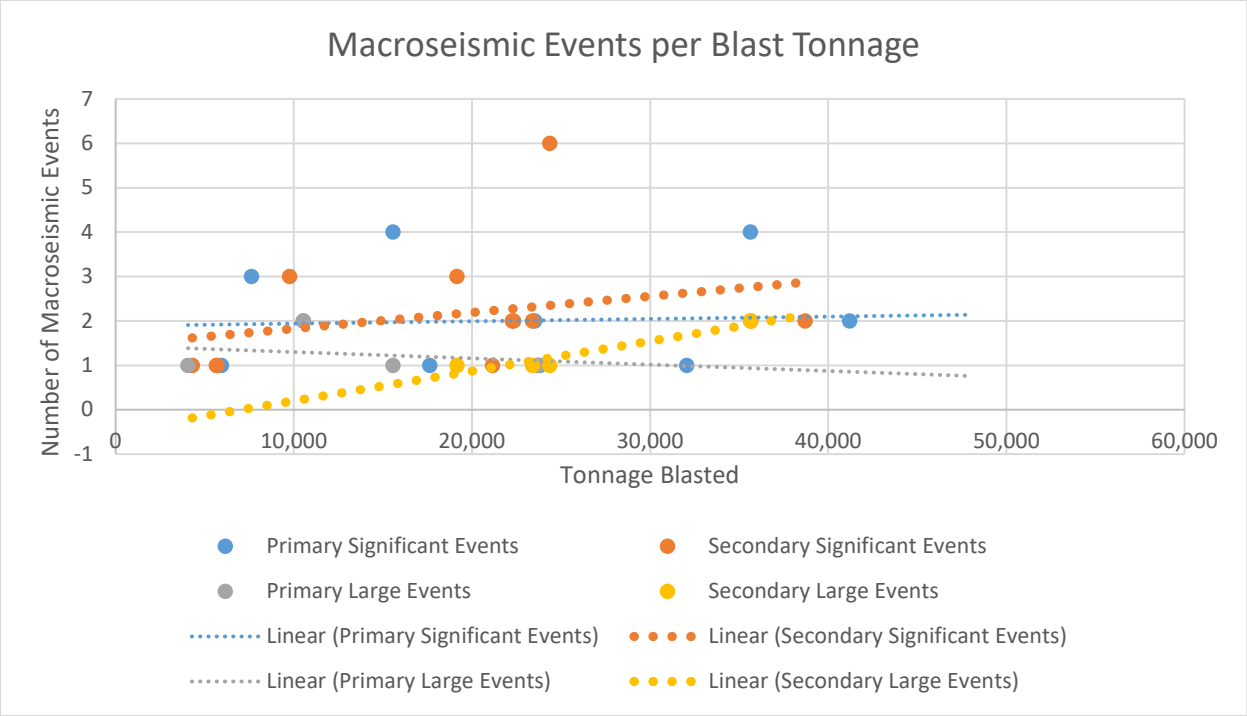

Figure 57 – Number of macroseismic events after production blasting compared to the tonnage of the production blast immediately preceding the response

4.6 Events per Mining Level (Depth)

Figure 58, shown below, is a longitudinal graphic of the Goldex Mine which shows the various ore zones within, as well as the level numbers. With respect to this thesis, the D1 Zone is the area of ore extraction in which the seismic response over time is being evaluated.

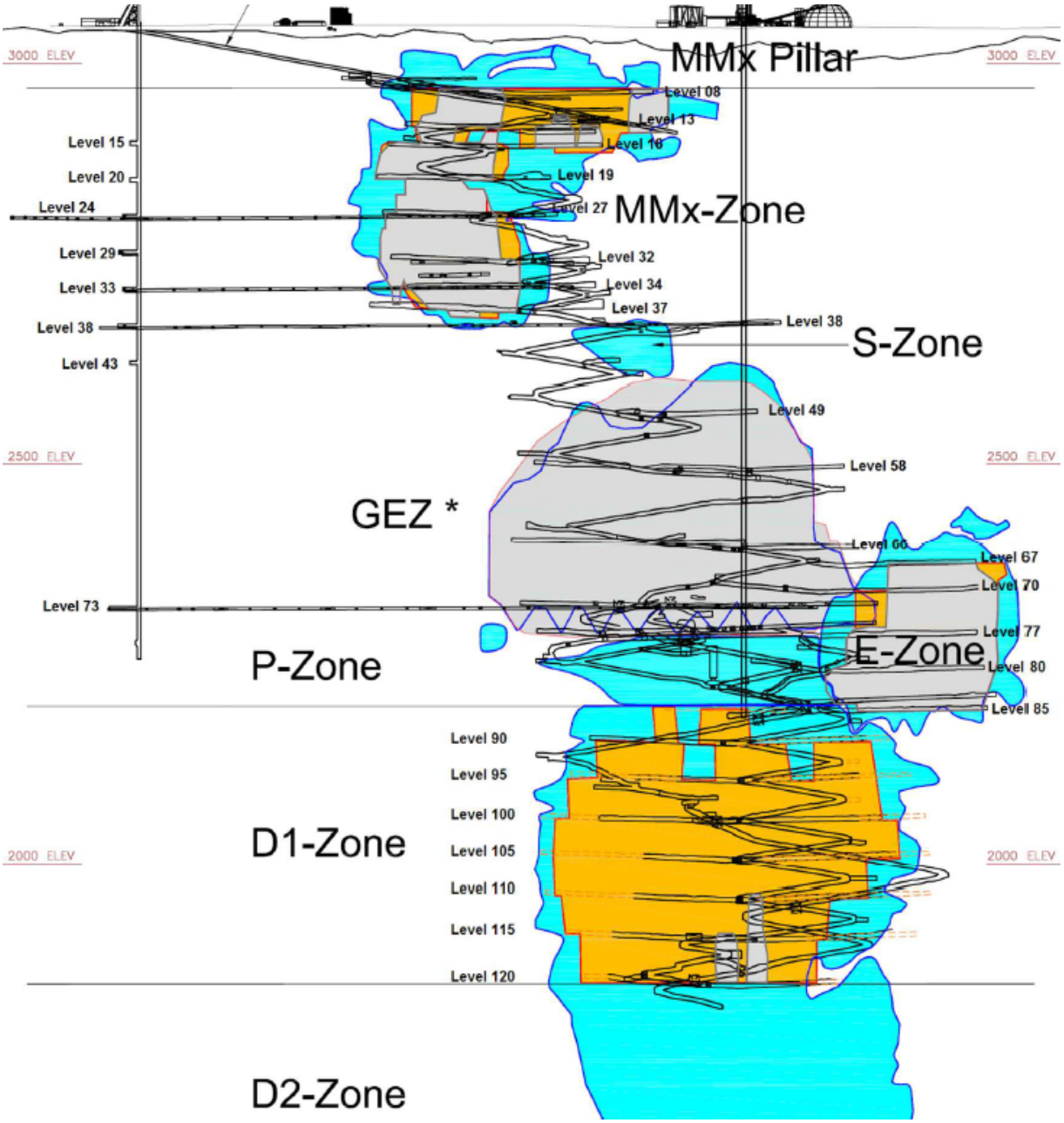

Figure 58 - Longitudinal view of Goldex Mine looking North. Reprinted from PROGRAMME EN CONTRÔLE DE TERRAIN, Mines Agnico Eagle, Mine Goldex, October 2018 (Doucet, 2018)

Conventional mining begins at the bottom of a given zone, removing ore from a level and then progressing upwards to the top of the zone over time. Since extraction of the entire length of the orebody can involve significant engineering complexities, the ore zone on a level is subdivided into manageable widths to be taken out one at a time across the level. These manageable widths

are referred to as panels, and in this particular zone the panels are numbered sequentially starting at around 120 on the west side and ending around 136 on the east. Panels generally run the entire depth of the mine, so panel numbers above or below those values may exist at elevations either well above or below the D1 Zone. Two such panels can be observed in Figure 58, one extending from the Level 120 to the Level 115, the other from Level 120 to Level 110, coloured in light tan.

Figure 59, below, shows a 3-d isometric view of this same zone, with the level development indicated in salmon and the various ore stopes located across the panels in contrasting colours. The stopes are in most cases one panel wide, with some potential deviation at the edges of the orebody.

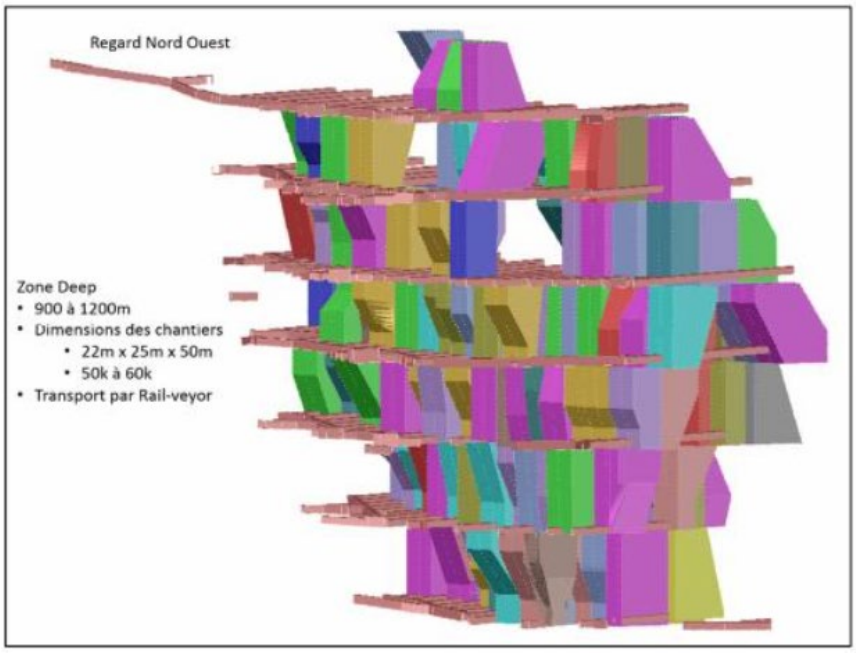

Figure 59 - Isometric view of D1 Zone looking North West. Reprinted from PROGRAMME EN CONTRÔLE DE TERRAIN, Mines Agnico Eagle, Mine Goldex, October 2018 (Doucet, 2018)

One final view, taken looking south, shows various panels and levels in stages of excavation with the 3-d wireframes representing ore that has been previously removed and backfilled. It is

apparent that every second panel is generally skipped during mining. These skipped panels are referred to as secondary panels. This mining method is done to both increase production by mining multiple panels at once, while also managing the changes in stress during the extraction process. The design intends to concentrate the stresses from the removal of the primary panels into the secondary panels, which will yield those secondaries, and ultimately push the stresses to the extents of the orebody and outside of the active mining zones.

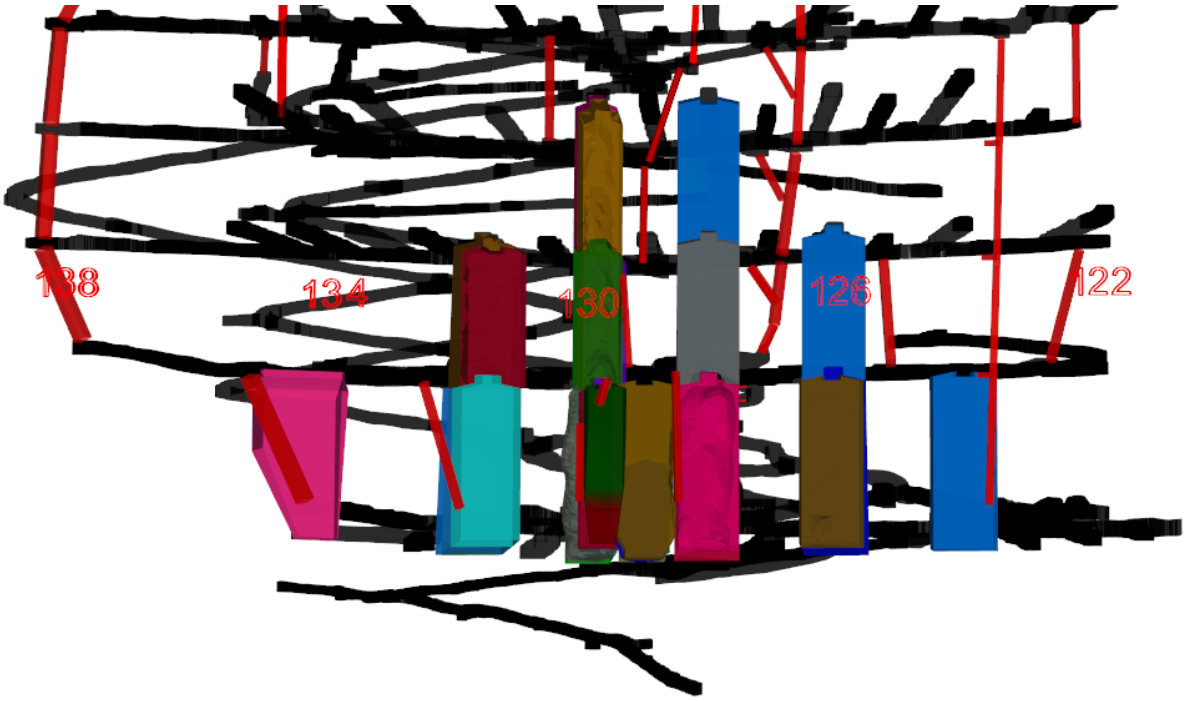

Figure 60 - South Facing 3-d view of extracted ore Q1 2019

4.6.1 Primary Stope Response per Level

Figure 61, seen below, shows the number of both microseismic and macroseismic events that occurred per level post-blasting using the dataset.

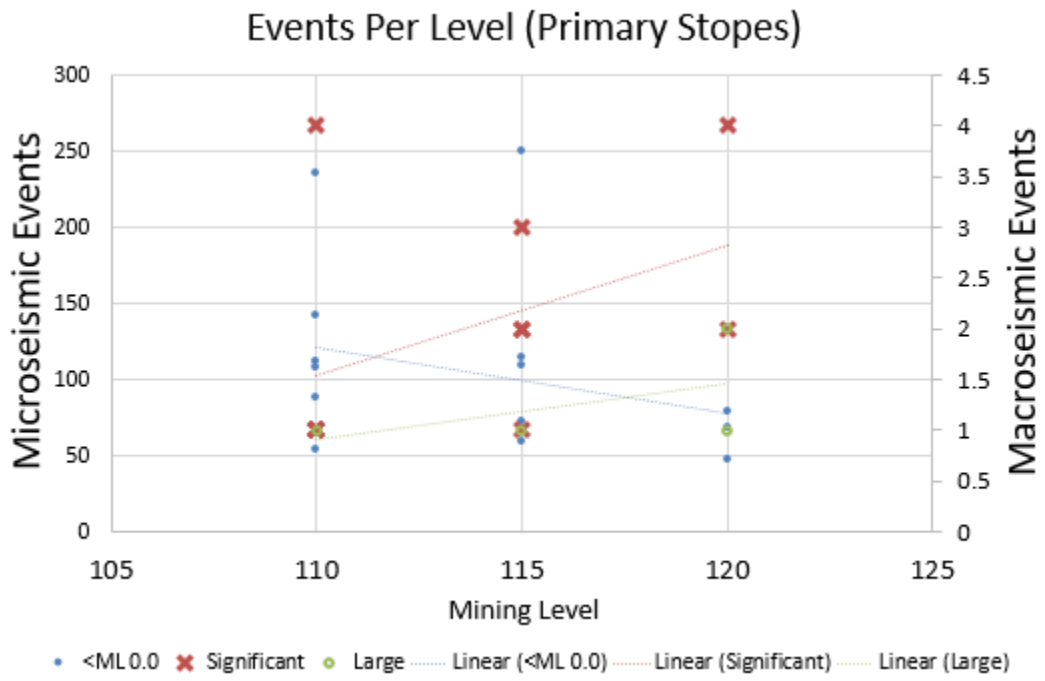

Figure 61 - Total number of seismic events recorded after production blasting per mining level of primary stopes

Figure 61 shows relations between the macroseismic events and levels within the D1 zone where they occurred throughout the dataset. In addition, it shows the microseismic events and that same relation. Normally, it would be expected that an increase in depth would relate to additional seismic response, due to an increase in *in situ* stress. In addition, over time a similar expectation to greater extraction would be expected, due to increases to the mining-induced stress.

What was observed during primary stope blasting, a time of generally lower extraction ratio than secondary blasting, an increasing trend between the depth and the macroseismic events was observed. This follows general trends identified in other work (Gibowicz and Kijko, 1994). Due to mine sequencing being from bottom to top, deep primary stopes which are associated with this increase in significant or larger events have been mined relatively early in the mining sequence, at a time when limited overall extraction of the level is achieved. This may be explained through

the remaining ore, which has not yet been extracted, experiencing sufficient confinement that deformation or yielding is problematic until significant stress changes had occurred – resulting in the larger seismic responses.

Conversely, the total number of events is trending downward with depth. This indicates that the failure mechanism between the large events and the small events is different. Initial investigation of significant structural geological features, such as the dyke swarm or the dylonite discussed in Section 3.2.2.1, showed no obvious trends. Further evaluation may assist in determination if structural geology plays a role in the larger event failure mechanisms. Further discussion on these different trends can be observed in other sections and is discussed in more detail in Section 4.3 and its relevant subsections.

4.6.2 Secondary Stope Response per Level

Over the time period evaluated, the mining sequence had not yet reached the extraction phase where secondary stopes had reached the same elevation as the primary stopes. This resulted in an evaluation of only the two bottom levels, with the results observable in Figure 62 below.

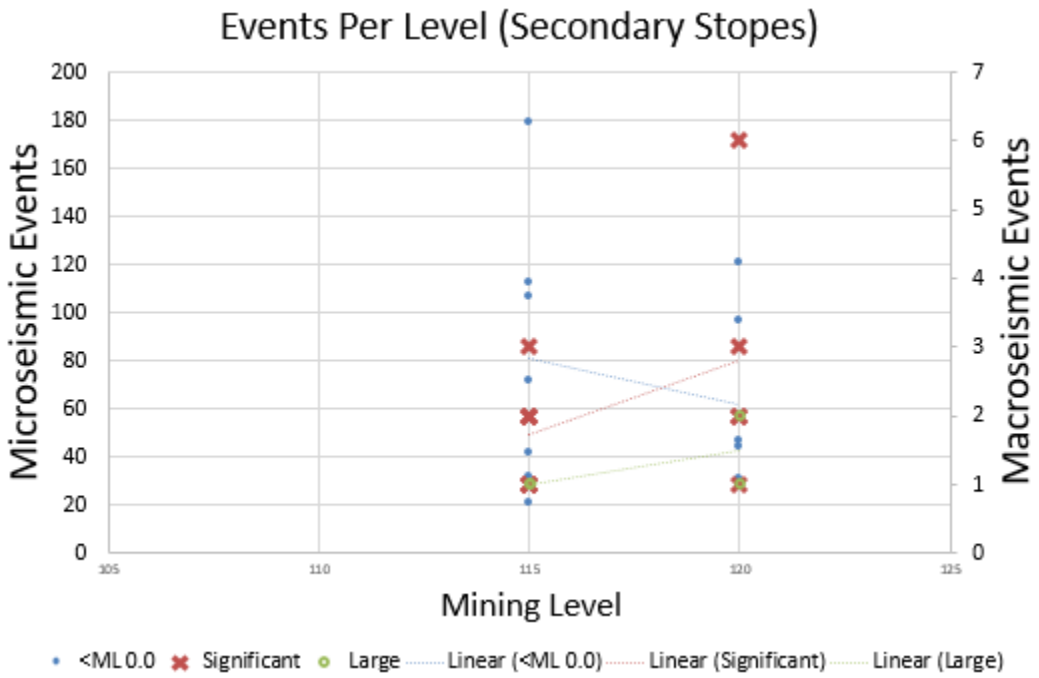

Figure 62 – Total number of seismic events recorded after production blasting per mining level of secondary stopes

As was observed with the primary stopes, a trend of larger seismic events with depth has appeared. In contrast, very weak correlation in trends of microseismic events between the levels was observed, indicating that, with respect to secondary stopes, the level is independent of the microseismic response.

4.7 Number of Seismic Events per Panel Blasted

Figure 58, Figure 59, and Figure 60 in Section 4.5 Events Per Tonnage of Blast (above) show the general arrangement of the panels relative to the overall orebody.

All stopes were plotted, regardless of depth, on a chart against the numbers of microseismic and macroseismic events that occurred during the seismic reponse to stope blasting within the panel. Figure 63 below shows the plot of that data. The panels are oriented West-East, with the 122

panel being furthest West and the 134 panel being furthest East. Figure 63 could be visualized as looking North.

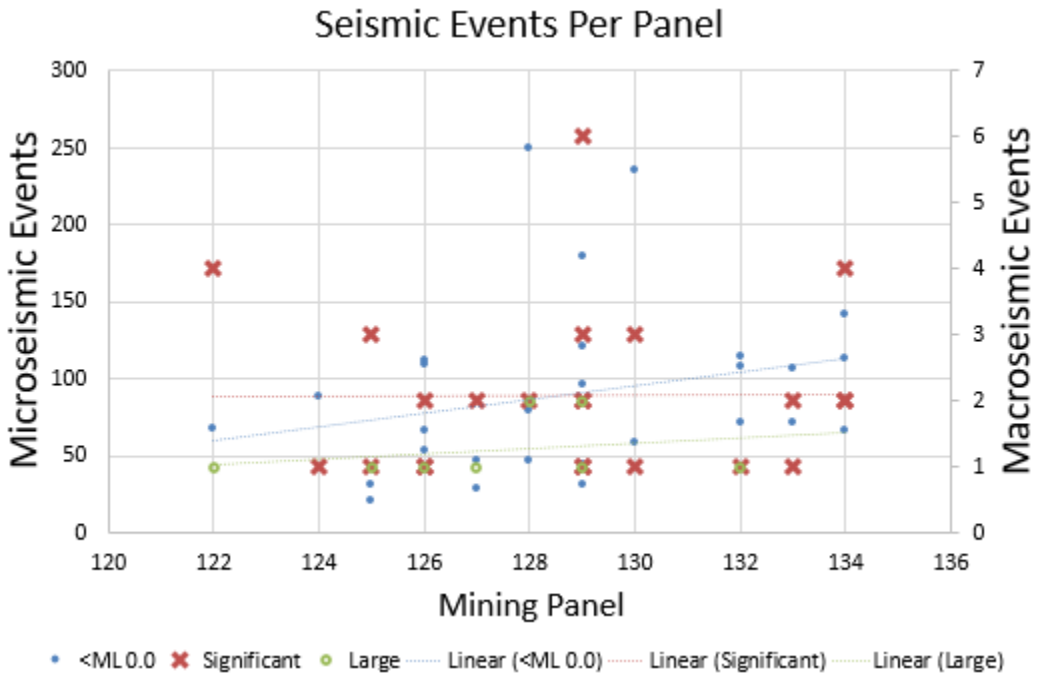

Figure 63 – Total number of seismic events recorded after production blasting per mining panel of the production blast

From this data, it is observed that the highest numbers of both macroseismic and microseismic events occur when blasting between the 128 and 130 panels. These panels were the lead panels when blasting this zone of the mine due to a series of factors including: ramp access; the thickest part of the orebody located in these panels; the desire to increase production by mining two fronts at a time (one East and one West of the primary panels); and the intent to reduce stress concentrations by not leaving substantial pillars behind during mining (only secondary stopes which were intended to yield in a controlled manner).

As observed in the level based analysis of seismic response, the earlier mined portions (in this case the lead panels), experience more macroseismic events. The panel based observation also shows an increase in microseismic response; a result not observed in early mining at depth. The

implication is that as the lead panels rise in elevation, the larger number of microseismic events increase, due to a change in mechanism.

This increase in response is likely due to the principal stress being East-West, which would exhibit the largest stress field changes when opening up the first openings in a North-South direction.

East side panels from panel 132 show a higher average total response (average 99) than West side panels below 128 (average 63). Conversely, the Western panels show more macroseismic events, which may be the influence of geological structures. A very brittle, soft dyke crosses through the lower west portion of the mine, which may contribute to greater levels of macroseismicity either within the dyke itself or in the adjacent more massive waste or ore.

The abutment panels (those furthest East or West of the orebody extraction) show elevated macroseismic events, with the East abutment also showing an increase in microseismic events. This is likely due to stress accumulations in the abutment in later extraction phases.

Comparing primary panels (even panels) to secondary panels (odd panels), 64% of significant or larger events occur in secondary panels. Thirty-one percent of all significant or larger events, in the dataset, are a direct result of mining in the 129 panel. Further examination of the mechanism at play may lead to an improvement of seismic hazard management.

4.8 S-Wave Energy to P-Wave Energy Ratio (Es:Ep) Median Response

As stated in Chapter 2, the ratio of s-wave to p-wave energy is an indicator of seismic source mechanism.

In order to evaluate this ratio, a series of events over a time period can be plotted on a cumulative frequency graph, an example of which can be seen below in Figure 64.

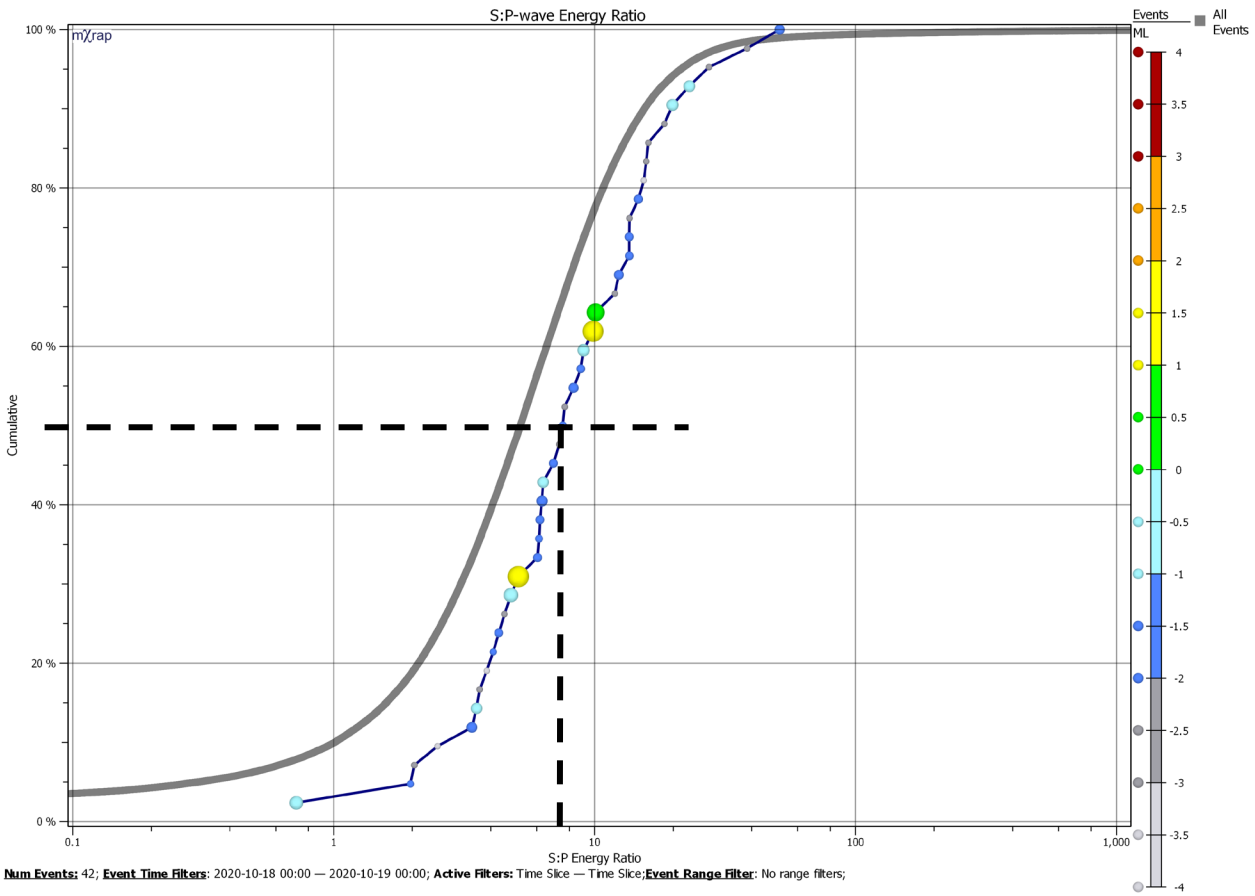

Figure 64 - S:P Energy Ratio (Es:Ep) of Seismic Response to Blasting a Primary Stope on October 18, 2020

Observing the median Es:Ep for the 24 hours following any given blast allows for an understanding of potential seismic source mechanisms among the events, and the total response. Similar to the use of median distance in Section 4.2 and median response time in Section 4.3 above, use of a single value for median Es:Ep will facilitate a simple value to quantify the response. Figure 64 shows a dashed line indicating a median Es:Ep in this case as 7.5.

Figure 65 below shows no observable changes over time to the median Es:Ep ratio. Overall values show relatively limited shear (Es:Ep >10), and almost no obviously attributible values to entirely volumetric fracturing (Es:Ep <3).

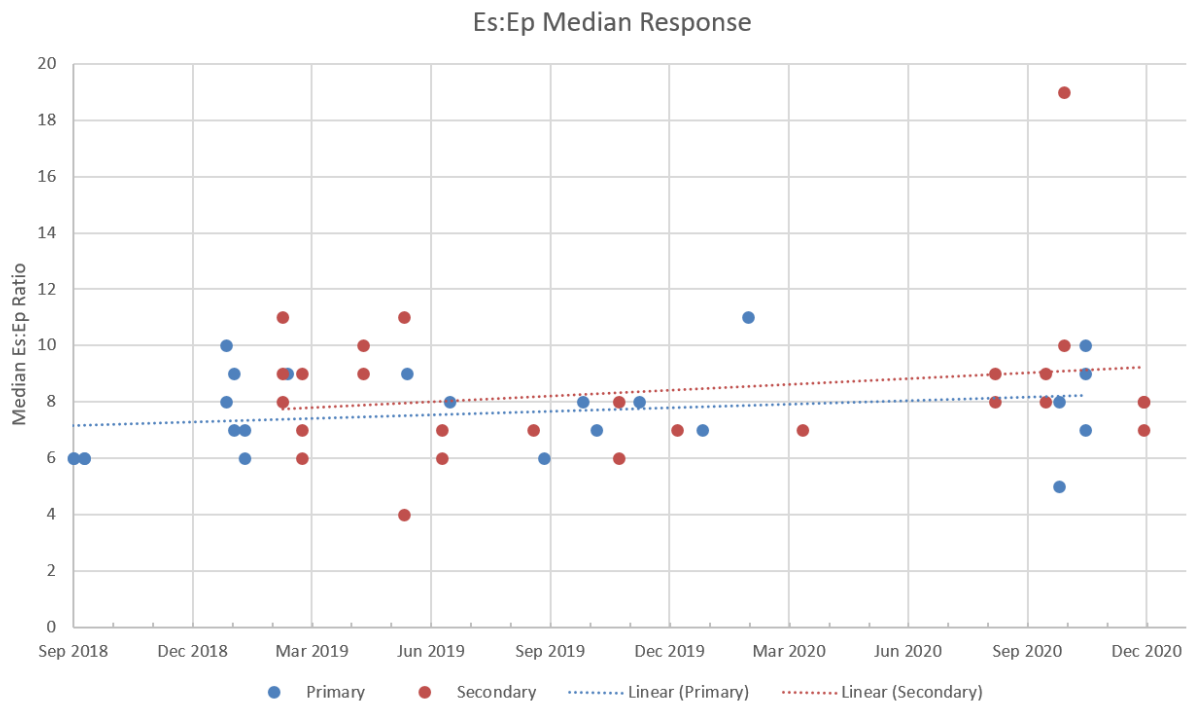

Figure 65 - Es:Ep median response for total seismic response in primary and secondary stopes following production blasting

4.9 S-Wave Energy to P-Wave Energy Ratio (Es:Ep) Percent Shear Response

In contrast to the median Es:Ep observations above, significant observations were available when the percent shear response was examined. A similar method to the determination of median Es:Ep was done for all populations of events, in place of using a median the percentage of events above an Es:Ep >10 were used. The percent shear response for the 24h following each blast in the dataset were compiled and is represented in Figure 66 below.

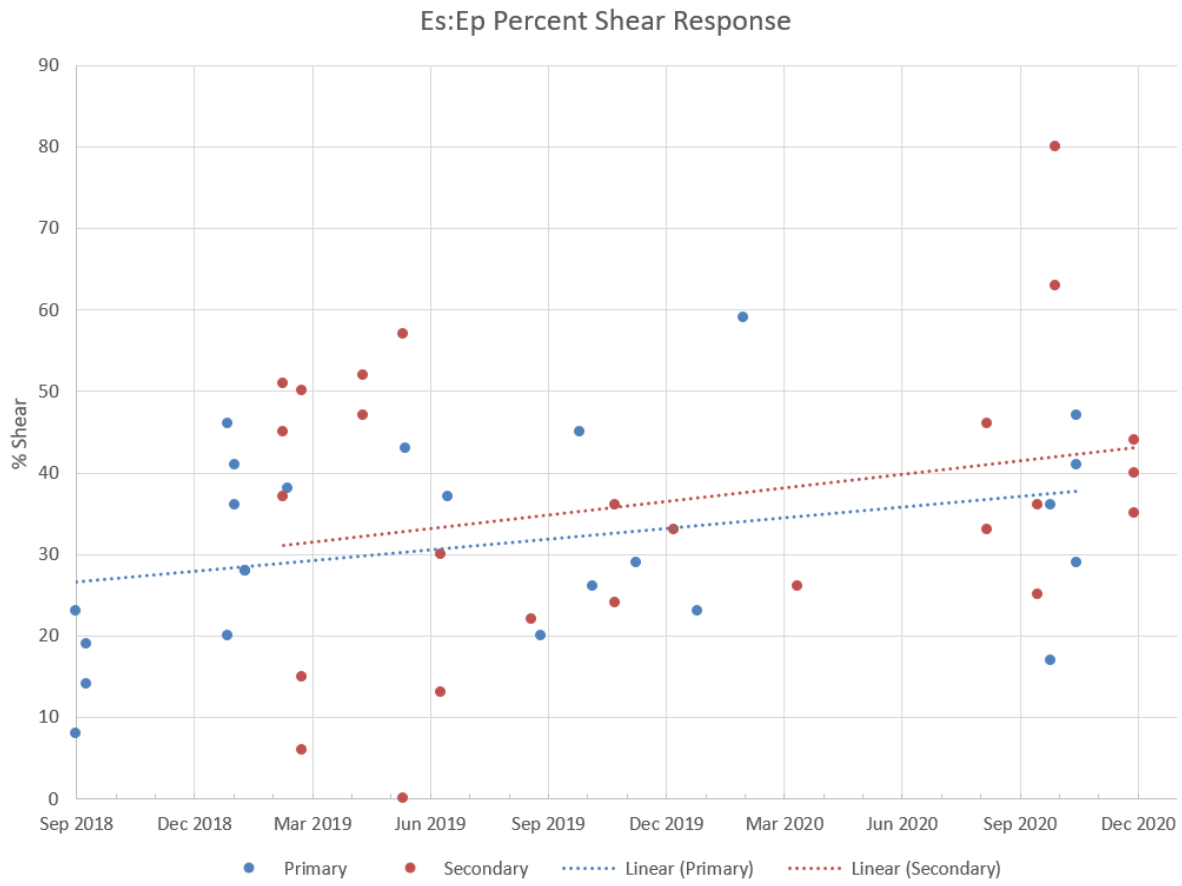

Figure 66 - Es:Ep percent shear response for total seismic response following production blasting

Over time, a gradual trend of increasing shear response was observed. This observation is supported by the increase in Es:Ep over time for both primary and secondary stopes.

The lowest values (<20%) were observed prior to Q2 2019; not only did those low values cease, the highest shear percentage values (>60%) began appearing Q3 2020. This change in percent shear indicates a significant change in mechanism over time.

The change in mechanism is further highlighted when it is observed that prior to Q2 2020, 49% of all responses in both primary and secondary stopes had less than 30% shear. After this time period, this reduces to 21%. This potential change in mechanism is more pronounced in the

primary stopes than the secondary stopes, with only 12.5% of late mining primary stopes having less than 30% shear response.

Plotting the Es:Ep values for the macroseismic events over top of the % shear response for the 24 hours following the blast resulted in Figure 67 below.

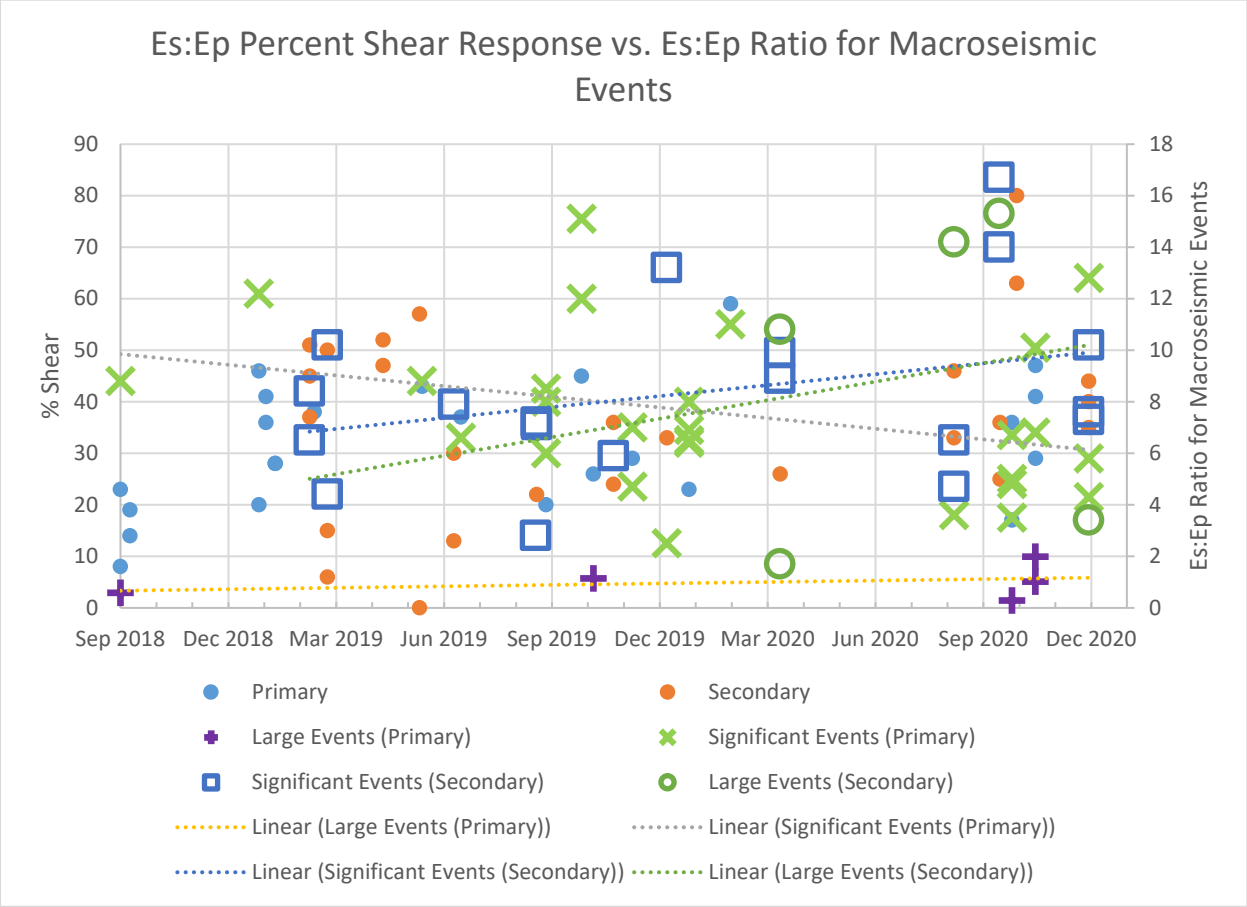

Figure 67 - Es:Ep percent shear response and Es:Ep ratio for macroseismic events following production blasting

From this figure, it is apparent that all but one primary macroseismic events are non shear up until late 2019. The macroseismic events post Q1 2020 show a similar lack of shear events, however have changed to more shear over time (32%).

Also of note from this figure, is the lack of any macroseismic activity following secondary blast responses which show a high percentage of shear response (above 52%)

The trends observed in this graph show the change in mechanism over time starting around late 2019.

4.10 d-value of Seismic Response to Blasting Over Time

d-value, a representation of the ratio of seismic moment to seismic energy, can indicate if the seismic response to a given stress change is "softer" (occurs more slowly with more moment for a given energy) or "harder" (occurs with less moment for a given energy). The value is a constant related to the stiffness of the rock mass system (Mendecki and van Aswegen, 2001). Average d-values in large populations of events in underground, Canadian Shield hard rock mining have been found to be between 1.31 (Carusone, 2018) and 1.14 (Brown, 2015). Figure 68 below shows the plot of the d-value of the seismic responses for all the blasts within the dataset used for this thesis.

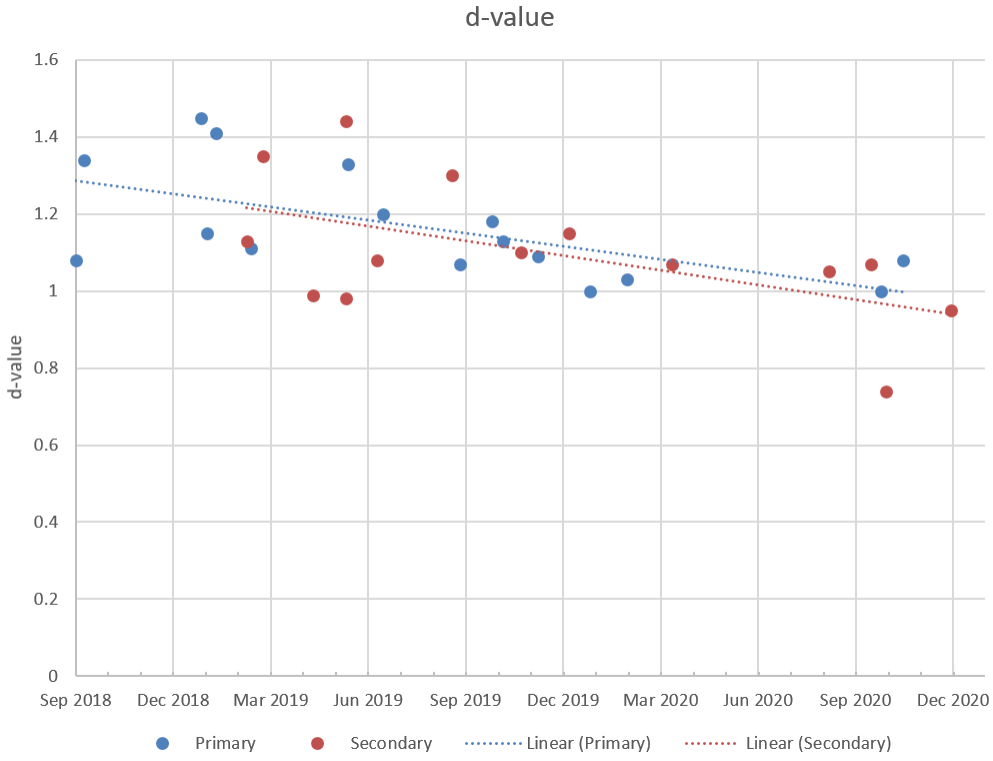

Figure 68 – Average d-values of total seismic response post blasting for primary and secondary stopes

It is observed that not only is there a very significant decreasing trend over time, but many values are well below averages found throughout similar mines. This indicates a very soft response, yet is in contrast to the previously discussed Es:Ep ratio percent shear response in the subsection above. The six d-values less than or equal to 1.0 indicate much softer stope responses over time, which contrasts with the numbers of significant events happening later in the dataset. Additionally, the observation that 29% of secondary stopes over the entire 16 month period are at or below a 1.0 d-value may stimulate further work.

Generally, higher d-values are more common in early mining (Mendecki *et al.*, 1999) whereas later mining involves yielding, and the associated lower values. Figure 68 shows this general relation.

4.11 Spatial Locations of the Aseismic Zone and Macroseismic Events

As discussed in Section 4.2, the macroseismic events related to primary stope blasting earlier in the mine life (Q1 2019) had a tendency to occur at the maximum extent of the total seismic response. Over time, the larger events for both primary and secondary stopes tended towards the median distance of events. Figure 69 shows early mining response, a stope with a contrasted with Figure 70 of a later mining response. Both figures show primary stope mining blasts. It was observed that the events migrated from the hanging wall of the orebody into the host rock and footwall.

Figure 69 - Primary Stope Blast December 31, 2018 Plan View

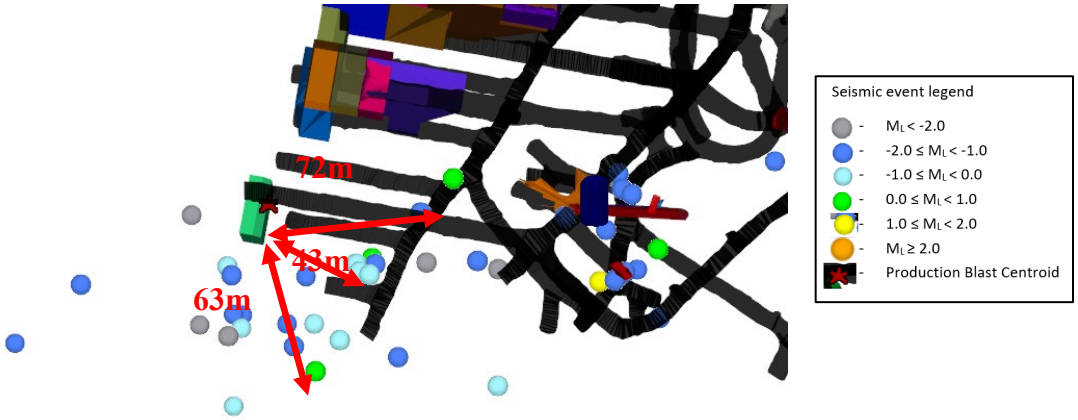

Figure 70 - Primary Stope Blast September 28, 2020 Plan View

The largest of the events also showed an increase in distance from the blast over time, in both primary and secondary stopes. This increase in distance corresponded with the median distance

of responses, and tended towards the footwall. Figure 71 shows the early mining large event distance contrasted with Figure 72 showing the later mining large event distance. These two figures show that secondary stopes over similar timeframes reacted in a similar manner to the primary stopes.

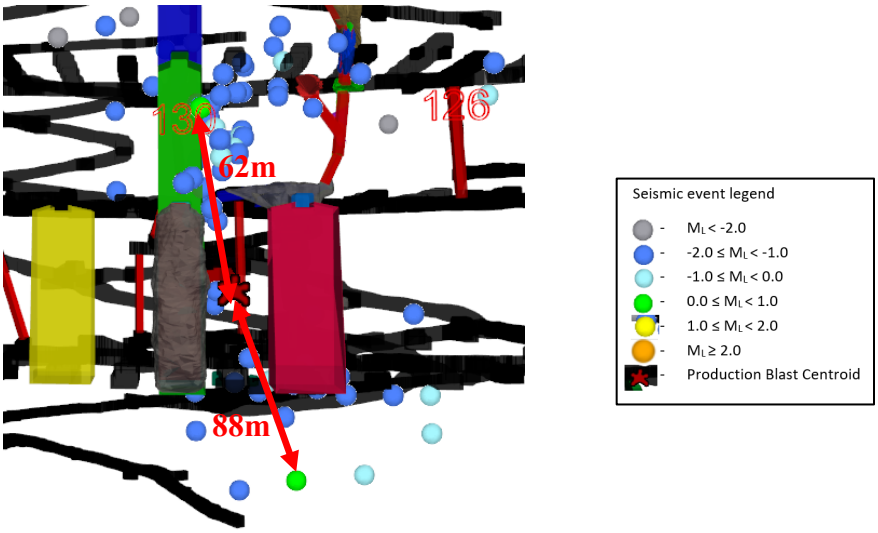

Figure 71 - Secondary Stope Blast February 27, 2019 Looking South

Figure 72 - Secondary Stope Blast August 23, 2019 Looking North

4.12 Production Blast Tonnage Impact on Number of Seismic Events

As discussed previously in Section 4.1.4, the relation between blast tonnage and seismic response has been established. An examination of this impact will be undertaken in this section.

4.12.1 Primary Stope Response

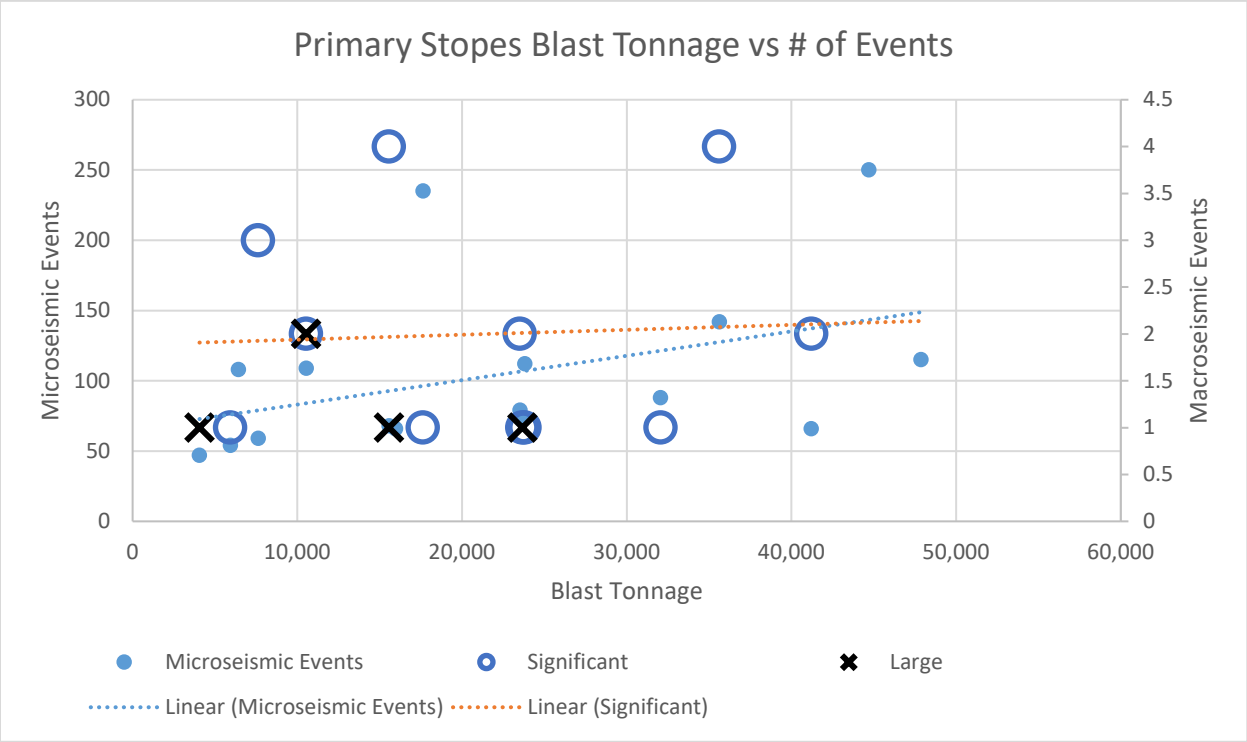

Figure 73 - Microseismic and macroseismic response to production blasting based on blast tonnage (primary stopes)

Although a trend appears for primary stopes in the total events per tonne blasted, there is no apparent correlation in macroseismic events observed in this dataset. It is also observed that the largest events only occurred in blasts under 25,000 tonnes, however it is a limited dataset.

Throughout the dataset, 1670 microseismic and 27 macroseismic events were recorded in the 24 hours following a total of 16 blasts. This results in an "average" blast response of 104 microseismic events and 1.7 macroseismic events per blast.

4.12.2 Secondary Stope Response

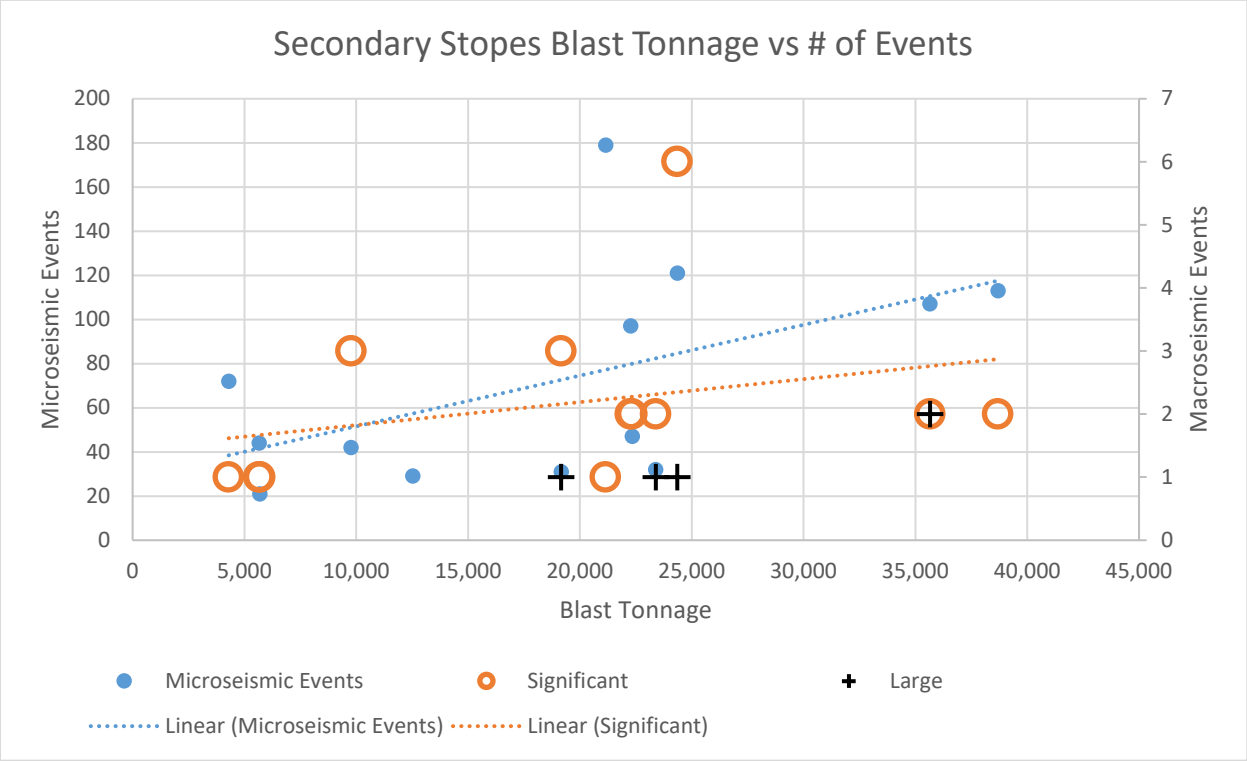

Figure 74 - Microseismic and macroseismic response to production blasting based on blast tonnage (secondary stopes)

As seen in the primary stopes, once again a trend appears for secondary stopes in the total events per tonne blasted. In this dataset, there is a weak trend in macroseismic events observed per tonne blasted. It is also observed that the highest accumulations of macroseismic events occur in a range of blasted tonnages, between 18,000 and 25,000 tonnes, with all large events occurring in blasts >18,000 tonnes

Throughout the dataset, 935 microseismic and 31 macroseismic events were recorded in the 24 hours following a total of 13 blasts. This results in an "average" blast response of 72 microseismic events and 2.4 macroseismic events per blast.

4.12.3 Conclusions Regarding Blast Tonnage and Response

In general, higher tonnage blasts increase the microseismic response. In secondary stopes, increasing the blast tonnage above 18,000 can result in large macroseismic events. This is in contrast to primary stopes, which tend to have the largest macroseismic events below 25,000 tonnes.

On average, the secondary stopes reviewed within the dataset were 41% more likely to generate a macroseismic event. This does not account for the fact that within this same set, the secondary stope blasts averaged 15% fewer tonnes than the primary blasts.

These differences may be accounted for differences in the mechanisms of failure, however more analysis would be required to better understand them. One possible explanation would be that primary stopes largely result in changes to mining-induced stress, whereas the secondary stope blasts are more likely to induce shear related failures.

4.13 Conclusions

A significant change in mechanism, from almost entirely non-shear response to a more shear response, has occurred over time starting around late 2019/2020.

Macroseismic events had shorter averages and less standard deviation in the primary stopes than the secondary stopes. Primary large events tend to occur within twelve hours after a blast. Some evidence of a trend between primary significant events and median response time also exists. The largest events resulting from primary stope blasts in this dataset occurred in blasts under 25,000 tonnes.

A trend may exist between blast size of secondary stopes and macroseismic response, specifically when the tonnage exceeds 18,000 tonnes.

Secondary stopes have an increased likelihood of producing significant or large events during a longer time frame than primary blasts. Sixty-four percent of all macroseismic events occur in secondary stope blasts, almost half of which occurred in the 129 panel alone. When comparing primary stope responses to secondary stope responses, despite a 15% lower average blast tonnage in the secondary stopes, there were 41% more macroseismic events.

In secondary stope blasts, the timing of large events can be seen to be very strongly correlated to the median response time.

Most events occurring over the entire time period of the dataset are non-shear in nature, however the amount of shear events is increasing over time. Shear events are more prevalent in secondary stopes, and tend to occur much longer after blasting. In cases where the 24 hour response following a secondary blast had a high percentage of shear response (above 52%), there were no associated macroseismic events.

Chapter 5

5 Discussion

Although this chapter includes all discussion, a significant portion of the discussion involves the examination of seismic hazard and practical implications of this work. Many of the observations made during this work have potential implications regarding both the relative seismic hazards and the evolution of those hazards over time. Understanding of these hazards may assist in seismic risk management through many different aspects, including: operational re-entry protocols; both dynamic and static ground control standards; production scheduling; distance of permanent infrastructure to the ore; and blasting practices. None of these items have been evaluated as a result of this work and may be considered through suitable risk assessment protocols.

5.1 Aseismic and Seismogenic Zone Development

Over time, a significant change in the seismic response was observed spatially. Early stope mining from within the dataset shows significant near field response, much of which is located in the immediate hanging wall off the orebody.

As mining developed both vertically and laterally across the D1 Zone, the distance from the mine blasts which both the microseismic events and the macroseismic events increased. This increase tended towards the footwall side of the ore, where much of the permanent mine infrastructure lies.

A very clear aseismic zone becomes apparent in both primary and secondary stopes, emerging in late 2019. Just outside of this aseismic zone, a region of seismicity is observed – the seismogenic zone.

This behavior is very reminiscent of the behavior seen around cave propagation in caving mines, such as that observed in the Telfer Mine (Abolfazlzadeh 2013) and Northparkes (Duplancic 2001). In contrast, the seismogenic zone observed at Goldex has progressed mostly laterally towards the footwall, where permanent infrastructure is located.

In the recent past, cave propagation has been monitored through the observations of seismic event locations over time (Reyes-Montes *et al*., 2010; Duplancic & Brady 1999). A characterization of this behaviour, showing a caved zone, air gap and zone of loosening making up the aseismic zone can be seen in Figure 75 below. The locations of the seismic events show the seismogenic zone which can be monitored in caving mines to understand the propagation of the cave.

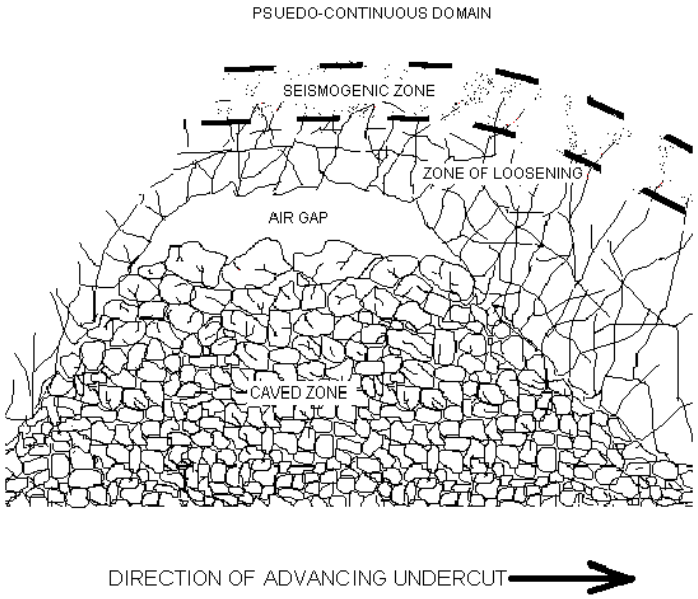

Figure 75 - Conceptual seismogenic zone showed above an advancing cave in a caving mine (Duplancic, 2001)

That being said, the proposed mechanisms (large scale deformation and/or yielding) from the caving mines does not appear to have any evidence of taking place within this dataset, nor have there been operational observations of whole-scale deformation within the orebody. Access to the ore zones for production purposes is through the aseismic zones, with considerable work being done within them for production mining. If significant loosening, yielding and/or failure had occurred, reports and observations in the field would support them.

Aseismic zones without wholesale deformation have been observed in open stoping mines, such as that at Creighton (Cotesta *et al*., 2014) or Lac Shortt mine (Ecobichon *et al*., 1992). Cotesta *et al*. postulated that the process at work at Creighton was an absence of seismicity due to completion of the stress cycle. Mining-induced stresses had reached the yield point of the rock mass in question, and it remained at the residual strength shedding excess stress to the seismogenic zone. Ecobichon *et al*. (1992) similarly believed stress change was the root cause of seismic response. Prior publications have focused on the mine planning aspect of this response.

Cotesta's conclusion was arrived at from changes in deviatoric stress contours overlaid with microseismicity, as can be seen in Figure 76 below. The aseismic zone, identified as the yield limit in this work, from 2002 is shown as a white line. When overlain on the 2008 deviatoric stress map it is clear that the aseismic zone has grown in size in all dimensions visible on this section of the mining region.

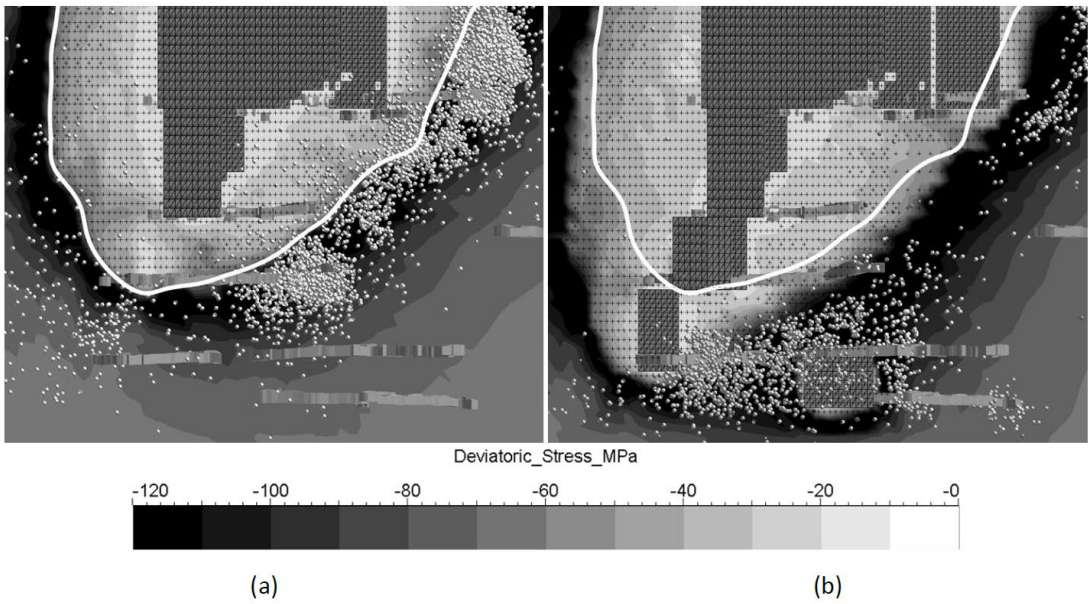

Figure 76 - Creighton mine showing (a) 2002 and (b) 2008 deviatoric stress contours, yielded regions (crosses), the 2002 yield limit (white line), and microseismicity (white spheres) (Cotesta *et al.*, 2014)

Similar to those publications, even with a poorly understood reason for the aseismic zone at Goldex, knowledge of its existence can be used for mine planning purposes, seismic hazard, and risk assessment. Since past seismicity can be a good indicator of future seismicity (Hudyma, 2008), the increases in both the number and magnitude of seismic events within the data set indicate an increase in seismic hazard over the time frame.

5.2 Macroseismic Event Distance in Relation to Aseismic Zone Development

In comparing the macroseismic events to the total events over time, some trends have been observed. Figure 77, below, shows that when all stopes in the dataset are observed, the macroseismic events fall in a narrower band of distances than the total population.

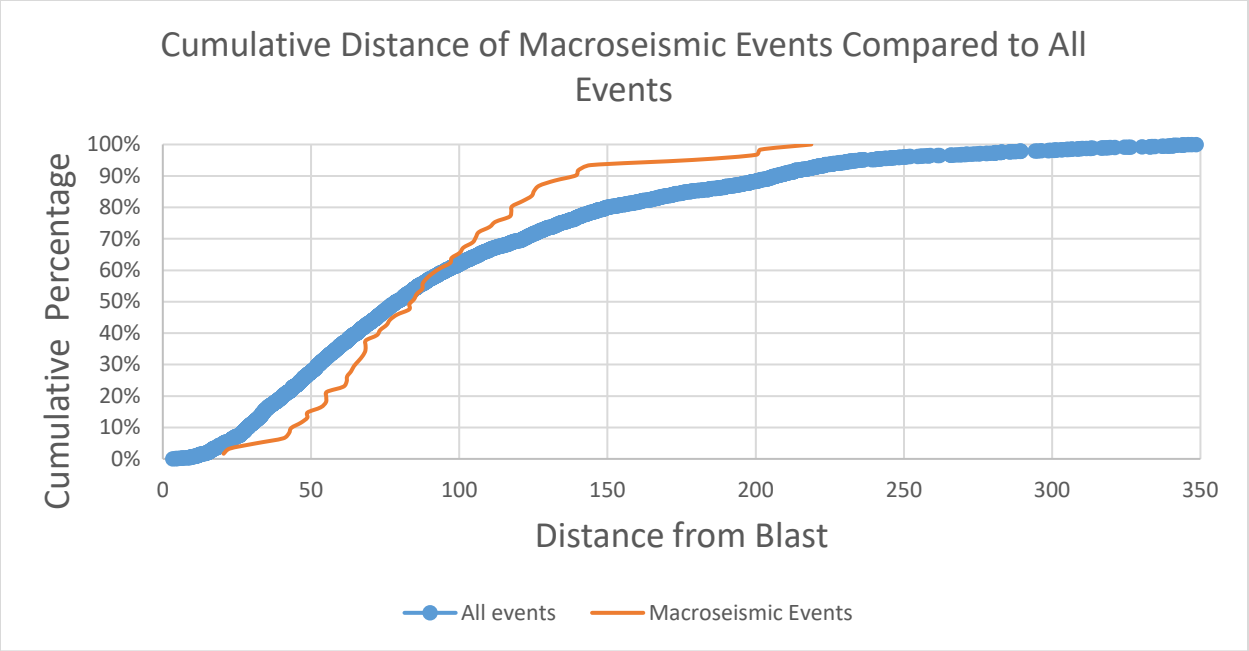

Figure 77 - Distance from the blast for macroseismic events compared to the total population

In total, only 15% of macroseismic events occur within 50m of the blast itself, however 95% of the events occur within 150m of the blasted stope. This response shows a relatively consistent slope along the graph, and given the distances involved are likely to include a stress driven response in the closer events.

When the data is evaluated on a primary stope basis, a similar response is observed to the total dataset, however with an even closer response to the blast. Figure 78 shows two different responses.

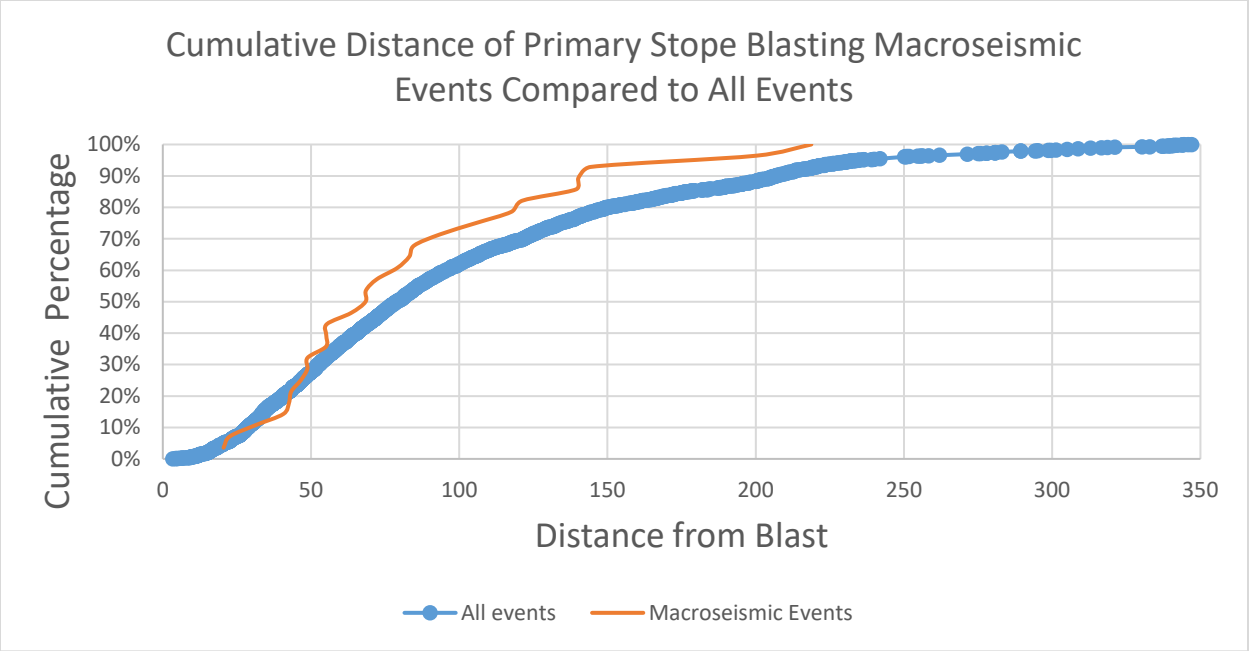

Figure 78 - Distance from the blast for macroseismic events after primary stope blasts compared to the total population of primary stope blast seismic responses

For the primary stopes, approximately 15% of macroseismic events occur within 40m of the blast and 94% occurring within 150m. Compared to the total population, the response within the 40m to 85m range, indicates a higher proportion of the larger seismic events to be stress driven over this time period. It is also observed that the microseismic response further than 250m from the blast is less for the primary stopes than the complete seismic record.

In contrast to the primary stopes, the secondary stope seismic response occurs over a narrower band of distances and is generally further away. Figure 79 shows this response on a cumulative basis.

Figure 79 - Distance from the blast for macroseismic events after secondary stope blasts compared to the total population of secondary stope blast seismic responses

For the secondary stopes, none of the macroseismic events occur within 50m of the blast and only 15% occur within 65m. At the upper end of the chart, 95% of the events occur within 130m of the blast.

In total, the data suggests that macroseismic events are more likely to occur within 150m of the blast location, with secondary stopes being somewhat more consistent between 50m and 130m. As for the total response, it is relatively rare for macroseismic events to occur in the immediate vicinity of the blast, with secondary stope responses being further away than primary stopes.

5.3 Dominant Seismic Responses

The seismic response behavior is characterized by the information gathered from and subsequently analyzed in the dataset. Several different dominant responses were observed, each of which will be discussed in the following sections.

5.3.1 Change in Mechanism Over Time

Two significant changes occurred over time which can be inferred to be a result of a change in mechanism. This includes the Es:Ep (which can be used to infer shear/non shear response) and d-value (which relates to rock mass stiffness). Both will be discussed.

5.3.1.1 Increase in shear response

A relatively significant change in mechanism first started to be observed in late 2019 in this dataset. Prior to this time period, almost all events in the dataset were non shear. This trend was observed in both microseismic and macroseismic events, and can be seen in *Figure 66* found in Section 4.9.

The post-2019 increase in shear events was more apparent in the seismic responses to secondary stope blasting than in primary stope blasting, yet existed in both. Due to shear events correlating with up to three times more energy for a given seismic moment, and also correlating with generally larger magnitude events (Nordström *et al*, 2017), it can be inferred that this change resulted in an increase in seismic hazard.

The increase in shear events was also represented in the significant ($M_L \geq 0$) and large ($M_L \geq 1.0$) events, elevating the already elevated seismic hazard associated with larger magnitude events. Figure 67, located in Section 4.9 shows this relation. This figure also shows that the largest magnitude events ($M_L \geq 2.0$) after a blast were observed to be less likely to occur in secondary stope responses, particularly if there was a significant microseismic shear response immediately following the blast.

An example of these behaviours can be seen in Figure 80, a blast of a secondary stope late in the data set. In this figure, the secondary stope blast itself is denoted by a red star, with the two adjacent primary panels visibly advanced towards the footwall. The seimsic response from this blast occurred primarily in the footwall, with a small response in a largely undeveloped secondary panel to the west (bottom of the figure).

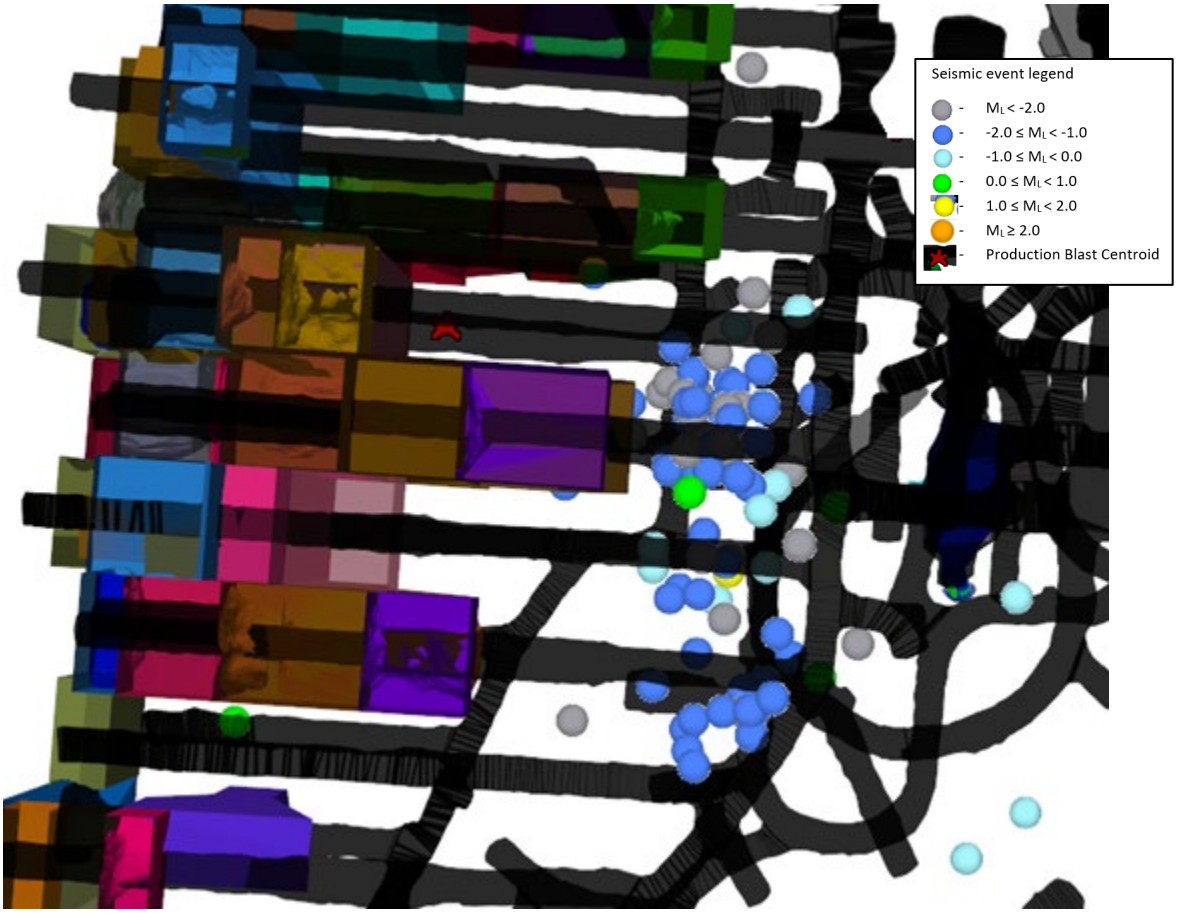

Figure 80 - Plan view of seismic response to blasting of secondary stope CH-120-129-F on December 2, 2020

From this figure, it can be observed that although a significant microseismic response occurred (97 events in the first 2 hours and 126 events in 24 hours), there were no observable largest magnitude events ($M_L \geq 2.0$).

Figure 81 shows the Es:Ep ratio for all of the events occurring following the CH-120-129-F stope blast.

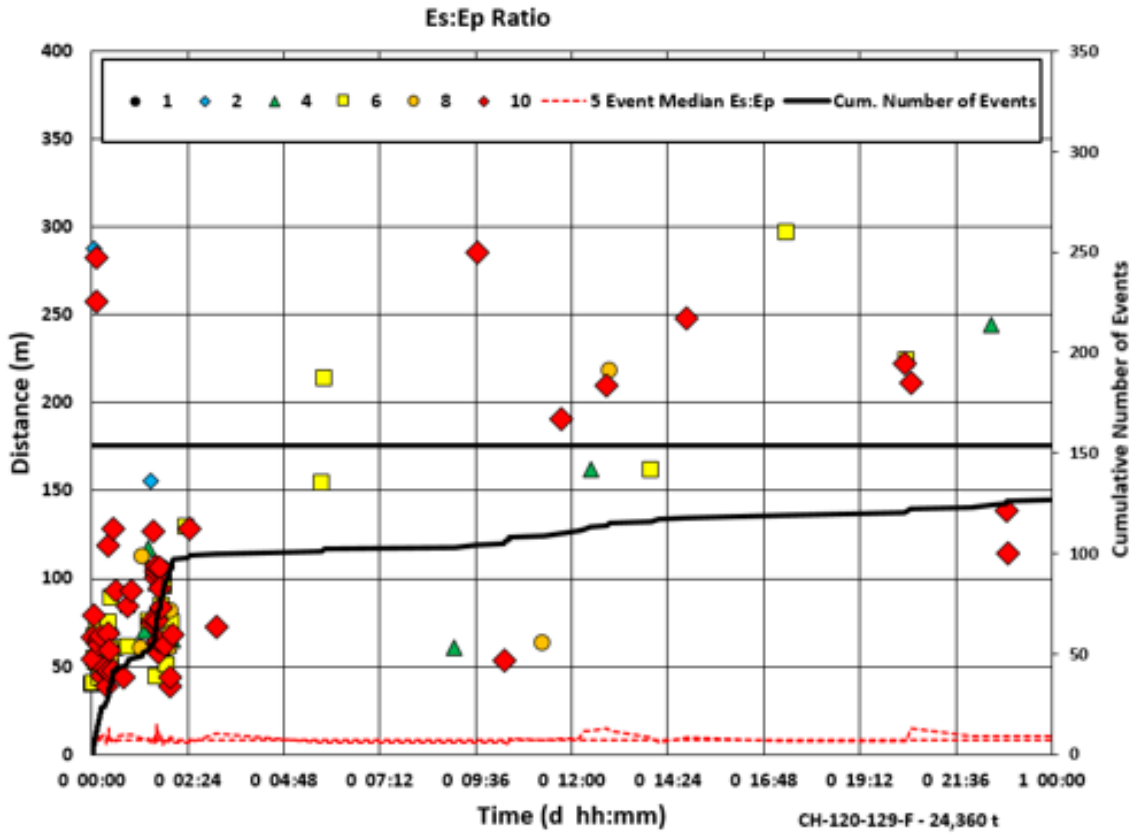

Figure 81 - Es:Ep Ratio for all seismic events in the seismic response to blasting the CH-120-129-F secondary stope

This figure demonstrates the large proportion of high Es:Ep ratio events, correlating with a high volume of shear mechanism events, and thus an increasing seismic hazard. This increase in hazard is tempered by the large response immediately after the blast (within the first 2 hours), in which all large events and all but a single significant event (M_L 0.34) occurred. This general trend indicates in cases of significant response immediately after the blast, the majority of the hazard passes quickly.

5.3.1.2 Decrease in d-value

d-value, the relation between moment and energy, was observed to have a significant decreasing trend over time, as can be seen in *Figure 68 – Average d-values of total seismic response post blasting for primary and secondary stopes* above in Section 4.10. Although observed in both primary and secondary stope blasting seismic responses, this decrease was particularly strong in secondary stopes.

This change in d-value may represent a softening of the rock mass over time, however it does not harmonize with the increase in shear events, as yielding ground was found to include a lower shear response. Mendecki *et al.* (1999) proposed a correlation between d-values and system stiffness within a given rock mass, illustrated in Figure 82 below.

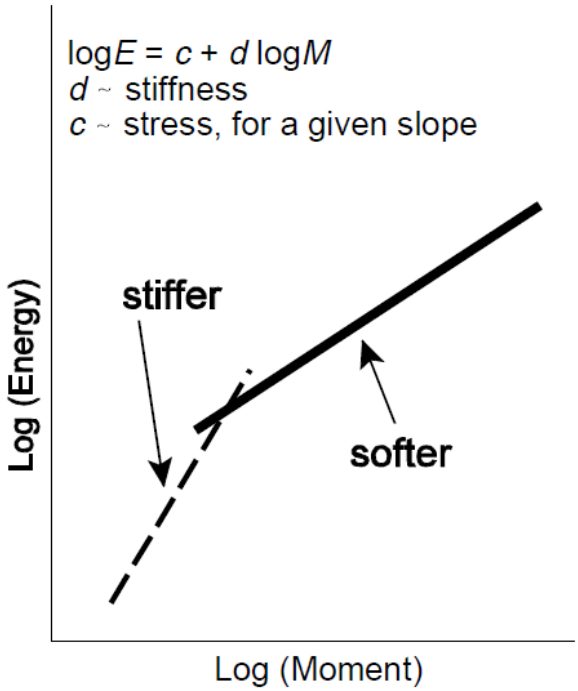

Figure 82 - Log energy vs. log moment plot showing lower d-values for a softer rock mass system response (Mendecki *et al.*, 1999)

Ultimately, the reduction in d-value may represent an increase in seismic hazard overall within the rock mass, especially in the yielded out areas identified as the aseismic zone. The seismogenic zone may have a stiffer response and thus a lower hazard, however due to the movement of the seismogenic zone over time it is problematic to gather sufficient numbers of events to provide a reliable d-value.

5.3.2 Timing of Seismic Response

Over the period of time in the dataset, it was observed that both: the time at which the median seismic event during the total seismic response to blasting; and the amount of deviation within the total response; were reducing. Although observed in both primary (*Figure 49 - Median seismic response time for 24h following production blasting for primary stopes*) and secondary (*Figure 50 - Median seismic response time for 24h following production blasting for secondary stopes*) stope responses, the responses from primary stopes occurred more quickly after production blasting.

This change in total response did not immediately correlate to the largest events, however some similar reductions may be occurring in the primary stope responses. A trend was observed that the largest events associated with primary blasting all occurred within twelve hours of the blast, and a very substantial portion of significant events did the same. Figure 83 shows this response more clearly below.

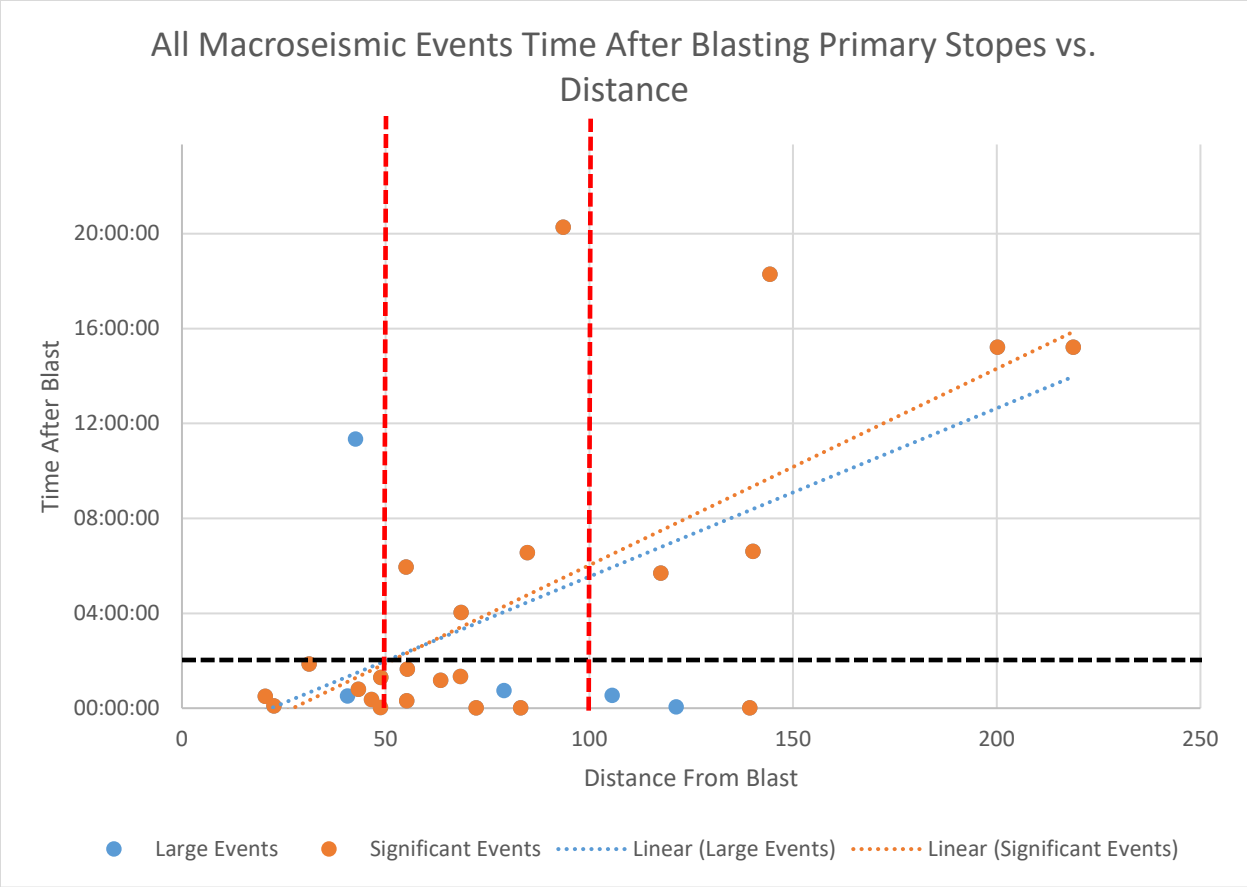

Figure 83 - Distance of macroseismic response compared to time after the blast (Primary stopes)

As observed from this figure, a significant proportion of the macroseismic response occurred in the first two hours (18/28 or 64%) after blasting a primary stope. Specific to the large events, 4/5 or 80% occurred within two hours. Due to the small sample size, it is unclear if this relation is significant, however future data may verify or refute this relation.

When timing was further correlated with distance, the following observations were made:

- 8/9 events occurring within 50m of the blast occurred in the first two hours following the blast
- 7/11 events occurring within 50m-100m of the blast occurred in the first two hours following the blast

- 3/8 events occurring greater than 100m from the blast occurred in the first two hours following the blast

The observation is that as distance increases, time of significant seismic events after a blast increases.

For the total 24 hour response after blasting:

- 9/28 occurred within 50m
- 11/28 occurred between 50m and 100m
- 8/28 occurred at distances greater than 100m

It could be concluded that there is a relatively even distribution of event distances throughout the entire 24 hours following a blast.

The secondary stopes showed considerably more variability in timing of the macroseismic events compared to the primary stopes, as can be seen in Figure 84.

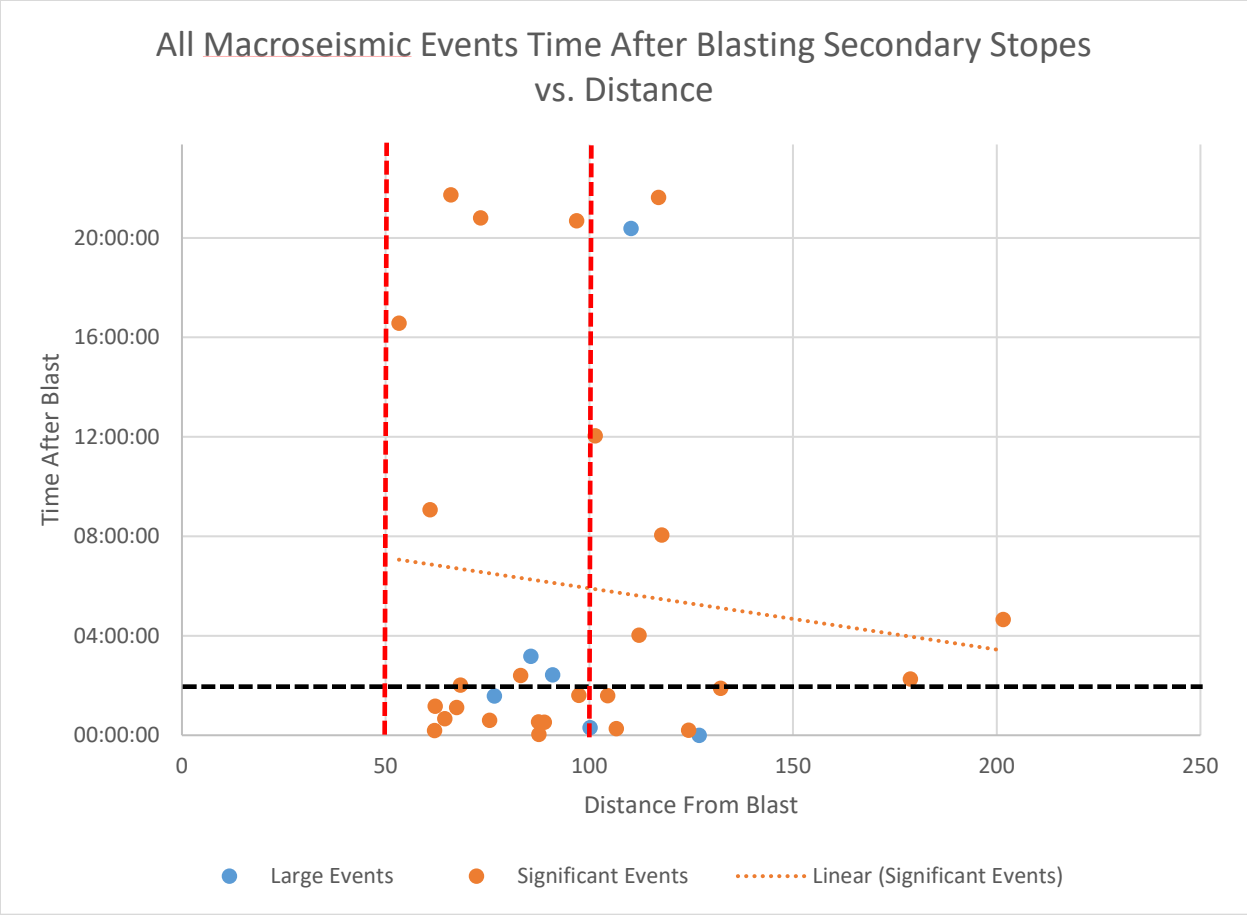

Figure 84 - Distance of macroseismic response compared to time after the blast (Secondary stopes)

The contrast from the primary stope response is very significant. No macroseismic events occurred within 50m of a secondary stope blast at any time. This observation is an indicator of an aseismic zone when blasting secondary stopes.

Using the previously recognized two hour response after a blast:

- 10/19 events occurring within 50m-100m of the blast occurred in the first two hours following the blast
- 6/13 events occurring greater than 100m from the blast occurred in the first two hours following the blast

Increasing the observation time to 4 hours after the blast:

- 14/19 events occurring within 50m-100m of the blast occurred in the first four hours following the blast
- 8/13 events occurring greater than 100m from the blast occurred in the first four hours following the blast

The observation is that increasing distance does not have a significant relation with time of events. However, the amount of time that a significant portion of the macroseismic events has almost doubled.

For the total 24 hour response after blasting:

- 0 occurred within 50m
- 19/32 occurred between 50m and 100m
- 13/32 occurred at distances greater than 100m

It is observed that the majority of events occurred between 50m-100m.

With respect to the median response time (*Figure 50 - Median seismic response time for 24h following production blasting for secondary stopes*), most macroseismic events related to secondary stope blasts were well correlated to the median. This may assist in real-time re-entry protocol development. Some evidence of a similar trend in primary stopes was also observed, but more research may be needed to draw more definite conclusions.

Secondary stope large events were more erratic and, although they appear to be decreasing in response time, have at times extended up to almost 24 hours after the blast. It is worth noting that this work did not evaluate any response after 24 hours from a blast as it was out of the scope. Further research in this area may assist in more understanding of long term, high magnitude seismic responses from secondary stope blasting.

5.4 Response Based on Stope factors

In addition to the various seismic source parameters, the stope planning and scheduling process has resulted in observable differences to the seismic response. These differences and their impact will be discussed below.

5.4.1 Stope Tonnage

In primary stopes, a trend between the total number of events and the stope tonnage blasted was observed in *Figure 73 - Microseismic and macroseismic response to production blasting based on blast tonnage (primary stopes)*. This trend would imply the greater the blast size, the greater the elastic stress change, and the greater the overall seismic response.

An inverse trend was also observed with respect to the largest macroseismic events – no events greater than a 1.0 local magnitude occurred within this dataset after any primary blast greater than 25,000 tonnes. There was no obvious minimum tonnage where these largest events occurred. This behaviour appears unexpected and unexplainable with techniques employed.

In secondary stopes, a similar trend between the total number of events and the stope tonnage blasted was observed in *Figure 74 - Microseismic and macroseismic response to production blasting based on blast tonnage (secondary stopes)*. This trend continued to the macroseismic events, where blast tonnages exceeded 18,000 tonnes the largest of the events within the dataset were observed to occur.

5.4.2 Stope Level

Normally, with depth, an associated increase in pre-mining stresses would be expected. This increase in stresses often correlates with more pronounced seismic response.

In the case of this dataset, the inverse was observed. Deep stope mining had less overall response than shallower mining. This may be an indication that the lower extraction ratio early on, when the deepest mining began, played a role in the seismic response. This observation was especially apparent in the primary stope mining (*Figure 61 - Total number of seismic events recorded after production blasting per mining level of primary stopes*). That being said, the macroseismic response in the deepest primary stopes was generally more significant than the shallower stope mining.

When mining secondary stopes, no trends were observed between seismic response of any sort and the depth in which mining was occurring (*Figure 62 – Total number of seismic events recorded after production blasting per mining level of secondary stopes*). This once again suggests a difference in seismic source mechanism between the primary and secondary stope blasting seismic responses.

5.4.3 Stope Panel

In this dataset, the largest seismic responses generally occurred in the middle lead panels within the orebody – typically between the 128 and 130 panels, as can be seen in *Figure 63 – Total number of seismic events recorded after production blasting per mining panel of the production blast*. Fourty-five percent of all recorded seismic responses came from these three panels, despite only a third of the total mining stopes being taken from these panels. The lead stopes

from these three panels represented approximately 2.5 times more seismic events than an average stope across the orebody.

It is hypothesized that this significant response was a result of a combination of early extraction ratios combined with the principal stress orientation. Mining from the middle of the orebody outwards is likely a production decision, which may benefit from re-evaluation in any subsequent ore mining below the D1-Zone.

In contrast to the increased early microseismic events, yet more similar to the level based analysis above, early panel mining had more macroseismic events.

In general, the east side panels showed more microseismic response and the west side panels showed more macroseismic response. These increases in responses may be attributable to either abutment stresses or geological structure.

5.4.4 Primary/Secondary Stopes

By using the same figure as stope panel (*Figure 63 – Total number of seismic events recorded after production blasting per mining panel of the production blast*), it can be observed that secondary stopes have an increased likelihood of producing significant or large events during a longer time frame than primary blasts. Sixty-four percent of all macroseismic events occur following secondary stope blasts, almost half of which occurred in the 129 panel alone. When comparing primary stope responses to secondary stope responses (*Figure 73* and *Figure 74*), despite a 15% lower average blast tonnage in the secondary stopes, they generated 41% more macroseismic events.

This observation could be a relation between confining stresses and seismic response. Secondary stopes are considerably more likely to have lower confining stresses due to mined-out regions

adjacent to them. This lower confining stress could result in lower strength of the rock mass, and ultimately smaller events, leading to deformation.

The development of an aseismic zone was different in both primary and secondary stope blasting responses. Primary stopes showed no such zone until early 2020, after which the distance of the aseismic zone increased with time. Secondary stopes showed an aseismic zone throughout the entire time of mining within the data set, which was larger in distance than the primary stopes.

5.5 Response Following Production Blasting

As can be observed in *Figure 51 - Median seismic response time for 24h following production blasting for all stopes, overlain with the significant (*ML >0.0*) and large (ML > 1.0) events*, 85% of the largest events occurred within 8 hours of primary stope blasting. This contrasts with the secondary stope response, where 35% occurred between 8 and 24 hours after a blast. In both cases, the macroseismic events had shorter median times and less standard deviation in the primary stopes than the secondary stopes. Also in both cases, the majority of all events occurred within 2.25 hours of the blast time.

This indicates that secondary stopes have an increased likelihood of producing significant or large events over a longer time frame.

Combined with the observations in Section 4.2, where Figure 45 and Figure 47 show primary stopes with 90% and secondary stopes with 94% of all significant and large events occur within 150m of the blast, this information may be useful for informing re-entry protocols for workers in a post blast environment. It is of note that those same last two figures show only 68% (primary) and 65% (secondary) of significant and large events occur within 100m.

5.6 Responses beyond the 24 Hour Window

In the time period and geographical coverage of the data set, there were 11 large events which had occurred. Of those events, all of them have been included in this analysis. With respect to significant events, 49 of the 61 events in the same period have been analyzed. Considerable additional work could have resulted in determining the impacts of development blasting, multiple production blasts, or the influence of time greater than 24 hours on these excluded significant events, however that fell outside of the scope of this work.

5.7 Final discussion

The existence of an aseismic zone and a seismogenic zone has developed over time in both primary and secondary stopes. Figure 85 shows what a typical responses were for stopes in 2019 and how that changes by the end of 2020.

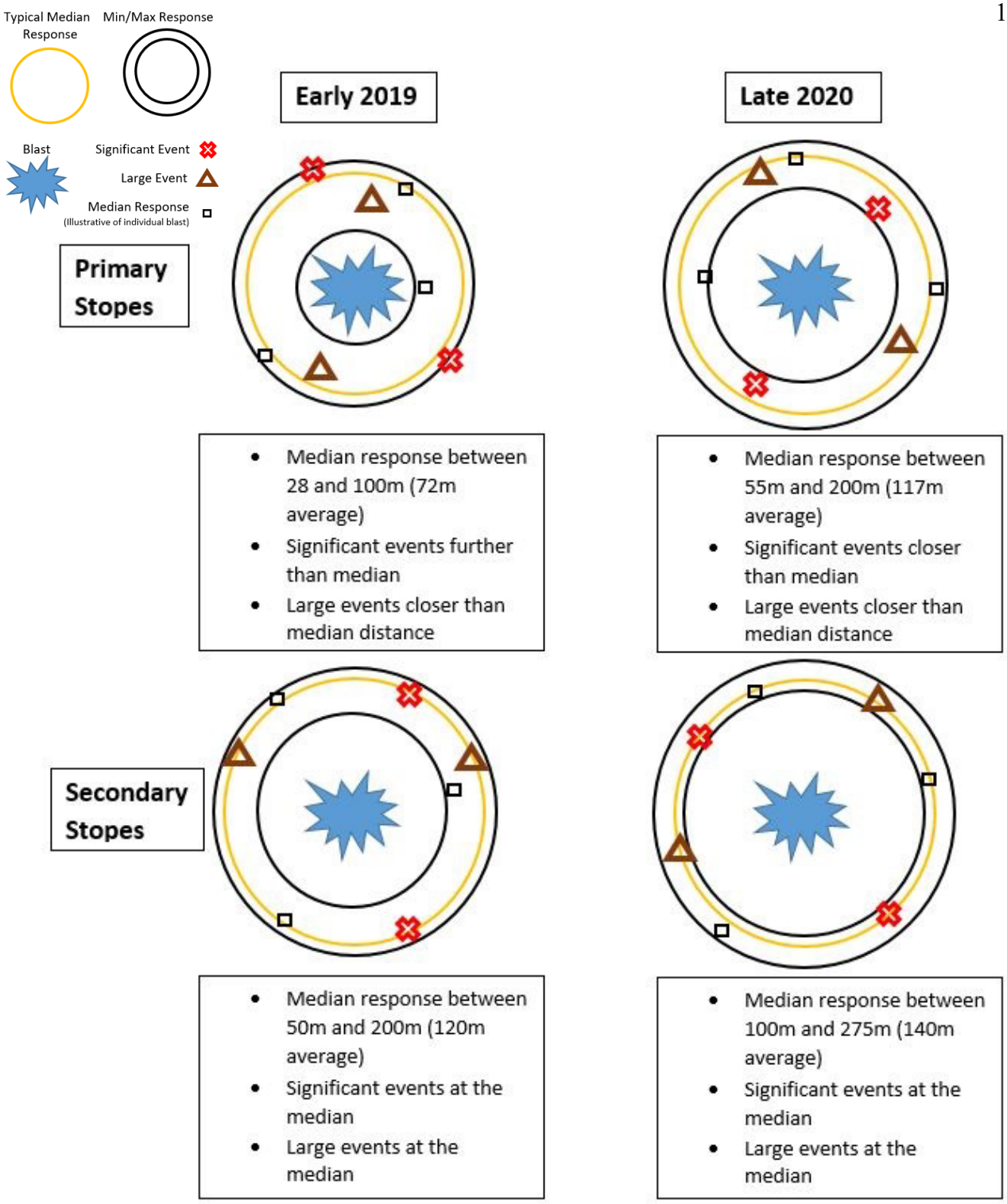

Figure 85 - Schematic of typical aseismic and seismic response over time in primary and secondary stopes

In the figure, the aseismic zones are represented by the areas around the centre without any seismicity, with the blast represented as a blue irregular shape. Median seismic responses are represented by black squares, with black circles representing the upper and lower bounds of where the median response occurred. The orange circle is the average of all median responses in the relevant time frame. Significant events and large events are represented by red crosses and brown triangles, respectively.

It is apparent that the aseismic zones are getting larger in all cases over time, and that all seismicity is migrating further away from the blasts. This is more pronounced in secondary stope blasts compared to primary stope blasts.

It is clear from the data observed that there are considerable differences in seismic responses between various categories of examination. With respect to seismic hazard, the highest importance is on the timing and magnitudes of the larger events. Based on the various parameters reviewed, some of the highest seismic response hazard would be late extraction centre orebody stopes. This includes the primary panels of 128 and 130, as well as the 129 secondary panel. Bottom up mining may be contributing the stress accumulation in the competent rock left above in the D1 Zone, which creates a stressed pillar between the previously mined out zones above.

Reduction in hazards from macroseismic activity appears to correlate with larger primary stope blasts and smaller secondary stope blasts.

Timing of macroseismic stope responses are generally under 8 hours for primary stopes, yet up to 24 hours for secondary stopes.

An evaluation of the various observed increased hazard conditions described in this work could be completed, resulting in a risk assessment detailing the various risk levels associated with

diverse mining strategies. Implementation of seismic monitoring protocols or the evaluation of re-entry times may be supportive controls in such situations.

Chapter 6

6 Conclusions and Recommendations

Throughout the mining of the D1 Zone at Goldex, there has been an ever evolving and increasing intensity in the seismic response to mining. As previously discussed, mining-induced seismicity at depth has been and continues to influence the hazards related to seismicity. This thesis has investigated the changes over time to the seismic response, and the associated changes in hazard.

The work done on this thesis, and any information, conclusions or findings generated therefrom, has been done on an empirical basis. Conclusions are an indication based on the limits of the data available at the time, and during the time periods included, but extrapolation outside of that data period is not appropriate.

6.1 Contributions of the Thesis

The main novel observation of this thesis is the identification of both an aseismic zone and seismogenic zone within the D1 Orebody, and the conditions under which the presence of both could be expected.

This thesis also presented:

- How the seismic response has changed, both in primary stoping and secondary stoping, throughout the extraction of the orebody
- Changes in hazard as a result of the changes to the seismic response
- Trends in seismicity which may be useful in evaluation of re-entry protocols

6.2 Recommendations for Further Work

The methodology in this thesis should be assessed against other mines of similar depths and seismic responses. Specifically, hard rock, longhole stoping mines located within the Canadian Shield.

This same methodoloygy should also be used against any data from the Goldex Mine extending from the end of the data set used in this work up until current day. Additional data and analysis could prove very useful in both verification of this work and potentially in seismic forecasting applications.

Additional investigation of the impact on seismic response and geological structure may yield additional information about the increase in shear seismic response over time.

Finally, a significant work involving numerical modelling to emulate the seismicity observed to better understand the mechanisms at play would be recommended. This could be used not only to better understand the mechanisms at work during the time period covered in this thesis, but also could serve to assist in future forcasting purposes.

References

Abolfazlzadeh, Y. (2013) Application of seismic monitoring in caving mines – case study of Telfer Gold Mine. M.A.Sc. Thesis, Laurentian University, Sudbury, Canada, 213 pages.

Agnico Eagle Mines Limited. (2021) Agnico Eagle Reports Fourth Quarter and Full Year 2020 Results. Date retrieved July 9, 2022. https://s21.q4cdn.com/374334112/files/doc_financials/quarterly/2021/Q4-2020_AEM-Results-February-11-2021-Final.pdf

Andrieux, P.P., Hudyma, M.R., O'Connor, C.P., Li, H., Cotesta, L., and Brummer, R.K. (2008) Calibration of large-scale three-dimensional non-linear numerical models of underground mines using microseismic data. *1st International FLAC/DEM Symposium.* Minneapolis, Minnesota. 8 pages.

Arjang, B. (1996) In situ ground stresses in the Abitibi Mining District. CIM Bulletin, vol. 89, no. 996, pp. 65-71

Barton, N.R, Lien, R., and Lunde, J. (1974) Engineering classification of rock masses for the design of tunnel support: Rock Mechanics, v. 6, p. 189-239.

Bawden, W.F. and Mercer, R.A. (1994) Some thoughts on hazard assessment for improved mine design. *Proceedings for Risk Assessment in Extractive Industries.* University of Exeter, United Kingdom.

Beck Engineering. (2013) Back analysis and E and M Stope forward analysis. Preliminary Draft Privileged – Prepared for Legal Counsel.

Bieniawski, Z.T. (1976) Rock Mass Classification in Rock Engineering, Editor: Bieniawski, Z.T., *Symposium on exploration for rock engineering*, Balkema: Rotterdam, p. 97-106.

Boatwright, J. and Fletcher, J.B. (1984) The partition of radiated energy between P and S waves. *Bulletin of the Seismological Society of America,* Vol. 74(2), pp. 61-376.

Brady, B.H.G. and Brown, E.T. (2006) Rock Mechanics for underground mining, 3rd ed. Springer, Dordecht, The Netherlands. 628 pages.

Brown, L.G. (2015) Seismic hazard evaluation using apparent stress ratio for mining-induced seismic events. M.A.Sc. Thesis, Laurentian University, Sudbury, Canada, 257 pages.

Brown, L.G. (2018) Qualification of seismic responses to mining using novel seismic response parameters. PhD Thesis, Laurentian University, Sudbury, Canada, 286 pages.

Brown, L.G. and Hudyma, M.R. (2018) Mining induced seismicity in Canada: A 2017 update. *Proceedings of Fifty-Second Rock Mechanics/Geomechanics Symposium.* Seattle, Washington, 8 pages.

Card, K.D. (1990) A review of the Superior Province of the Canadian Shield, a product of Archean accretion. *Precambrian Research,* Vol. 48, Issues 1-2, pp. 99-156.

Carusone, O.T.S. (2018) Interpretation of rock mass yield using apparent stress of microseismic events – examples from Glencore's Nickel Rim South Mine. M.A.Sc. Thesis, Laurentian University, Sudbury, Canada, 302 pages.

Cichowicz, A., Green, R.W.E., Brink, A v Z, Grobler, P., and Mountfort, P.I. (1990) The space and time variation of micro-event parameters occurring in front of an active stope. Editor: Fairhurst, C. Rotterdam: A.A. *Proceedings of Rockbursts and Seismicity in Mines.* Balkema, pp 171-175.

Cook, N.G.W. (1976) Seismicity associated with mining. *Engineering Geology,* Vol. 10, pp. 99-122.

Coulson, A.L. (2009) Investigation of the pre to post peak strength state and behaviour of confined rock masses using mine induced microseismicity. PhD Thesis, University of Toronto, Toronto, Canada, 493 pages.

Corthésy, R. and Leite, M.H. (2006) Mesures des contraintes in-situ Mine Goldex. École Polytechnique, Montréal, 88 p.

Cotesta, L., O'Connor, C.P., Brummer, R.K., and Punkkinen, A.R. (2014) Numerical modelling and scientific visualization – integration of geomechanics into modern mine designs. Editors: Hudyma, M., Potvin, Y. *Deep Mining 2014: Proceedings of the Seventh International Seminar on Deep and High Stress Mining.* Australian Centre for Geomechanics, Sudbury, ON, pp. 377-394.

Deere, D.U., Hendron, A.J., Patton, F.D., and Cording, E.J. (1967) Design of surface and near surface construction in rock. Editor: Fairhurst, C. *Failure and breakage of rock, proceedings of the 8th U.S. Symposium on Rock Mechanics.* Society of Mining Engineers, American Institute of Mining, Metallurgical, and Petroleum Engineers. New York, USA, pp. 237-302

Doucet, C. (2018) Programme en Controle de Terrain, Mine Agnico Eagle – Mine Goldex. Unpublished report.

Doucet, C. (2021) Dylonite.pdf. Unpublished PowerPoint Presentation.

Duplancic, P. (2001) Characterization of caving mechanisms through analysis of stress and seismicity. PhD Thesis, University of Western Australia, Perth, Australia, 227 pages.

Duplancic, P. and Brady, B.H. (1999) Characterization of caving mechanisms by analysis of seismicity and rock stress. Editors: Vouille, G., Berest, P. *Proceedings of the Ninth*

International Congress of Rock Mechanics. International Society for Rock Mechanics and Rock Engineering, Lisbon, Portugal, pp. 1049-1053.

Ecobichon, D., Hudyma, M.R. and Laplante, B. (1992) Understanding geomechanics problems through microseismic monitoring at Lac Shortt. *Proceedings of 94th Annual General Meeting of the CIM: Rock Mechanics and Strata Control Sessions.* Montreal, Canada, pp. 1-13.

Gibowicz, S.J. (1990) The mechanism of seismic events induced by mining. Editor: Fairhurst, C. *Proceedings of the 2nd International Symposium of Rockbursts and Seismicity in Mines.* Balkema, Rotterdam, pp. 3-27.

Gibowicz, S.J. and Kijko, A. (1994) An introduction to mining seismology, 1st ed. Academic Press, San Diego, California, 396 pages.

Google. (2022) [Google Maps showing Goldex – Mines Agnico Eagle Ltée, 3e Avenue, Val-d'Or, QC, Canada]. Date retrieved July 7, 2022. https://goo.gl/maps/B1vi39WpE3RW5bkS9

Gutenberg, B. and Richter, C.F. (1994) Frequency of earthquakes in California. *Bulletin of the Seismological Society of America,* Volume 34(4), pp. 185-188.

Hanks, T.C. and Kanamori, H. (1979) A moment magnitude scale. *Journal of Geophysical Research,* Vol. 84, pp. 2348-2350.

Hasegawa, H.S. Wetmiller, R.J., and Gendzwill, D.J. (1989) Induced seismicity in mines in Canada – an overview. *Pure and Applied Geophysics* Vol. 129, No. 3/4, pp. 423-453.

Hedley, D.G.F. (1992) Rockburst handbook for Ontario hardrock mines. CANMET Special Report SP92-1E, 305 pages.

Hoek, E. (2006) Practical rock engineering. Self published, online. 341 pages. Retrieved July 9, 2022. https://www.rocscience.com/assets/resources/learning/hoek/Practical-Rock-Engineering-Full-Text.pdf

Hoek, E., and Brown, E.T. (1980) Underground excavations in rock. London: The institution of Mining and Metallurgy, 527 pages.

Hudyma, M.R. (2008) Analysis and interpretation of clusters of seismic events in mines. PhD thesis, University of Western Australia, Perth, Australia, 409 pages.

Hudyma, M.R., Frenette, P., and Leslie, I. (2010) Monitoring open stope caving and Goldex Mine. Editor: Potvin, Y., *Caving 2010: Proceedings of the Second International Symposium on Block and Sublevel Caving.* Australian Centre for Geomechanics, Perth, Australia, pp. 133-144.

Hudyma, M.R., Heal, D., and Mikula, P. (2003) Seismic monitoring in mines - Old technology – New applications. *Proceedings of the 1st Australasian Ground Control in Mining Conference.* University of NSW, Sydney, Australia, pp. 201-218.

Kaiser, P.K., McCreath, D.R., and Tannant, D.D. (1996) Canadian rockburst support handbook MIRARCO: Geomechanics Research Centre, 324 pages.

Kgarume, T.E., Spottiswoode, S.M., and Durrheim, R.J. (2010) Deterministic properties of mine tremor aftershocks. Editors: Van Sint Jan, M. and Potvin, Y. *Proceedings of Deep and High Stress Mining.* Australian Centre for Geomechanics, Santiago, Chile, pp. 227-237.

Ortlepp, W.D. (1997) Rock fracture and rockbursts, an illustrative study. The South African Institute of Mining and Metallurgy, Monograph Series M9, Johannesburg, South Africa, 98 pages.

Madariaga, R. (1976) Dynamics of an expanding circular fault. *Bulletin of the Seismological Society of America,* Vol. 66(3), pp. 639-666.

Mendecki, A.J. (2013) Mine seismology: Glossary of selected terms. Editors: Malovichko, A., Malovichko, D. *The 8th Rockburst and Seismicity in Mines Symposium*. Geophysical Survey of Russian Academy of Sciences, Mining Institute of Ural Branch of Russian Academy of Sciences, St. Petersburg-Moscow, Russia, pp. 527-551.

Mendecki, A.J. and van Aswegen, G. (2001) Seismic monitoring in mines: selected terms and definitions. Editors: van Aswegen, G., Durrheim, R.J., and Ortlepp, W.D. *Proceedings of Rockbursts and Seismicity in Mines.* RaSiM 5, South African Institute of Mining and Metallurgy, Johannesburg, South Africa, pp. 563-570.

Mendecki, A.J., van Aswegen, G., and Mountfort, P. (1999) A guide to routine seismic monitoring in mines. In book: A handbook on Rock Engineering Practice for Tabular Hard Rock Mines. 1st ed. The Safety in Mines Research Advisory Committee, Johannesburg, South Africa, pp. 287-309.

Mercer, R.A. and Bawden, W.F. (2005) A statistical approach for the integrated analysis of mine induced seismicity and numerical stress estimates, a case study – Part I: developing the relations. *International Journal of Rock Mechanics and Mining Sciences,* Vol. 42, pp. 47-72.

Nordström, E., Dineva, S. and Nordlund, E. (2017) Source parameters of seismic events potentially associated with damage in block 33/34 of the Kiirunavaara mine (Sweden). *Acta Geophysica,* Vol. 65, pp. 1229–1242.

Nuttli, O.W. (1973) Seismic wave attenuation and magnitude relations for eastern North America. *Journal of Geophysical Research,* Vol. 78(5), pp. 876-885.

Ortlepp, W.D. (1992) Invited Lecture: The design of support for the containment of rockburst damage in tunnels – An engineering approach. Editors: Kaiser, P.K. and McCreath, D.R. *Proceedings of Rock Support and Underground Construction*, Rotterdam, A.A. Balkema, pp. 593-609.

Reyes-Montes, J.M., Sainsbury, B.L., Pettitt, W.S., Pierce, M., and Young, R.P. (2010) Microseismic tools for the analysis of the interaction between open pit and underground developments. Editor: Potvin, Y. *Proceedings of the Second International Symposium on Block and Sublevel Caving.* Australian Cenre for Geomechanics, Perth, Australia, pp. 119-131.

Richter, C.F. (1935) An instrumental earthquake magnitude scale. *Bulletin of the Seismological Society of America,* Vol. 25, pp. 1-32.

Simser, B.P. (2006) Mine wide seismic monitoring at Falconbridge's Craig Mine. *Proceedings of the 41st US Rock Mechanics Symposium (USRMA): 50 Years of Rock Mechanics – Landmarks and Future Challenges.* Golden, Colorado.

Stacey, T.R., and Ortlepp, W.D. (2001) Tunnel surface support – capacities of various types of wire mesh and shotcrete under dynamic loading. The *Journal of South African Institute of Mining and Metallurgy,* Vol 101(7), pp. 337-342.

Tarasov, B.G., and Randolph, M.F. (2011) Superbrittleness of rocks and earthquake activity. *International Journal of Rock Mechanics and Mining Sciences,* Vol. 48(6), pp. 888-898.

Thurston, P.C., Ayer, J. Goutier, J. and Hamilton, M.A. (2008). Depositional gaps in Abitibi greenstone belt stratigraphy: A key to exploration for syngenetic mineralization. *Economic Geology,* Vol. 106, No. 6., pp 1097-1134.

Urbancic, T.I., Young, R.P., Bird, S., and Bawden, W.F. (1992). Microseismic source parameters and their use in characterizing rock mass behaviour: Considerations from Strathcona Mine. *94th Annual General Meeting of the CIM: Rock Mechanics and Strata Control Sessions,* pp. 36-47.

Vallejos, J.A.M. (2010) Analysis of seismicity in mines and development of re-entry protocols. PhD thesis, Queen's University, Kingston, Canada. 372 pages.

Wawersik, W.R. and Fairhurst, C. (1970) A study of brittle rock fracture in laboratory compression experiments. *International Journal of Rock Mechanics and Mining Sciences,* Vol. 7(5), pp. 561-575.

Wyss, M. and Brune, J.N. (1968) Seismic moment, stress and source dimensions for earthquakes in the California-Nevada region. *Journal of Geophysical Research,* Vol. 73(14), pp. 4681-4694.